AFRL-RV-HA-TR-2007-1124

Seismic Energy Generation and Partitioning into Various Regional Phases from Different Seismic Sources in the Middle East Region

Yefim Gitterman
Vladimir Pinsky
Rami Hofstetter

Geophysical Institute of Israel
P.O.B. 182, Lod 71100
ISRAEL

Final Report

20 September 2007

AIR FORCE RESEARCH LABORATORY
Space Vehicles Directorate
29 Randolph Road
AIR FORCE MATERIEL COMMAND
Hanscom AFB, MA 01731-3010

NOTICES

Using Government drawings, specifications, or other data included in this document for any purpose other than Government procurement does not in any way obligate the U.S. Government. The fact that the Government formulated or supplied the drawings, specifications, or other data does not license the holder or any other person or corporation; or convey any rights or permission to manufacture, use, or sell any patented invention that may relate to them.

This report was cleared for public release and is available to the general public, including foreign nationals. Qualified requestors may obtain additional copies from the Defense Technical Information Center (DTIC) (http://www.dtic.mil). All others should apply to the National Technical Information Service.

AFRL-RV-HA-TR-2007-1124 HAS BEEN REVIEWED AND IS APPROVED FOR PUBLICATION IN ACCORDANCE WITH ASSIGNED DISTRIBUTION STATEMENT.

//Signature//	//Signature//
ROBERT RAISTRICK Contract Manager	BRIAN GRIFFITH, Maj, USAF, Chief Battlespace Surveillance Innovation Center

This report is published in the interest of scientific and technical information exchange, and its publication does not constitute the Government's approval or disapproval of its ideas or findings.

REPORT DOCUMENTATION PAGE

Form Approved
OMB No. 0704-0188

1. REPORT DATE *(DD-MM-YYYY)*	**2. REPORT TYPE**	**3. DATES COVERED** *(From - To)*
20-09-2007	Final Report	01-01-2004 to 30-06-2007

4. TITLE AND SUBTITLE
Seismic Energy Generation and Partitioning into Various Regional Phases from Different Seismic Sources in the Middle East Region

5a. CONTRACT NUMBER
F19628-03-C-0124

5b. GRANT NUMBER
N/A

5c. PROGRAM ELEMENT NUMBER
62601F

6. AUTHOR(S)
Yefim Gitterman, Vladimir Pinsky and Rami Hofstetter

5d. PROJECT NUMBER
1010

5e. TASK NUMBER
SM

5f. WORK UNIT NUMBER
A1

7. PERFORMING ORGANIZATION NAME(S) AND ADDRESS(ES)
Geophysical Institute of Israel
P.O.B. 182, Lod
71100 Israel

8. PERFORMING ORGANIZATION REPORT NUMBER
542/260/07

9. SPONSORING / MONITORING AGENCY NAME(S) AND ADDRESS(ES)
Air Force Research Laboratory
29 Randolph Rd.
Hanscom AFB, MA 01731-3010

10. SPONSOR/MONITOR'S ACRONYM(S)
AFRL/RVBYE

11. SPONSOR/MONITOR'S REPORT NUMBER(S)
AFRL-RV-HA-TR-2007-1124

12. DISTRIBUTION / AVAILABILITY STATEMENT
Approved for Public Release; Distribution Unlimited.

13. SUPPLEMENTARY NOTES

14. ABSTRACT
The project was focused on studying, experimentally, features of seismic energy generation and partitioning of P and S waves from different explosive seismic sources, at near-source and regional distances, in the time and spectral domain. An extensive database of Ground Truth single-fired explosions was created. The explosions selected contain a broad variety of design features (buried and surface sources, tamped and decoupled shots, large diameter 0.5-0.8m borehole and near-spherical cavity charges), charge weight (100-32500kg), depth (14–62m), scaled burial depth (1.0-3.9m/$kg^{1/3}$), emplacement rocks (alluvium, basalts, marls) and geological settings.
The highlight of this project was the source phenomenology experiments: Decoupling and Depth-of-Burial (DOB) explosion series at the phosphate quarry Oron, Negev. A special technology was used for creation of large cavities (up to 3.5 m) at different depths, to accommodate large near-spherical ANFO charges. Extensive observations in the near-source zone (100-800 m) and remotely (up to 350 km) demonstrated signal characteristics and energy generation features; decoupling factors were estimated.
The design and configuration of the Oron DOB experiment were preferable in design to the previous Balapan DOB experiment (1997): media homogeneity, small aspect ratio (~1), full containment and small separation (~200 m) of the shots. The crossover point of spectral dominance at ~10 Hz for different depth shots, observed at ranges 0.2-230 km, was remarkably consistent with the Mueller/Murphy source model predictions.

15. SUBJECT TERMS
Decoupling factor, DOB experiment, seismic energy generation

16. SECURITY CLASSIFICATION OF:			**17. LIMITATION OF ABSTRACT**	**18. NUMBER OF PAGES**	**19a. NAME OF RESPONSIBLE PERSON**
a. REPORT	**b. ABSTRACT**	**c. THIS PAGE**			Robert J. Raistrick
UNCLASSIFIED	UNCLASSIFIED	UNCLASSIFIED	SAR	83	**19b. TELEPHONE NUMBER** *(include area code)* 781-377-3726

Table of Contents

Figures

Tables

Acknowledgments

Many individuals and organizations contributed to the success of the project explosion experiments. Special thanks to A. Dainty for useful discussions before and after the experiments. We are thankful to B. Hayoun of Tamar Ltd., Y. Levi and U. Yassur of Rotem Amfert Negev Ltd. for their crucial role in preparation and conducting the explosions of special design with near-spherical charges. Y. Ben-Horin of Israel NDC provided excellent records of the Oron DOB experiment by a portable tripartite array. The staff of the Geophysical Institute of Israel performed technical support throughout the project: preparation of measuring equipment and computer procedures, portable observations during the experiments, data processing and analysis - thanks to U. Peled, M. Kalmanovich, N. Perelman, H. Dan, M. Ezersky, A. Polozov, V.Giller, L. Feldman, A.Shvartsburg, Y.Lifshitz.

1. SUMMARY

The project was focused on studying, experimentally, features of seismic energy generation and partitioning of P and S waves from different explosive seismic sources, at near-source and regional distances, in the time and spectral domains. An extensive database of Ground Truth single-fired explosions was created, presenting a broad variety of design features (buried and surface sources, tamped and decoupled shots, explosions in large diameter 0.5-0.8 m boreholes, and near-spherical cavity charges), charge weight (100-32500 kg), depth (14–62 m), scaled burial depth (1.0-3.9 m/kg$^{1/3}$), emplacement rocks (alluvium, basalts, marls) and geological settings.

We have conducted several series of single-source contained explosions, of a special design, simulating nuclear test conditions: short charges in large diameter boreholes and near-spherical charges of different yields and depths. Two explosion series with different charge weight in the range 0.3-32.5 tons, placed in large diameter boreholes, were conducted in different geological environments: soft sediments (alluvial conglomerates) in the Negev desert in the South (Sayarim Valley) and hard basalt rocks in the Galilee region in the North (Beit-Alpha quarry), different types of explosives (ANFO and TNT) were used.

Source scaling estimations based on BB records at local distances of the Sayarim series showed similar yield scaling parameters (0.87-0.93) for different regional phases. The power law parameter values were found to be in close agreement with the constants for nuclear explosions in Nevada and chemical explosions in Wyoming.

The highlight of this project was source phenomenology experiments: Decoupling and Depth-of-Burial (DOB) explosion series at the phosphate quarry Oron, Negev. A special technology was used for creation of large cavities (up to 3.5 m) at different depths, and accommodation of large near-spherical ANFO charges. A high seismic efficiency of this explosion design provided a broad recording range from relatively small experimental shots. Extensive observations in the near-source zone (100-800 m) and larger distances (up to 350 km) demonstrated the signal characteristics and energy generation features; decoupling factors were estimated.

The design and configuration of the Oron DOB experiment, providing the first DOB data in the Middle East) were preferable in experiment design to the previous Balapan (Kazakhstan) DOB experiment (1997): media homogeneity, small charge aspect ratio (~1), full containment and small separation (~200 m) of the shots. An important goal of our experiment was to eliminate the asymmetry effect caused by the difference of lithostatic pressures between top and bottom of a vertical cylindrical explosive source, typical for borehole chemical explosions, and to study the generation of shear waves for spherically symmetric sources, typical of nuclear tests.

An important effect observed for near-source accelerometer records was a clear trend of the signal peak amplitude and energy enhancement with increase of charge depth. This effect was accompanied by a significant increase in signal frequency, providing empirical verification and estimation of decreasing seismic source size due to increase of overburden lithostatic pressure. High frequencies of the radiated signal resulted in rapid attenuation of seismic energy with distance, and a clear expected tendency of signal energy and magnitude reduction with depth is observed at regional distances. Analysis of seismic waveforms (in the broad band 1-20 Hz) at close local and regional distances (3.5-

240 km) demonstrated a clear decrease of peak amplitude and energy for S-phase and corresponding S/P ratios for deeper shots.

The frequency dependence of spectral amplitudes on shot depth was observed at most stations for both phases in the broad range 0.2-230 km: a decrease of amplitudes with increasing shot depth between about 1 and 10 Hz changes to the opposite trend at higher frequencies ~10-20 Hz. This dependence and the crossover point of spectral dominance at ~10 Hz are remarkably consistent with the Mueller/Murphy source model predictions specific for the Oron DOB experiment parameters.

Reliable identification of an unknown seismic source and estimation of its parameters, especially Depth-of-Burial and yield, are important tasks in nuclear test monitoring. The yield estimations are based mainly on seismic magnitude, correlated with energy of the recorded signals, which can depend also on source rock media, coupling conditions and the DOB. Therefore the knowledge of relationships between buried explosion source parameters and energy/spectral features of seismic signals at remote stations is crucial, and the explosion experiments conducted present an important contribution of the Geophysical Institute of Israel (GII) to improvement of nuclear test monitoring.

1. INTRODUCTION

This section provides some background and introductory material. In Section 3 we present the instrumentation, methods and procedures used to perform experimental explosions, carry out near-source and regional observations, and provide the required processing of seismic signals. Section 4 contains descriptions of the explosion series conducted, data obtained, processing and analysis of records, and discussion of results. Concluding remarks are presented in Section 5.

To improve nuclear test monitoring related to identification of seismic sources and estimation of source parameters, we should better understand earthquake and explosion phenomenology. Understanding the main features of seismic energy generation from point-source (explosion) and distributed (earthquake, quarry blast) sources, and the partitioning of energy between P and S waves, provides a basis for effective event discrimination tools.

The generation of S waves from explosions is still a topic of debate in the seismological literature. There are several physically based theories, including P-to-S conversion at the free surface or crustal interfaces, rock cracking and spall, scattering of short-period surface waves (Rg), and tectonic release (e. g. Vogfjord, 1997, Day and Mclaughlin, 1991, Myers et al., 1999, Wallace et al, 1985).

Determination of accurate regional magnitude-yield relationships (Khalturin et al., 1998) and dependence of signal features at regional distances on source depth, based on Ground Truth experimental explosions, contributes to the development of procedures for estimation of seismic source parameters (yield and depth) for clandestine explosions. Based on Israeli Ground Truth data, regional magnitude-yield equations for quarry blasts and underwater shots were developed (Gitterman, 1998). An empirical formula $M=0.285+\log_{10}(W,kg)$ for underwater explosions, based on the Dead Sea experimental explosions (Gitterman and Shapira, 2001), was used to estimate the TNT equivalent charge weight (lower bound values) for the two "Kursk" explosions (Gitterman, 2002).

In the 1997 Balapan (Kazakhstan) Depth-of-Burial (DOB) experiment, three 25-ton explosions were detonated at depths of 50, 300 and 550 m (Leith and Kluchko, 1998). The main objective of this series was to study DOB effects on the excitation of regional phases, and important data and results were obtained (Glenn and Myers, 1997). Nevertheless, due to circumstances at the experiment site, some conditions of the experiment were not ideal: 1) the rock media were not homogeneous (the shallow shot was deployed in the sedimentary shale subsurface layer, and two deeper shots in granites); 2) the shot spacing (2.5-8 km) provided close to identical ray paths for far-regional stations, however the paths to close local stations were quite different making single station comparison difficult; 3) scaled depth $h=Hc/W^{1/3}$ was 113, 968 and 1823 $m/kT^{1/3}$, while the range for NTS nuclear tests was $h=95\text{-}425\ m/kT^{1/3}$ (Springer et al., 2002); 4) the explosions were not fully contained: the 50-m shot created a 40-m crater, for deeper shots the casing was ejected; 5) cylindrical charges with a large aspect ratio (34) were far from spherical, as nuclear sources are. For a long vertical source the decrease in pressure at shallow depth causes much stronger non-linear deformation above the explosion than below it, and this asymmetry results in direct generation of shear waves, which would not be generated by purely spherical sources (Stevens, 2006).

Near-spherical charges (~1 ton) were used in the Rotem single-fired multiple-source calibration 25-ton explosion conducted by the GII (Gitterman et al., 2002). A special experimental design and technique were applied, creating cavities of ~1 m size in holes at a depth ~14 m, used for accommodation of explosives. This approach provided a basis for realization of an improved DOB experiment with more ideal conditions.

Recently NORSAR recorded several decoupled chemical explosions in large chambers of underground mines in Sweden (Stevens et al., 2003), however a reference (tamped) shot was not conducted. Lack of reference data did not allow comparison of signals from decoupled and coupled explosions and direct estimation of the decoupling effect. Application of the technique described above may improve the experiment conditions.

Reliable identification of a suspected seismic source and estimation of its parameters, especially Depth-of-Burial and yield are important tasks in nuclear test monitoring. This importance was demonstrated recently after the North Korea test in October 2006, which invoked debates on its nature, chemical or nuclear, and controversial estimations of the yield, from data at regional seismic stations. The yield estimations are based mainly on seismic magnitude, correlated with the energy of recorded signals, which depend also on source rock media, coupling conditions and the DOB. Therefore the knowledge of relationships between buried explosion source parameters and dynamic features of seismic signals at remote stations is crucial for improvement of nuclear test monitoring.

2. TECHNICAL APPROACH

3.1. Special Charge Design of Experimental Explosions

In developing the charge design for the project for buried experimental explosions we tried eliminate the large aspect ratios representative of long cylindrical charges in small diameter boreholes, thus providing seismic sources more similar to the spherical nuclear sources we wanted to model. Two design techniques were chosen: 1) short cylinder charges in large-diameter boreholes; 2) near-spherical charges in specially created cavities. The first method, more simple technically but more expensive, was used in the Sayarim (Southern Israel) charge weight explosion series in dry alluvium (2004), and the Beit-Alpha (Northern Israel) charge weight and type of explosive series in weathered basalt rocks (2005). The second design, more complicated, but cheaper, was applied to the Decoupling (2006) and Depth-of-Burial (2007) Experiments at Oron phosphate quarry (Northern Negev desert) (Figure 1).

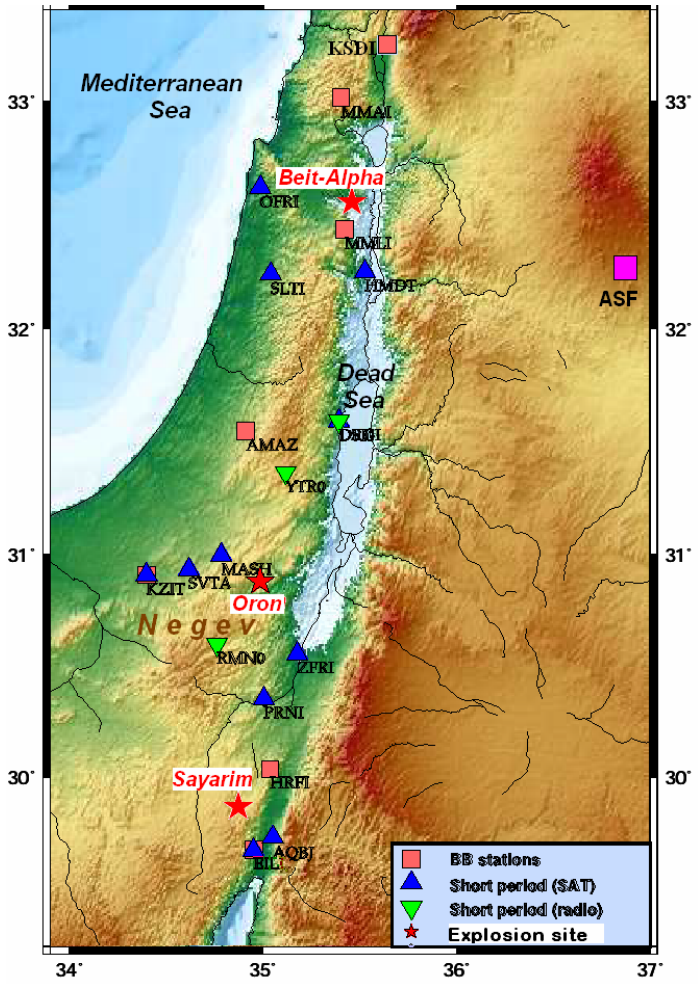

Figure 1. Map of explosion sites and permanent seismic stations that recorded signals.

3.1.1. Large-Diameter Boreholes

Sayarim Experiment. A Micropile machine with a drilling head of maximum diameter 60 cm was used for drilling in non-consolidated soils. A total of 13 boreholes were prepared with depth varying from 17 to 20.5 m (mostly ~20 m) (Figure 2a). An enlarged variable diameter of 60-80 cm was realised for all holes due to crumbling of the borehole inner walls (see Figure 2b), that allowed us to reduce the charge length. Heavy cardboard casing tubes were installed in the upper part of drilled boreholes (Figure 2c) to prevent collapse of loose rocks and provide safety for people.

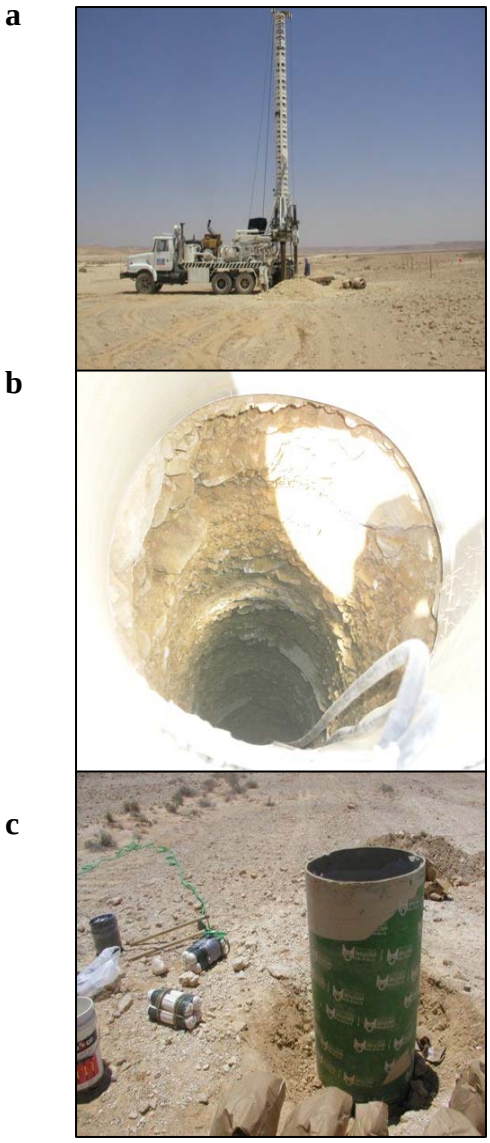

Figure 2. Micropile machine (a) provided boreholes of large variable diameter 60-80 cm in loose alluvial conglomerates (b), that required casing installation (c).

Beit-Alpha experiment. A special machine was used with a drilling head of maximum diameter 50 cm intended for drilling in hard basalt rocks (Figure 3a). A total of 24 boreholes were prepared under very heavy drilling conditions with depth varying from 14 to 16 m (maximum for this machine). An enlarged variable diameter of 55 cm was realised for many holes due to crumbling of the borehole inner walls (see Figure 3b), that allowed us to reduce the charge length.

a **b**

Figure 3. Special drilling machine (a) provided boreholes of large variable diameter 50-55 cm in hard basalt rocks, fractured in the upper part (b).

The calculated aspect ratio for all charges in large diameter holes did not exceed 10-15.

3.1.2. Near-Spherical Charges in Cavities Beforehand Created

A special design and technology were utilized, developed by Rotem Amfert Negev Ltd. and Tamar Advanced Quarrying Ltd.: deployment of explosives in a cavity, created beforehand by a series of small shots, thus forming near-spherical sources. The technology includes checking the inner configuration and size of a cavity created after a preliminary small shot by a GeoVISION borehole camera with an attached meter stick and monitoring video-recorder (Figure 4). Small diameter (~6.5 inch) boreholes are used, with rather cheap drilling. The hole of a preliminary shot is not stemmed, causing ejection of gases, crushed rocks and dust over ~20-30 sec (Figure 5). Successive detonations of specified charges provide enlargement of the cavity to the necessary size.

This approach was applied in two Source Phenomenology Decoupling and Depth-of-Burial Experiments, conducted at the Oron phosphate quarry, and after numerous trial shots cavities of ~3-3.5 m size were created in marl rocks at a depth of up to 63 m, allowing accommodation of ANFO charges ~5 tons and more.

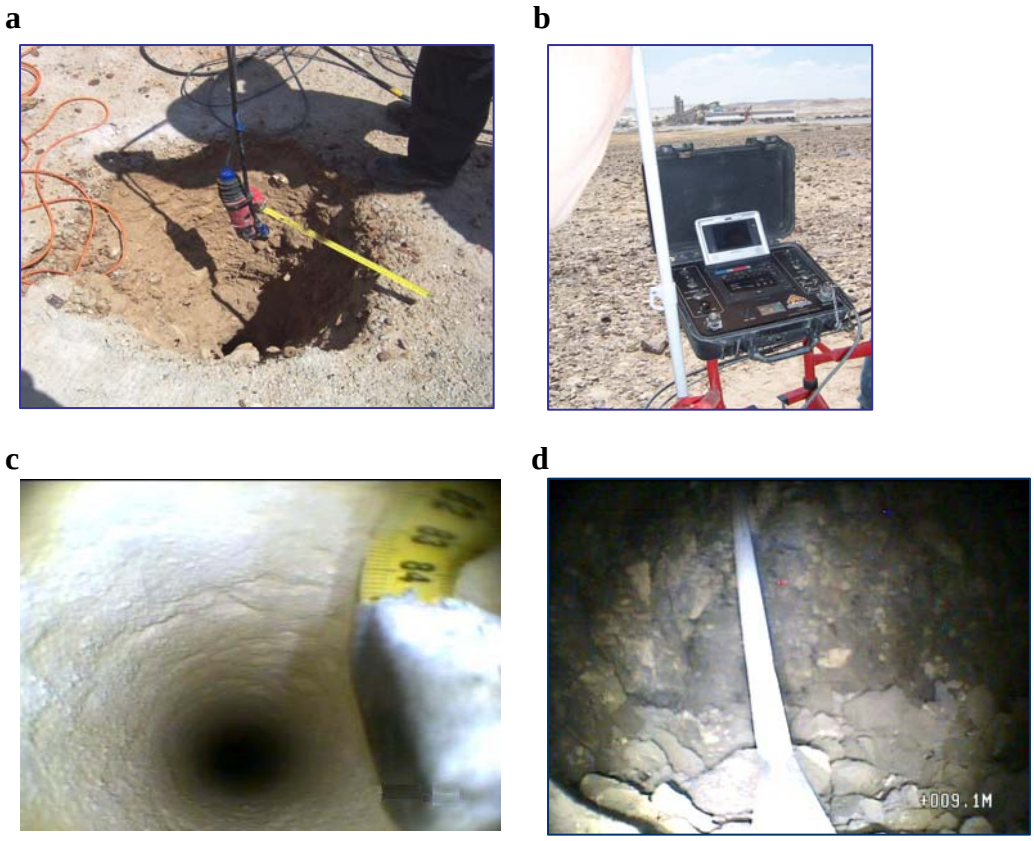

Figure 4. GeoVISION borehole camera with attached meter stick and special lighting (a), and monitoring video-recorder (b), used for checking a small diameter borehole before a preliminary small shot (c), and testing inner configuration and size of a cavity created after the shot (d).

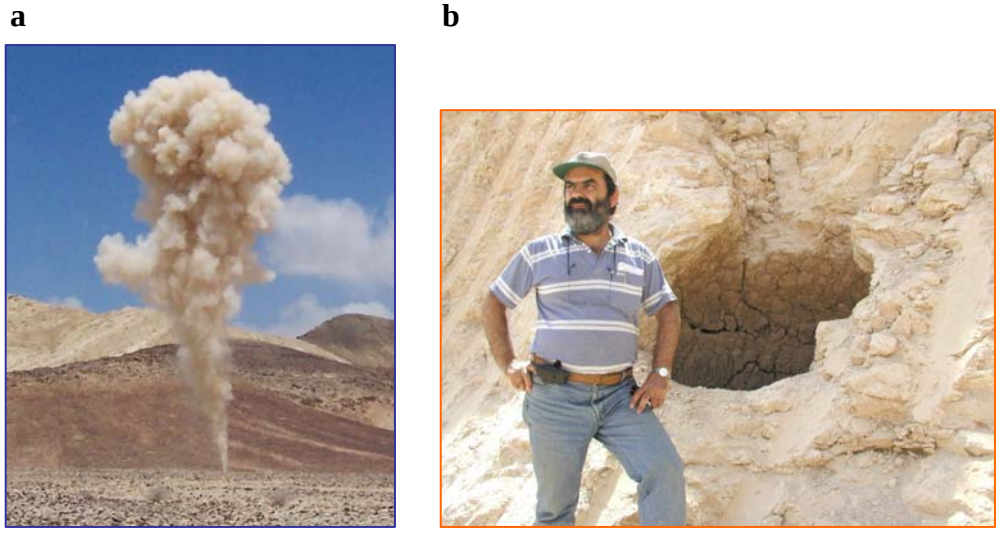

Figure 5. Ejection of gases, crushed rocks and dust during a preliminary shot for creation of a cavity, the shot hole is not stemmed (Oron quarry, 2006) (a); a sample cavity (d~1 m) revealed by an excavator (Rotem quarry, 2002) (b).

3.2. Recording Equipment and Data Acquisition System

Near-source seismic observations. A number of portable instruments were installed during the explosion series to investigate waveforms and spectral features of radiated seismic waves at close distances:

- 9-10 accelerometers (ETNA and K2) in the near-source zone at distances of 100-900 m, sampling rate 200-250 sps, with a flat observation frequency range of 1-100 Hz;
- five 3C short-period (SP) seismic stations (seismometer L4C, f_0~1Hz) at distances 0.6-17 km, sampling 200 sps, frequency range 0.5-50 Hz;
- three 3C engineering seismic sensors BlastMateIII, deployed near sensitive quarry structures at distances of 500-1000 m, for monitoring ground vibrations after each explosion (used only in the Decoupling Experiment).
- tripartite array of SP vertical seismometers with a central 3C element (Lennartz, f_0~1Hz,) at 24 km, sampling 200 sps (deployed, at our request, by the Israel NDC team, headed by Dr. Y. Ben-Horin, during the Oron DOB experiment).

All recording systems were equipped with GPS devices providing accurate times. The exact detonation time was measured by a PC-based GPS system, with a vertical SP seismometer deployed at ~100-300 m from an explosion, for additional Origin Time control. The PC-SDA data acquisition system developed in GII was used for digital recording of seismic signals at portable seismic stations.

a **b** **c**

Figure 6. Sample portable deployment of an ETNA accelerometer, Sayarim valley (a), a 3C SP seismic station (L4C) (b) and a sensor BlastMateIII, Oron quarry (c).

Regional Observations. We collected all available recordings at permanent seismic stations in Israel and Jordan (see Figure 1):

- SP vertical and 3C stations of the Israel Seismic Network (ISN) (seismometer L4C, f_0~1Hz), sampling rate 50 sps, flat observation frequency range 0.5-12.5 Hz; the Network was triggered manually a few minutes before each experimental explosion, using the ISDA data acquisition system developed in GII;
- SP vertical stations of the Jordanian Seismic Network (JSN) - only the largest Sayarim borehole explosion (32.5 tons) at the single station AQBJ - also Oron Decoupling and DOB explosions;
- 5 Broad-Band (BB) Israel Cooperating National Facility (CNF) stations (HRFI, KZIT, AMAZ, MMLI, KSDI) equipped with STS-2 seismometers and Quanterra data loggers, sampling rate 40 sps, useful frequency range 0.5-20 Hz;
- 3 stations of the International Monitoring System (IMS): 3C stations EIL and ASF (Jordan), and seismic array MMAI (AS49) at Mt. Meron, sampling rate 40 sps, useful frequency range 0.5-20 Hz (Figure 7).

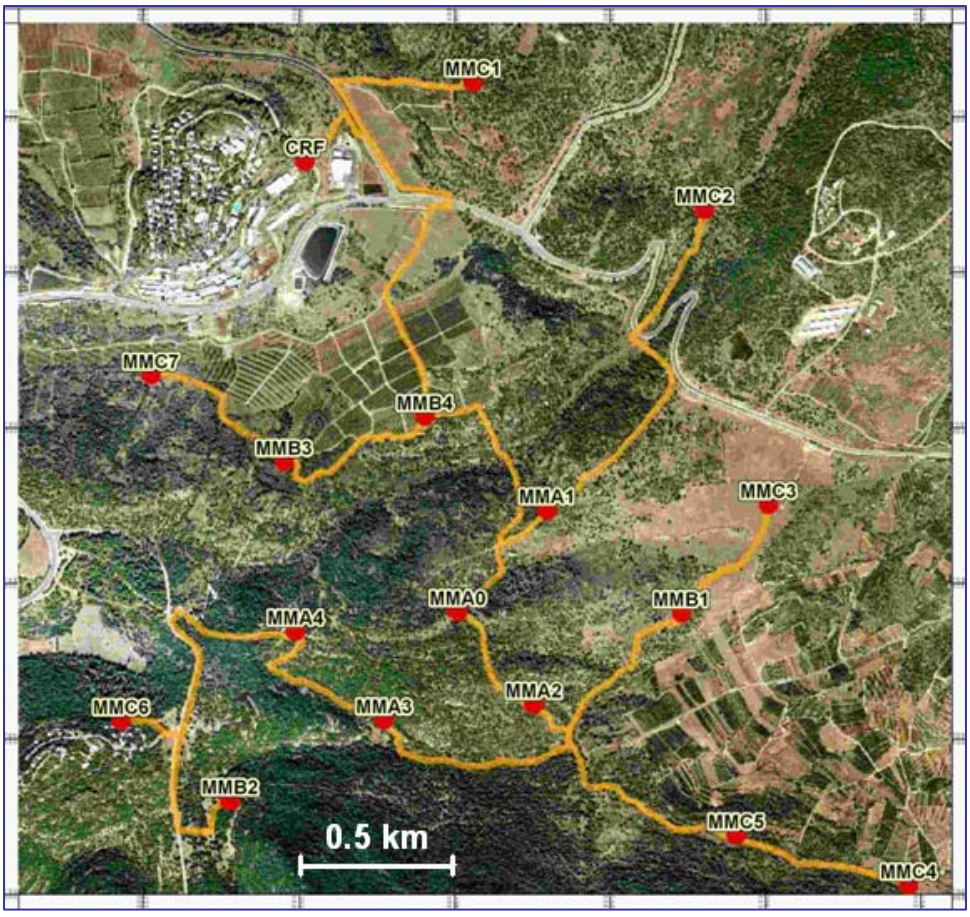

Figure 7. Seismic Array MMAI (AS49) of IMS at Mt Meron, Israel.

3.3. Software Used for Data Processing and Analysis

Existing GII software for visualization and preliminary processing of accelerograms and seismograms was modified and adapted for the project goals, including SEISPECT (analysis of spectra and spectral ratios), and jSTAR (waveform analysis of different data formats). Appropriate software for the S/P amplitude and energy ratios estimation was also developed.

3.3.1. SEISPECT Procedure

The GII newly-developed (by N. Perelman) software SEISPECT was utilized for visualization and preliminary processing of near-source observations of accelerometers ETNA and portable seismic stations. The program, created in the PC-Windows environment using the MATLAB platform, was modified to read ETNA source records in format *.evt, and compute FFT spectra and spectral ratios (Figure 8).

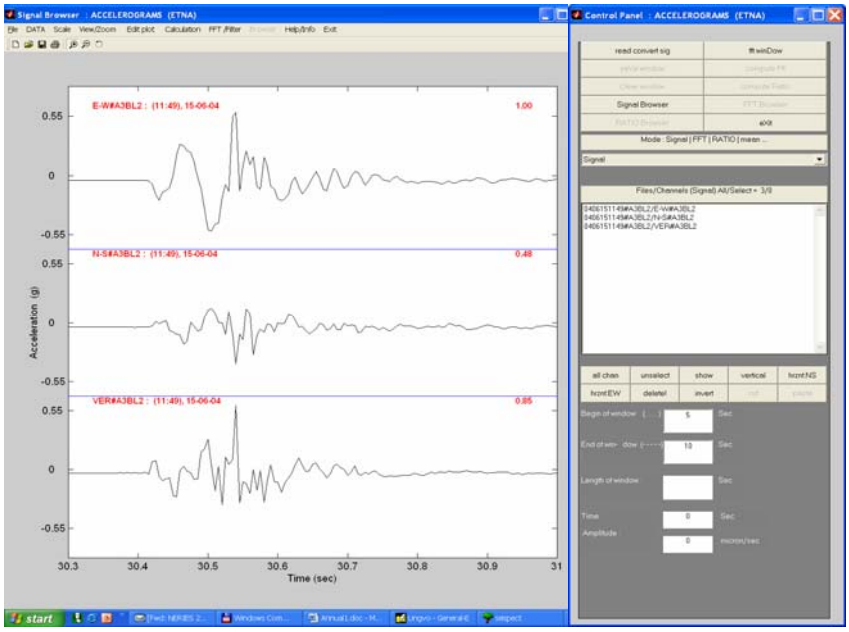

Figure 8. Graphic interface of SEISPECT program reading an ETNA accelerogram from a Sayarim explosion of 2 tons.

3.3.2. jSTAR Software

For visualization and preliminary processing of all data from seismic stations collected with different formats, we applied the newly-developed software jSTAR (former AIST and jSEIS) (by A. Polozov and V.Pinsky, GII). The program was modified to read data from the short-period stations of Israel (format *.dta) and Jordanian (format *.gse) networks, and broad-band stations (formats SEED and SAC), and provide joint visualization and analysis of waveforms from a single event in different record formats (Figure 9):

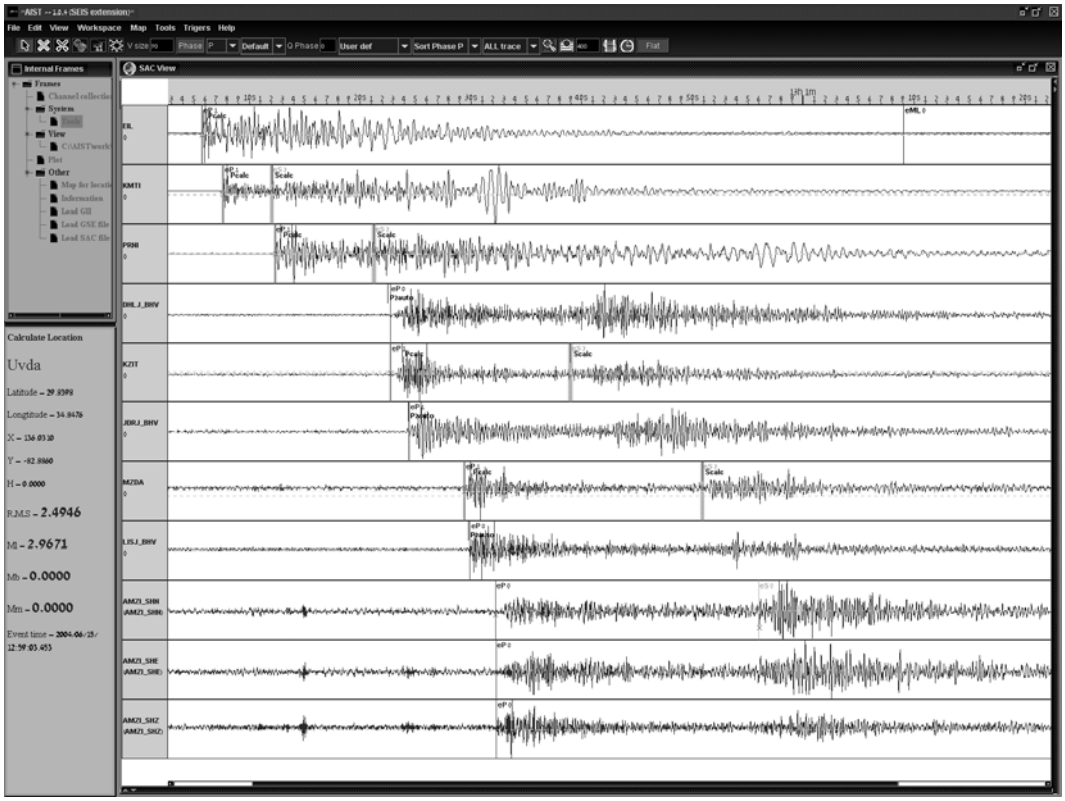

Figure 9. jSTAR interface including regional waveforms of the largest Sayarim explosion 32.5 tons recorded in different formats at ISN stations (format *.dta), JSN stations (*.gse) and BB station AMZI (format SAC).

During the project significant new features were incorporated in the software: transformation of the ground motion components, spectral and sonogram analysis of seismic and infrasound signals, calculation of energetic statistics for recorded waveforms in the time and frequency domain.

Transformation of the Ground Motion Vector Components. In order to enhance the manifestation of S-waves, Rg, and Lg regional phases in observations from different sources, and following estimation and analysis of seismic energy partitioning, the procedure was added of transformation of ground motion standard vector components – Vertical, North-South and East-West (Z, NS, EW) – to Vertical, Radial and Transversal (Z, R, T). The radial direction is chosen automatically if the source location is known (in a phase file loaded together with the waveform data), or assigned from manually inserted source coordinates.

Spectral and Sonogram Presentation of Signals. Procedures of spectral analysis in jSTAR were modified and improved to provide joint analysis and interpretation of amplitude spectra from several stations for a fixed event, or from different events at a specific station. A sample of the procedure is presented in Figure 10. Processing options include a variety of smoothing options (convolution, filter, average) and plot parameters that can be selected in interactive windows.

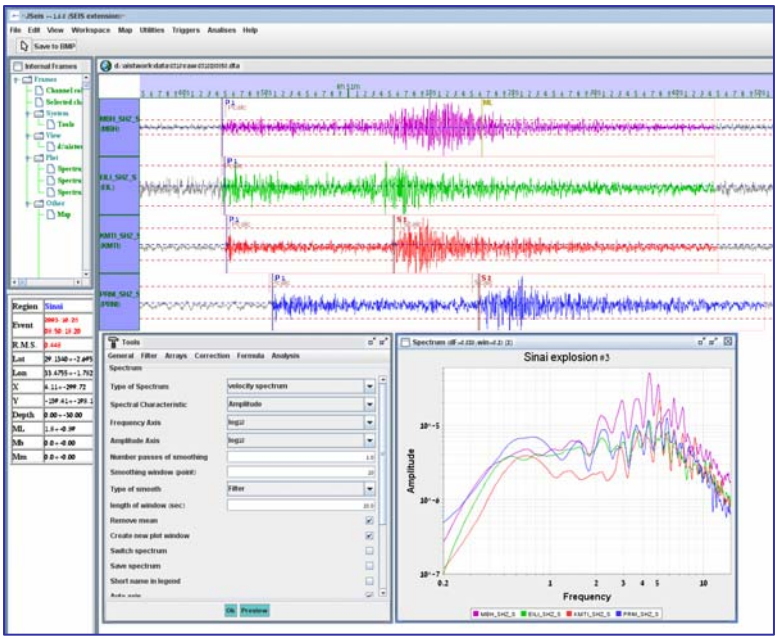

Figure 10. jSTAR interface for spectral analysis of regional waveforms from an explosion (Sinai). Selected time windows (60 s) are shown on the seismogram.

Another type of spectral analysis was included in the jSTAR software – two-dimensional time-frequency presentation of signals known also as a sonogram. This analysis can be useful for characterization of seismic signal energy changing in time, i.e., for different regional phases, and also for identification of different seismic sources (Figure 11).

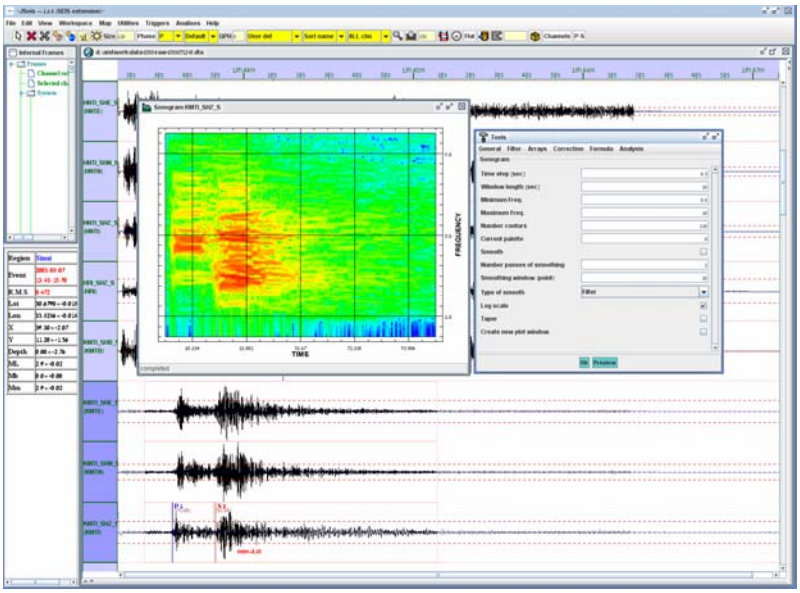

Figure 11. jSTAR interface for sonogram analysis of regional waveforms from an explosion (Sinai) at station KMTI (vertical). Distinct energy distribution in the time-frequency domain for P and S regional phases is clearly presented.

3.3.3. Software for Calculation of Seismic Signal Energy

A number of programs and scripts was developed for calculation of seismic energy of different regional phases observed on seismograms (by V.Pinsky). The processing procedure includes the following elements:

1) Data for each seismic event is given in "dta" format (short-period ISN stations) and SAC format (BB stations). Based on the AIST software interface the data is analyzed and filtered in a specified frequency band.

2) Using the AIST interface data files of an event (with instrument response removed) are transferred from the original formats to special ASCII format files for each channel.

3) Further data processing is accomplished by a shell script using the list of channels of the 3C stations (CICLION3C) and CICLION1C for vertical stations.

4) The CICLION3C script filters each of the channels in the prescribed frequency band.

5) Then the 3C channels of the stations are selected to compute a vector trace:

$$G(t)=[X(t)^2+Y(t)^2+Z(t)^2]^{0.5} \quad (1)$$

For each station in the list.

6) For each station the distance is computed using Cartesian coordinates of the source Xe, Ye, and station Xs, Ys:

$$D= [(Xe-Xs)^2+(Ye-Ys)^2]^{0.5} \quad (2)$$

7) Travel times for the first P and S waves arrivals: $\boldsymbol{TT_p}$ and $\boldsymbol{TT_s}$ are computed according to the local 1D layered velocity model used in GII for routine location by the TTCOMP procedure (by A. Shapira).

8) From the calculated travel times and known origin time T_0 (for the Ground Truth explosions) the theoretical arrival times TA_p and TA_s are computed for each trace: $\boldsymbol{TA=T_0+TT,}$ and constitute the left limit of the analysis windows for P and S phases on the seismograms.

9) The right limit is determined by the length of the window WL, which in the present study was chosen as 2 sec for P and S phases.

10) The surface Rayleigh wave window starts 0.5 sec after the S wave window and ends at twice the travel time for S waves $\boldsymbol{TE= T_0+2TT_s}$.

11) The whole signal window starts at $\boldsymbol{TA_p}$ and ends at $\boldsymbol{TE}$.

12) Seismic wave energy in each of the specified windows – the whole signal window AW, P window PW, S window SW and Rayleigh wave window RW - is calculated:

$$E = \sum_{t \in W} G(t)^2 \quad (3)$$

13) Energy in the specified windows are presented in the table of results as percent % of energy $\boldsymbol{E}$ computed in the whole signal window AW, and in appropriate plots.

3. RESULTS AND DISCUSSION

The results of this project were presented during a series of AFRL reviews and SRR Symposiums in 2004-2006 (Gitterman et al, 2004, 2005a, 2006a), and also placed (in part) on the GII Website: http://www.gii.co.il/html/seis/seis_fs.html. These results are summarized below. Material of more interest to the general seismological community was presented at several international conferences (see Gitterman et al, 2005c, 2006b).

4.1. Sayarim Charge Weight Series

Single-fired experimental explosions of 0.3, 2 and 32.5 tons of ANFO in boreholes were conducted in Sayarim Valley, Israel, providing a series for the yield-dependent analysis of regional waveforms (see Figure 1). The large shot, considered as a calibration shot, was mostly supported by the US AID MERC program (Gitterman et al., 2005b).

Explosion Design and Geological Settings. Geologically the area is a graben filled by Quaternary alluvial conglomerates, underlain by consolidated limestone, chalk and chert rocks. A seismic refraction survey provided a P-velocity estimate Vp~1600-1700 m/sec in the upper layers of soft sediments, and Vp~2000 m/sec in deeper consolidated rocks, evidently chalk (Figure 12a).

Ground Truth parameters of the large-scale buried explosions and a surface military shot are presented in Table 1, while locations of the explosion boreholes is shown on Figure 12b. Explosives were placed in boreholes of large diameter (0.6-0.8 m) with depth of 17-21 m, drilled in dry alluvial sediments (Figure 12a). The large diameter of the hole led to a small linear size of the cylinder charges, approaching a near-spherical configuration and allowed spatial concentration of explosives for the largest shot (only 11 holes for 32.5 tons). Estimated scaled depths $h=H_c/W_e^{1/3}$ ($m/kg^{1/3}$) for equivalent TNT charges are presented in Table 2.

Table 1. Design parameters of Sayarim buried explosions and a surface military shot.

Expl. No.	Total W, ton	Date	Origin time (detonation)	Lat. Long.	Boreholes			Mag. M_L
					No.	Depth H, m	Diam. D, m	
S1	0.3	13.06.04	12:20:01.19	29.842	1	20	0.6-0.8	-
S2	2	15.06.04	11:49:39.35	34.859	1	20		2.0
S3	32.5	15.06.04	13:00:01.49		11	17-20		3.0
S4	10	07.06.04	15:06:28.4*	29.991 34.798*	surface shot in a shallow (~1m) trench			2.5

* estimated from ISN records

Table 2. Estimated equivalent (single borehole) charges and scaled depth.

Ex. No	Single charge W1, kg	TNT equiv. W_e, kg	Charge (center) depth H_c, m	Scaled depth, $m/kg^{1/3}$
S1	300+20 (booster)	262	19.5	3.05
S2	2000 +20	1635	16.5	1.40
S3	3000 +20	2442	15	1.11

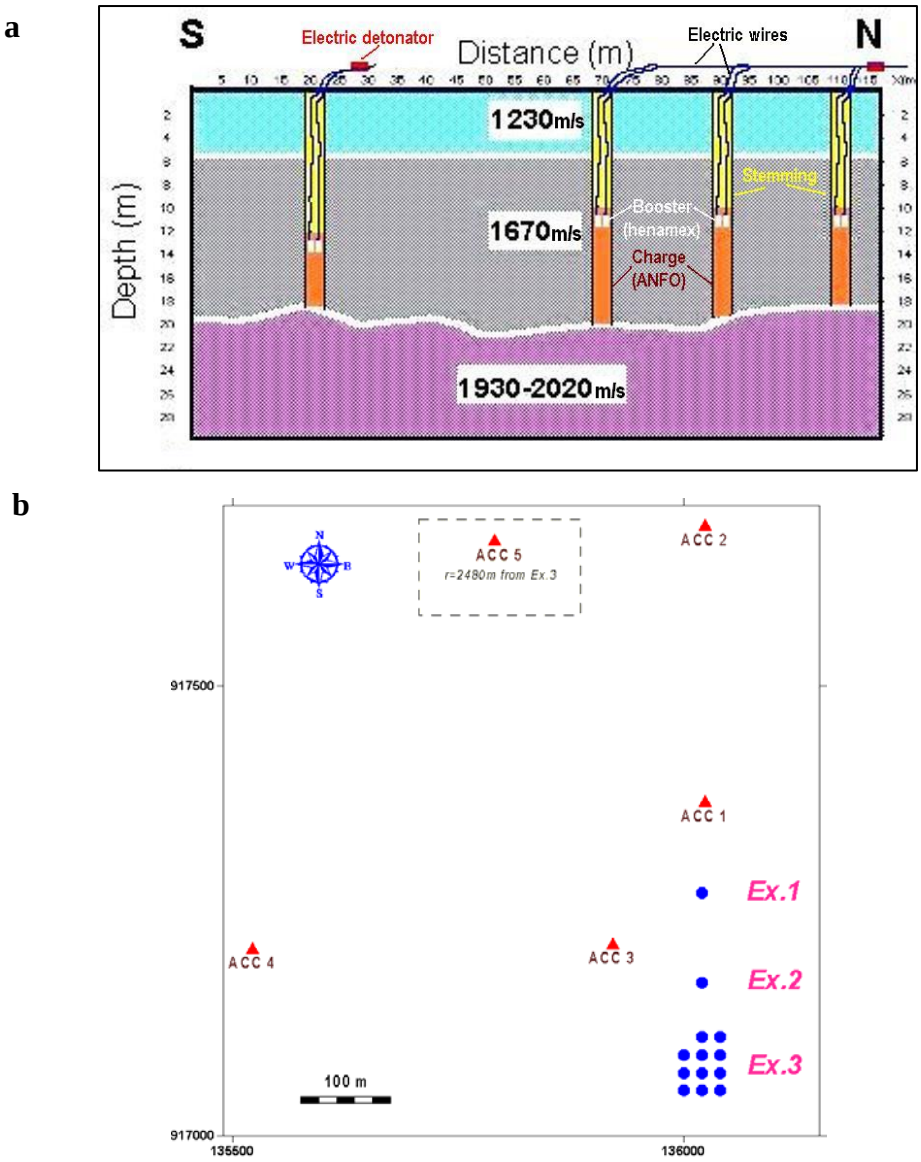

Figure 12. Charge design and accommodation in near-surface layers (a); borehole configuration and location of near-source portable accelerometers ETNA (b).

The two larger shots were not contained. The conditions for this site (hole depth) did not prevent rock spall and energy losses into the air, especially for the largest explosion (Figure 13), and craters were created.

Near-Source Observations. Good waveform records were obtained for the explosion series by portable accelerometers at distances of 100-500 m (Figure 12b), sample records are presented in Figure 14. Seismic source complexity for explosion S3 conducted in 11 boreholes was observed at the closest accelerometer, with two wave groups (separated by ~0.2 sec) found on all three components; the first group is like the signal from single-hole shot S2 (Figure 14). The accelerogram is similar to the data from Lyaur explosions with delayed detonations in multiple rows (Negmatullaev et al., 1999). All 11 charges were detonated simultaneously, but due to hole spacing, a distance difference from the closest

Figure 13. Sayarim buried explosions: (a) ground uplift for the 2-ton shot (video snapshot ~1 sec after detonation); (b) view of the largest explosion 32.5 tons.

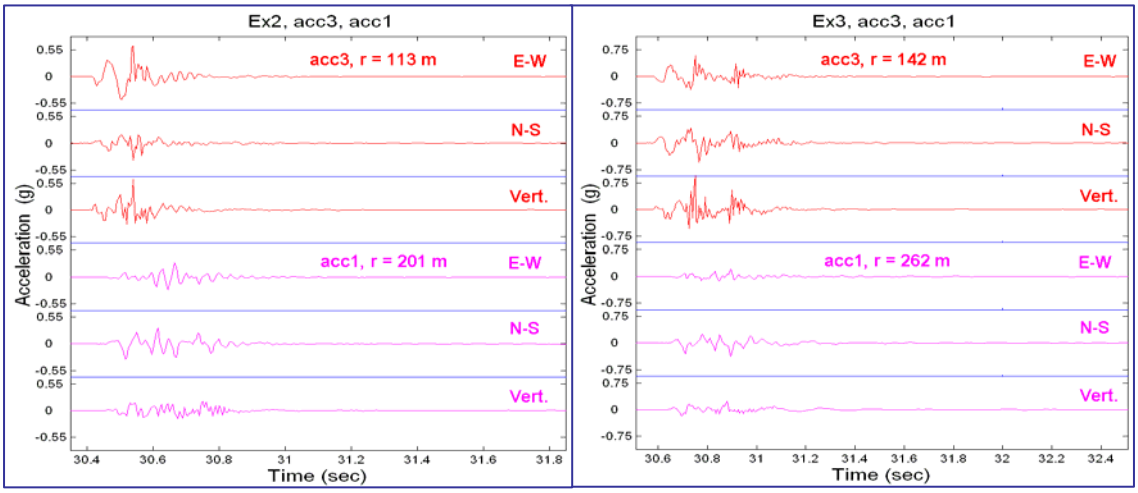

Figure 14. Acceleration waveforms for a single-hole shot S2 (left) and multiple-hole explosion S3 (right) of the Sayarim experiment.

and remotest charges to station ACC3 was ~60-70 m, and the time shift could reach ~0.2 sec (assuming S-wave velocity ~300-350 m/s).

We estimated attenuation of the vector and vertical component with distance *r*. The maximum vector of Peak Ground Acceleration (PGA) was calculated as**:**

$$PGA_{vector} = (PGA_{EW}^2 + PGA_{NS}^2 + PGA_{vert}^2)^{1/2} \quad (4)$$

The data are fit with the power relation:

$$PGA_{(cm/s^2)} = a * r_{(m)}^{b} \quad (5)$$

Similar attenuation parameters b_i were obtained for all three explosions (Figure 15a). Therefore we applied an average fixed value $b = -1.74$ for the 3 shots to estimate the scale coefficients a_i, and used them for yield scaling parameter estimation. The results showed that in the near-source zone peak accelerations (both vertical and vector) increase roughly as the square root of the charge weight W:

$$PGA \sim W^{0.58} \quad (6)$$

Using the scaled distance $R=r/W^{1/3}$ reduced but but did not remove the difference of the three attenuation lines (Figure 15b). (To compute R for the multiple-hole shot S3, we used the closest hole charge W_e, instead of the total weight of the explosive ANFO). The divergence for the three Sayarim shots is due to different scaled depth (Table 2), and contribution of more than one hole charge for the multiple-hole S3 explosion.

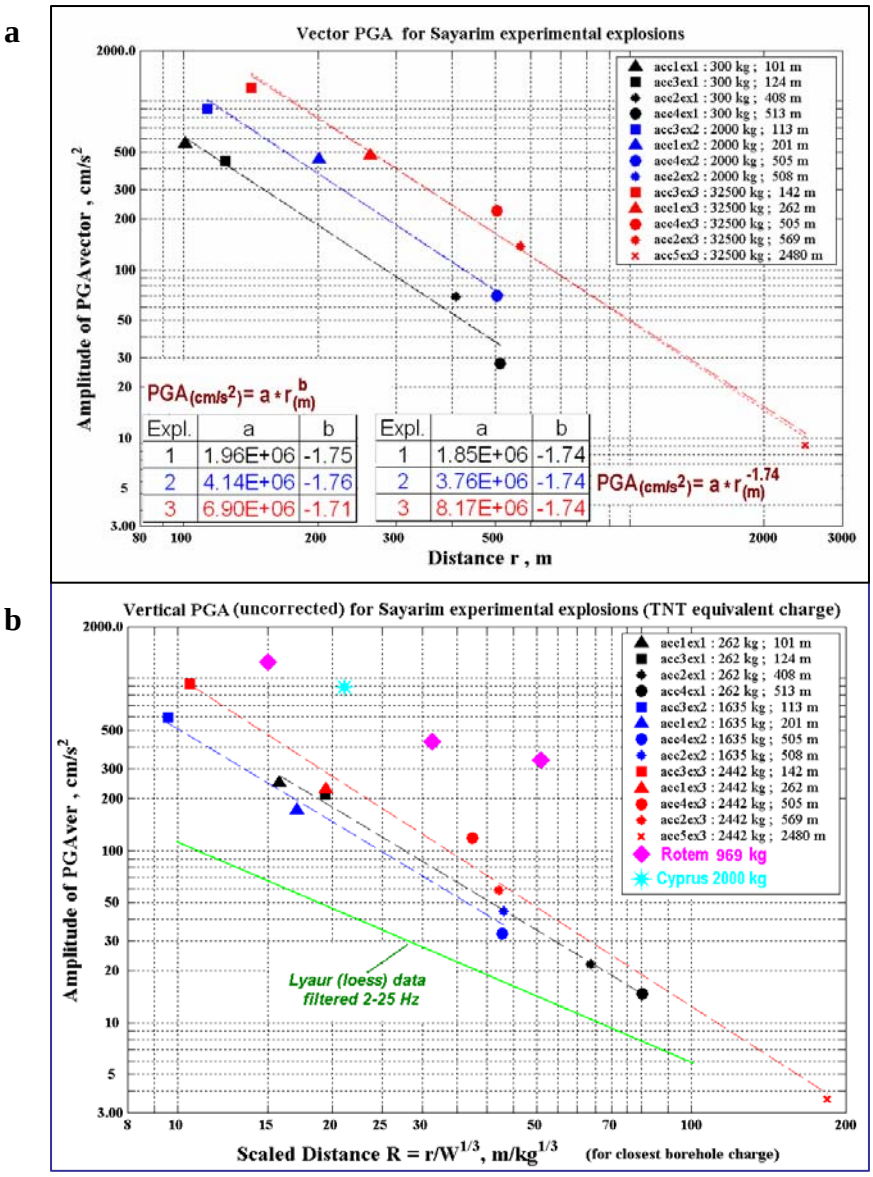

Figure 15. (a) PGA vector attenuation versus distance; (b) attenuation of the vertical peak acceleration vs scaled distance for different shots and geological settings.

The amplitudes for the Sayarim shots in dry alluvium/conglomerats are higher than for Lyaur explosions in loess (Negmatullaev et al., 1999), and lower than for explosions in consolidated sediments (Rotem kaolins) (Gitterman et al., 2002) and hard rock (Cyprus diabases) (Gitterman et al., 2004) conducted by GII.

Peak Amplitude Scaling at Close local Distance. All three Sayarim explosions were well observed at IMS BB station EIL (r~21 km), providing data for the source-scaling analysis (Figures 16, 17). Inspection of observed waveforms on 3C records (Figure 17a) identifies regional phases Pg, Sg and Rg (surface waves). First arrival of Rg, carrying most of the signal energy, can not be distinguished due to the small distance range, the Rg group velocity is estimated as 1.0-1.3 km/sec.

a **b**

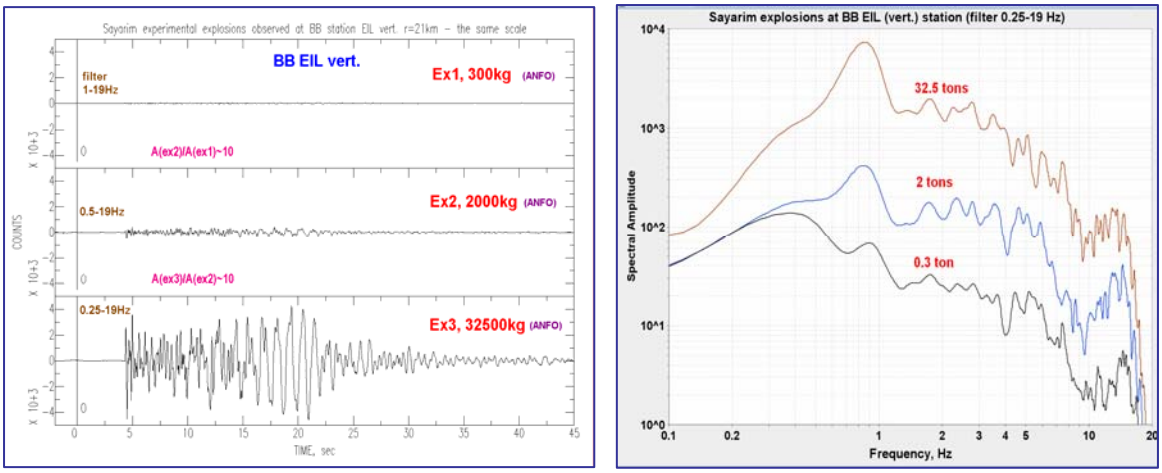

Figure 16. Vertical records (in absolute scale) of Sayarim shots at EIL, the TIME axis starts at the detonation moment (a), spectra showing low-frequency energy (0.5-1.5 Hz) of radiated signals (b).

Vertical Peak Amplitudes (VPA, micron/sec) were measured for each of the phases and plotted against charge weight for shots S1-S3 (Figure 17b). TNT equivalent charges were used (Table 2) and for the multiple-hole explosion S3 the total charge was used.

a **b**

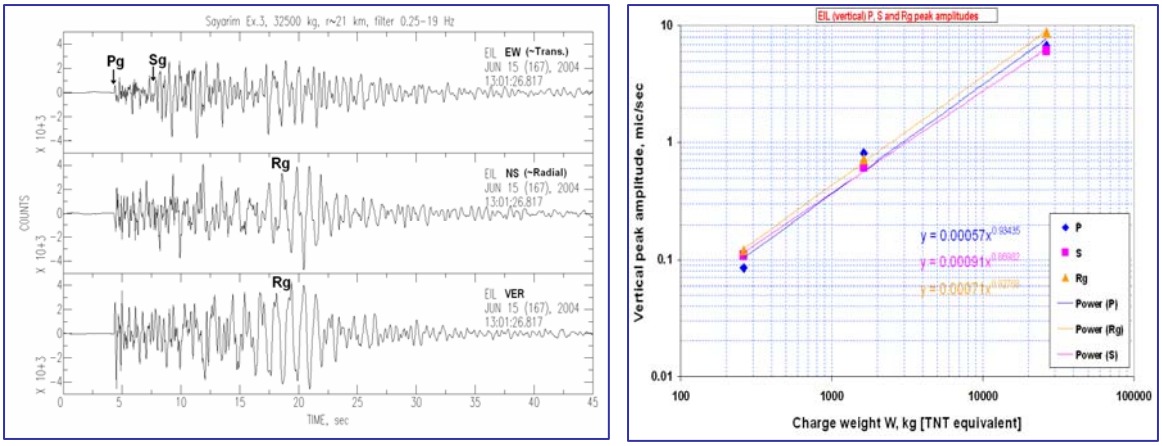

Figure 17. Observed wave phases at close local distances (station EIL) (a), used for source scaling analysis, based on peak vertical amplitudes of the phases (b).

The data for each phase are fit with the power equation:

$$VPA_{(mic/sec)} = A * W_{(kg)}^{B} \quad (7)$$

The r.m.s. procedure provided estimates of *A* and *B* for each of phases Pg, Sg and Rg (see Figure 17b); similar power law scaling parameters were determined for each of the dominant regional phases.

Power law fits to each phase shows little difference between the source yield scaling parameter *B* for the different phases: P (0.93), S (0.87) and Rg (0.93). The *B*-values obtained are in close agreement with the scaling parameter of Vergino and Mensing (1983) for Pn waves from nuclear explosions in Nevada, and Stump et al. (2003) for Pn, Pg, and Lg regional phases (0.84-0.91) from chemical explosions in Wyoming. The *A* value depends on distance and site conditions and for the station considered (EIL) is comparable for all three phases, similar to estimations of Stump et al. (2003) for Pg and Lg phases.

Low frequency signals were radiated from the charges in soft sediments (see Figure 16b), resulting in low attenuation of seismic energy. As expected, for the large explosion of 32.5 tons clear regional seismic phases were observed at the remote IMS array AS49 (Mt. Meron) at distance of ~350 km (Figure 18).

a **b**

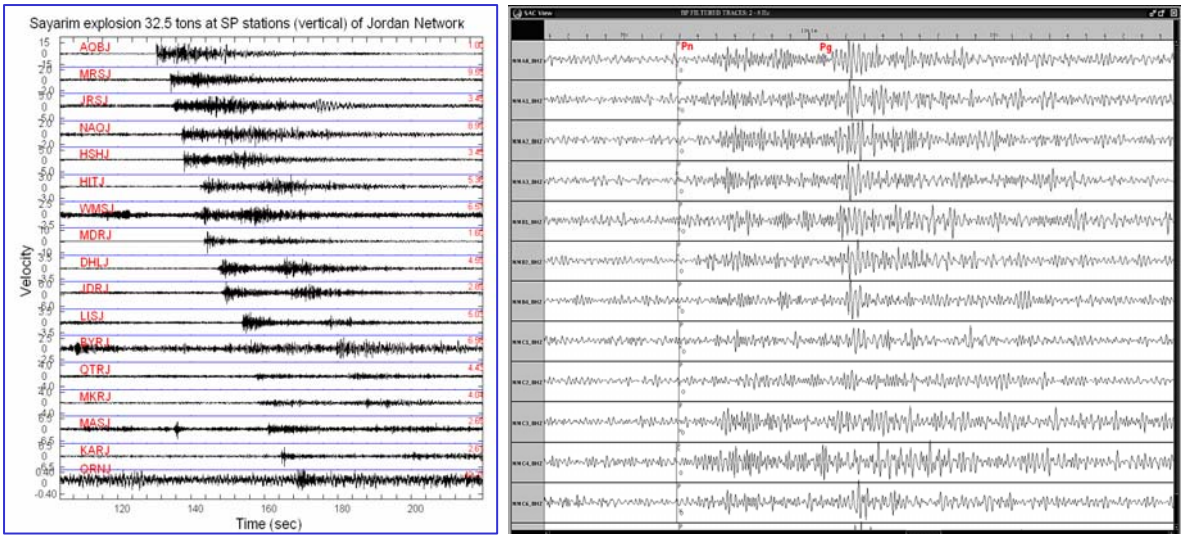

Figure 18. Seismograms of the largest Sayarim explosion of 32.5 tons (ANFO) recorded at seismic stations of Jordan network at distance range 22-285 km (a), and at IMS array MMAI (AS49) at 350 km, BP filtered 2-8 Hz (b).

S/P Maximum Amplitude Ratios in Different Frequency Bands. Different amplitude and spectral ratios for different wave phases are used for discrimination purposes (see e.g. the review of Blandford, 1995, and more recent research of Walter et al., 2004). We analyzed the S/P maximum amplitude ratio in different frequency bands,

using the software developed (Kurpan, 2004) based on the SEISPECT program. For the case study we used data from the three Sayarim charge weight series of buried explosions and a nearby military surface shot of about 10 tons of old ammunition (see Table 1). Seismograms at ISN vertical stations were filtered in three bands: 0.5-3 Hz (low filter), 3-6 Hz (medium filter) and 6-9 Hz (high filter), and maximum amplitudes were measured in windows 3-5 sec after P and S arrivals. A broad filter (0.5-12 Hz) including the whole recording frequency range is also used in the analysis.

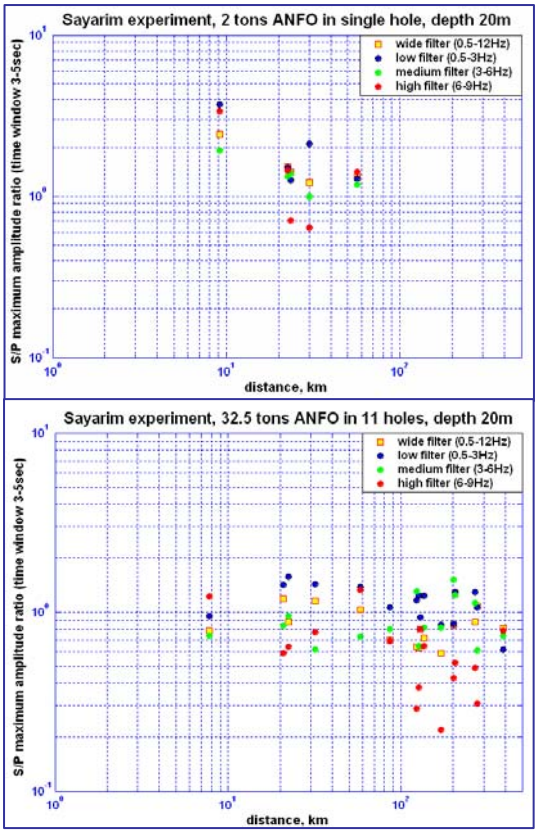

Figure 19. S/P ratios vs distance for different SP ISN stations from shots S2 (top) and S3 (bottom).

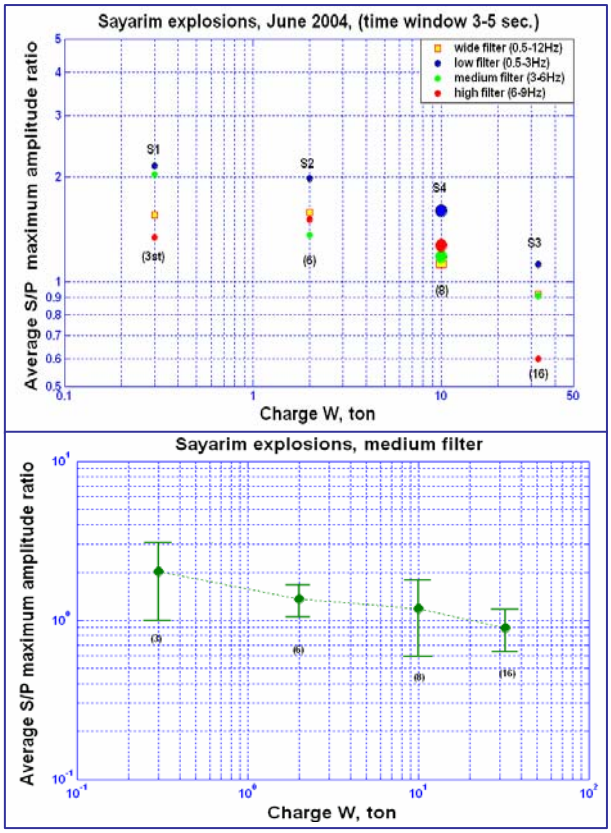

Figure 20. S/P ratios vs charge averaged for ISN stations (top); mean and standard deviations for the medium filter (3-6Hz) (bottom). Number of stations (in parentheses) is shown.

The S/P maximum amplitude ratios for different ISN stations presented in Figure 19 do not manifest a clear dependence on distance and frequency band. If the ratio values for a fixed shot are averaged over the stations, then two obvious tendencies can be observed: a decrease with charge (especially for low and medium filters) and higher ratios for lower frequency band (Figure 20). Note that the explosion S4 of 10 tons TNT on the surface is consistent with the three borehole ANFO shots located in the same area.

This S/P parameter shows a potential for identification of explosion seismic sources and discrimination between earthquakes and explosions, and will be tested on other explosions and earthquakes.

4.2. Sayarim Surface Military Detonations: Ground Truth and Record Collection

GT0 data and records for 13 explosions were collected in May-June 1998 during a joint experiment of the Israel Defense Forces (IDF) and the US Army Corps of Engineers at the Sayarim military range (Gitterman et al., 2001). The point-like single charges in the range of 215-2200 kg with different configurations and explosive composition (TNT, ANFO and Khanit) were detonated on the ground surface (Lat 29.9378ºN, Lon. 34.8185ºE). A similar explosion series of half-spherical charges at about the same site (Lat. 29.95429ºN, Lon. 34.82911ºE) was conducted in October 2003, we collected data for three shots (Figure 21, Table 3). A significant feature of all the shots was that the charges consisted of pure explosives of exactly known weight.

To extend the observation distance range for surface seismic sources we used data from nearby large explosions (4.5-8.5 tons) to destroy outdated ammunition. We visited the explosion site (Lat. 29.99140ºN, Lon. 34.80469ºE) on December 6-7, 2005, observed and collected Ground Truth Information for three shots placed on the ground surface and open to the air (Figure 22). Equivalent TNT charge weight was estimated allowing for shell casing and different explosive type (Table 3).

We measured detonation time and recorded seismic and acoustic waves by near-source portable seismic stations. A low-frequency infrasound sensor (Chaparral 2) was installed in 2005 at Zofar village at 73 km range; high-quality signals were observed that will be used in future research (Figure 21b).

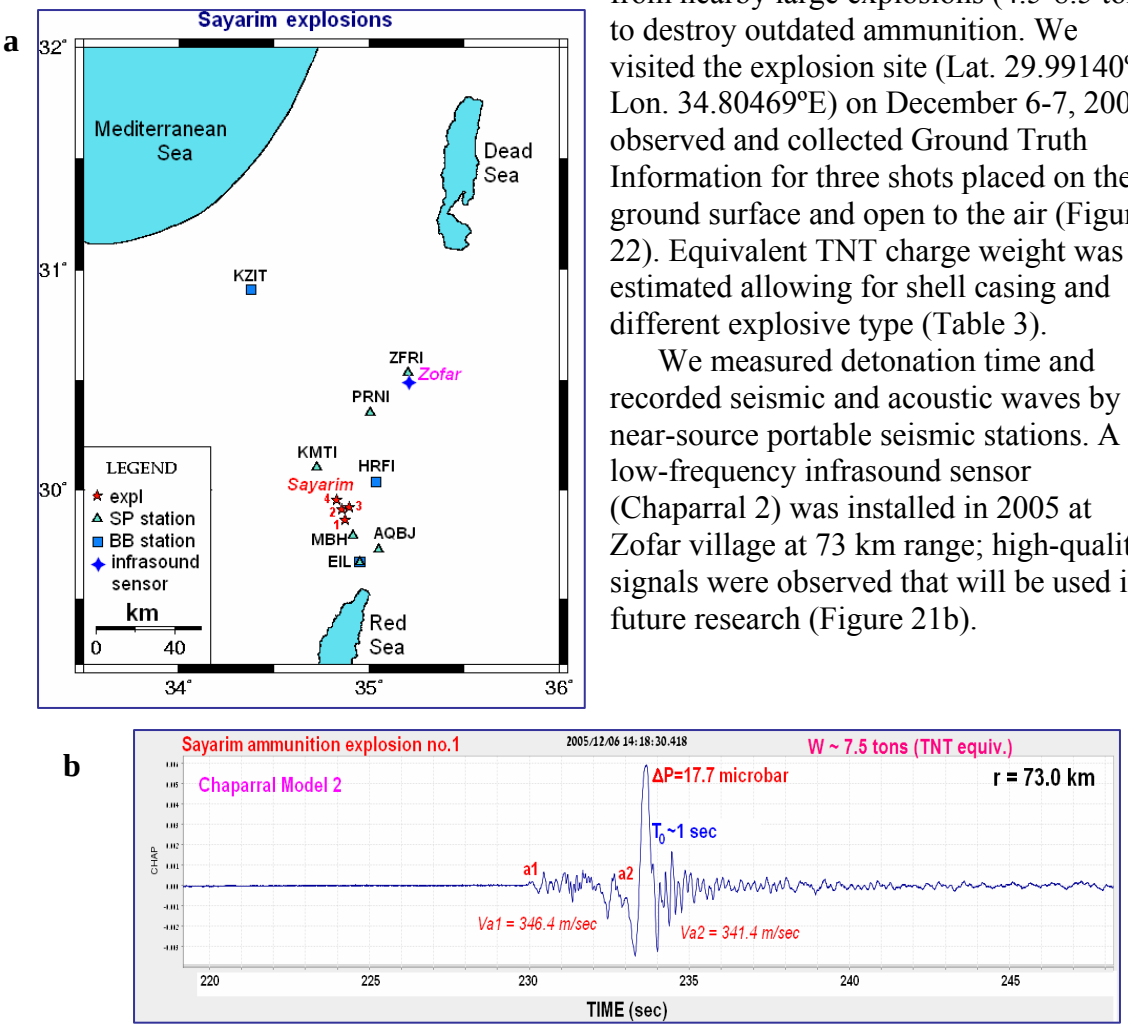

Figure 21. (a) Location of controlled Sayarim explosions and recording stations: 1 - buried charge-weight series in 2004, 2&3 – surface experimental series in 1998&2003, 4 – old ammunition detonations in 2005; (b) infrasound signal recorded at Zofar in 2005.

Table 3. Ground Truth parameters (GT0) collected for surface experimental shots and detonations of old ammunition at Sayarim military range.

Ex. No	Date	O.T.	Charge W, kg	Design	TNT equiv.[§]	Distance to EIL, km
1	20.05.98	11:37:47.5*	830	TNT cylinder, d~1m, h~1.5m, detonation down	830	32.2
2	24.05.98	14:37:13.70	830	TNT half-spherical, detonation up	830	
3	26.05.98	14:44:02:69	1000	ANFO, detonation down	800	
4	28.05.98	12:25:29*	1000	ANFO	800	
5	02.06.98	09:18:46.67	480	TNT half-spherical, detonation up	480	
6	02.06.98	16:30:18*				
7	03.06.98	09:08:57*				
8	03.06.98	15:50:35.68				
9	03.06.98	16:31:06.16				
10	04.06.98	16:43:58.90	1000	ANFO	800	
11	07.06.98	15:16:56.8*	202	H6, warhead MK83	215	
12	08.06.98	09:49:07.9*	1025	830 TNT (cubic), 195 ANFO	986	
13	08.06.98	16:15:58.0*	2200	TNT+hanit	2200	
14	27.10.03	11:30:44.75	830	TNT half-spherical	830	33.5
15	30.10.03	10:59:29.60	830	TNT half-spherical	830	
16	06.11.03	09:00:31.00	100	TNT cylinder	100	
17	06.12.05	14:18:47.5*	8500	7.5 ton henamit (emulsion) 1 ton TNT (ammunition shells)	7375	38.3
18	07.12.05	13:24:38.6*	4680	4.23 ton henamit (emulsion) 0.45 ton compositeB (ammun. mines)	4086	38.6
19	07.12.05	13:30:15.8*	8570	7.57 ton henamit (emulsion) 1 ton TNT (ammunition shells)	7434	38.3

* O.T. is estimated from records of close SP and BB stations;
[§] Explosive TNT equivalent: ANFO – 80%, henamit – 85%, compositeB – 109%.

All explosions selected were well recorded by IMS BB station EIL; some shots were observed also at SP ISN stations (up to 150 km), and close BB stations HRFI, KZIT (in 2003 and 2005).

Figure 22. Sayarim ammunition explosion on Dec. 6, 2005 (Ex.17). Industrial explosive (ANFO-like emulsion Henamit) was added to provide full demolition of the shells (left). The right photo is made from the distance ~3 km, with a large zoom (courtesy of Y. Hamashdyan of IDF).

The three explosions in 2003 were also recorded by portable stations of a special design. The acoustic sensors (low-frequency electret condenser microphones in a resonance box) were grouped in triangles, each side 100 m long, forming a tripartite array (Figure 23). Each array included a vertical SP seismometer (L4C) collocated with one of the microphones. The acoustic sensor geometry is configured to provide better estimation of source location, a major goal of the observations (Pinsky et al., 2005).

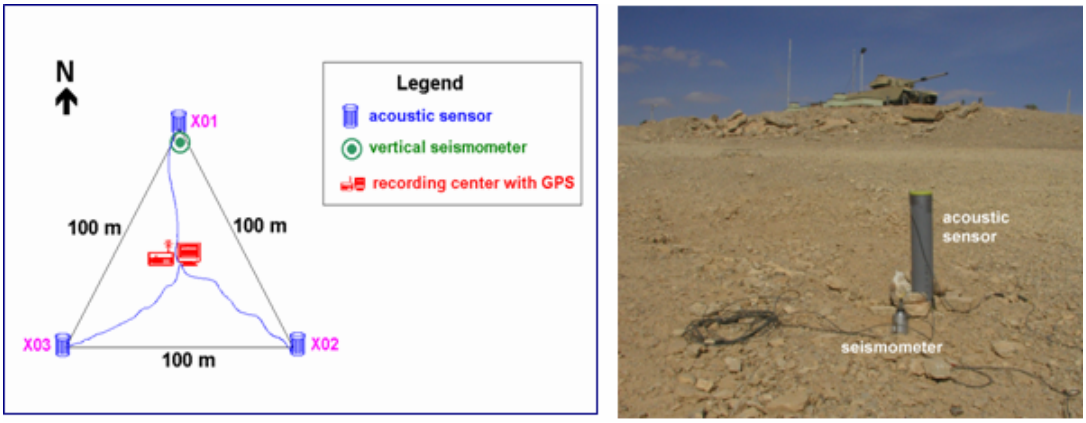

Figure 23. Observations in 1998: (a) Configuration of a hybrid seismic/acoustic portable tripartite array; (b) installed sensors in the Northern apex of the station triangle during one of the shots.

Energy Generation and Source Yield Scaling for Sayarim Surface Explosions. Strong infrasound phases were observed on seismic channels of local SP and BB stations, in some cases showing much higher amplitudes than seismic waves (Figure 24). Figure 24 also shows three striking examples of directional effects on acoustic phases at two SP stations situated at the same epicentral distance from the explosion site but in opposite directions (roughly, south and north). Ex.14, Oct. 27, 2003, and Ex 15, Oct. 30 2003, show high amplitudes to the South and low to the North; Ex.16, Nov. 6, 2003, the opposite. These observations illustrate that acoustic amplitudes and phase propagation time depend strongly on atmospheric conditions along the infrasound propagation path, especially the altitude distribution of wind direction and velocity (Stump et al., 2002).

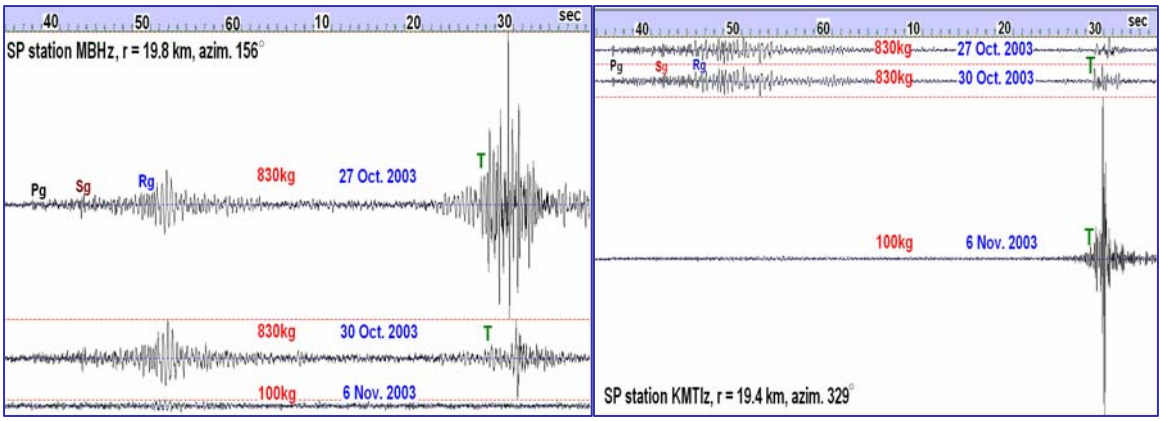

Figure 24. Observations of diverse acoustic phases (T) from surface shots in 2003 at two ISN seismic stations (plotted in absolute scale, filter 1-15 Hz is applied).

The extensive GT0 dataset of about 20 closely-spaced explosions in a broad range of charges (100-8500 kg), recorded at numerous SP and BB stations, facilitate the analysis of seismic energy generation dependence on yield. For a preliminary analysis of energy characteristics we selected observations at IMS BB station EIL, located at 32-38 km from the explosions (Table 3). Spectra of pre-signal noise showed an energy maximum at ~0.2-0.3 Hz, up to ~1 Hz; accordingly, seismograms were filtered in the frequency band 1-20 Hz for 80 Hz data and 1-10 Hz for 20 Hz data (Figure 25). Initially we measured maximum signal amplitudes, which are closely correlated with the energy of radiated seismic waves. For Sayarim shots, observed at EIL station, maximum amplitudes are found in the first arrivals (P-phase, Pg), while S waves are not manifested clearly (Figure 25a). Spectral amplitude shapes of seismic phases are similar in general over the 5 fold charge increase (Figure 26). For surface (Rg) waves the dominant frequency and simple spectral shape are about the same for the four shots, only the maximum spectral amplitude is increased ~4 times between smallest and largest, whereas spectra of P (Pg) phase are more complicated and the dominant frequency varies from 2.8 Hz for the largest explosion to 5-6 Hz for smaller shots.

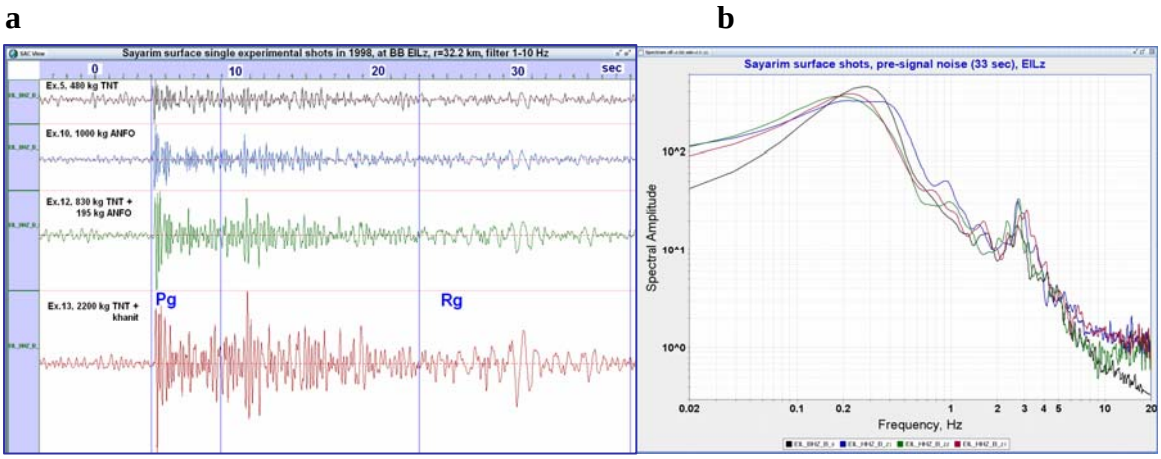

Figure 25. (a) Seismograms (in absolute scale) of 4 selected Sayarim surface explosions at BB station EIL (vertical), low-frequency noise (f<1 Hz) is filtered out, vertical lines show windows for spectral analysis; (b) spectra of pre-signal noise (curve colors correspond to the appropriate seismograms).

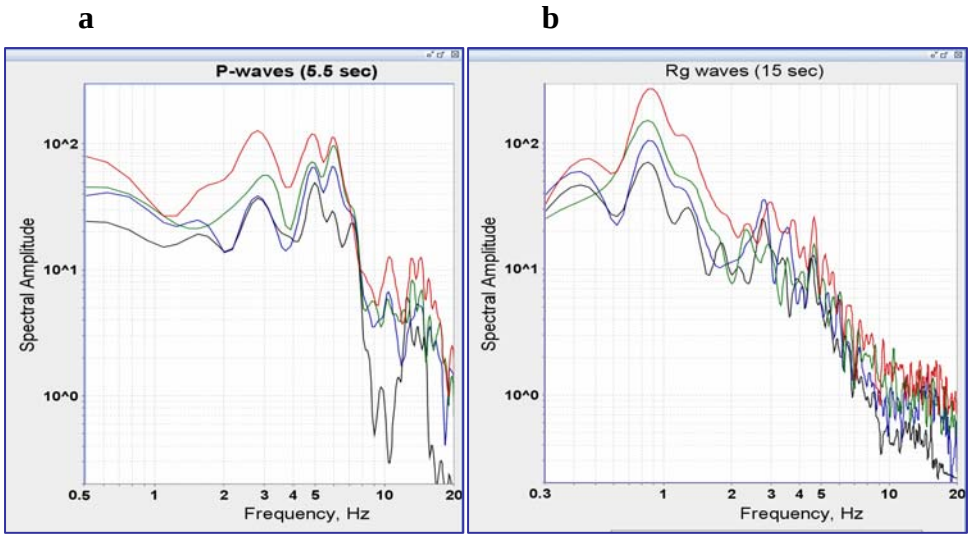

Figure 26. Spectra of P-waves (a) and surface waves (Rg) (b) at EIL (vertical) for 4 explosions (the data were pre-filtered in the 0.5-20 Hz band). Curve colors correspond to the seismograms in Figure 25.

We evaluated a source scaling relationship of surface shots based on records at BB station EIL. Measured Vertical Peak Amplitudes (VPA, micron/sec) for the Pg phase were corrected for distance r (VPA~ $r^{-1.7}$, r_0=35 km) and for different explosive type (estimating ANFO energy as ~80% of TNT) (Gitterman et al., 2001). The corrected Vertical Peak Amplitudes are plotted against charge weight W (kg) for 19 shots (Figure 27). The data were fitted to the power law equation: VPA (mic/sec) = $a*W_{(kg)}^{b}$.

The r.m.s. procedure produced estimates of a = 0.0002258 and b = 0.918 for the Pg phase at station EIL.

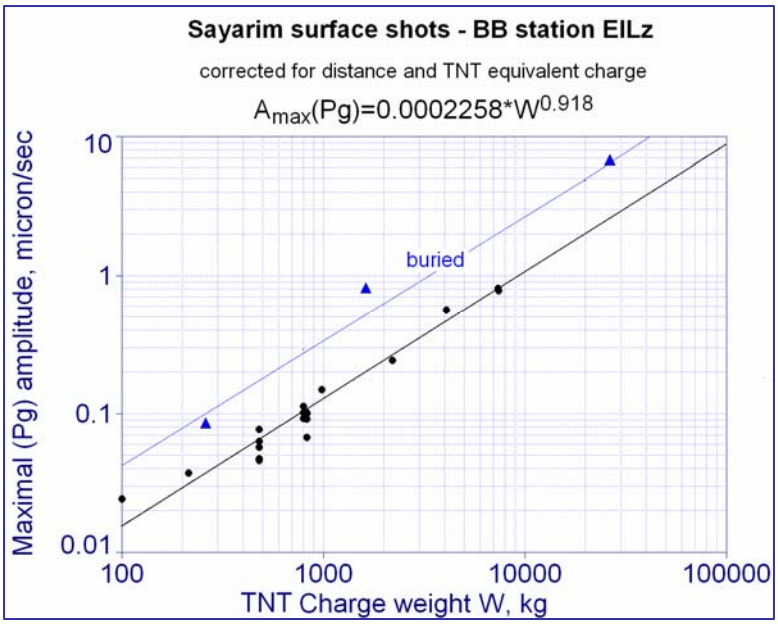

Figure 27. Yield scaling of surface seismic sources at BB station EIL. Data of 3 buried Sayarim experimental explosions (2004) at EIL are also shown for comparison (▲).

Comparison of Surface and Buried Seismic Sources. The high scaling power law parameter for P-waves b=0.918 is similar to b=0.93 for the nearby buried explosions (in boreholes of large diameter ~0.6-0.7 m, depth 20 m) conducted by GII in 2004, observed at the same BB station EIL (Gitterman et al., 2005a) (Figure 27). A lower *b*-value might be expected due to the small charge-rock contact surface for single surface charges resulting in a decrease of the share of explosive energy transferred to the ground for larger shots. Apparently the 3 ammunition detonations with the largest, multiple, charges, placed on a large enough area (~25 m^2, see Figure 22), compared to a small area (1-3 m^2) for other single experimental shots in the dataset, produced enhanced Pg-amplitudes, resulting in the high *b*-value.

We compared waveforms and spectra for Sayarim surface and buried (2004) explosions. A sample comparison is presented in Figure 28 for a pair of sources with similar charge weight (~2 tons), observed at BB station EIL, with the same propagation path (North-South). The buried explosion was in a single borehole, partially contained, with the scaled depth h=1.4 m/$kg^{1/3}$. Both explosions produced maximum amplitudes in the P-waves on the vertical component and a clear Rg wave on the vertical and near-radial (NS) components, but the S-wave manifestation is different: an obvious Sg arrival on the near-transversal (EW) component is seen for the buried shot, whereas it is not visible on the surface shot record.

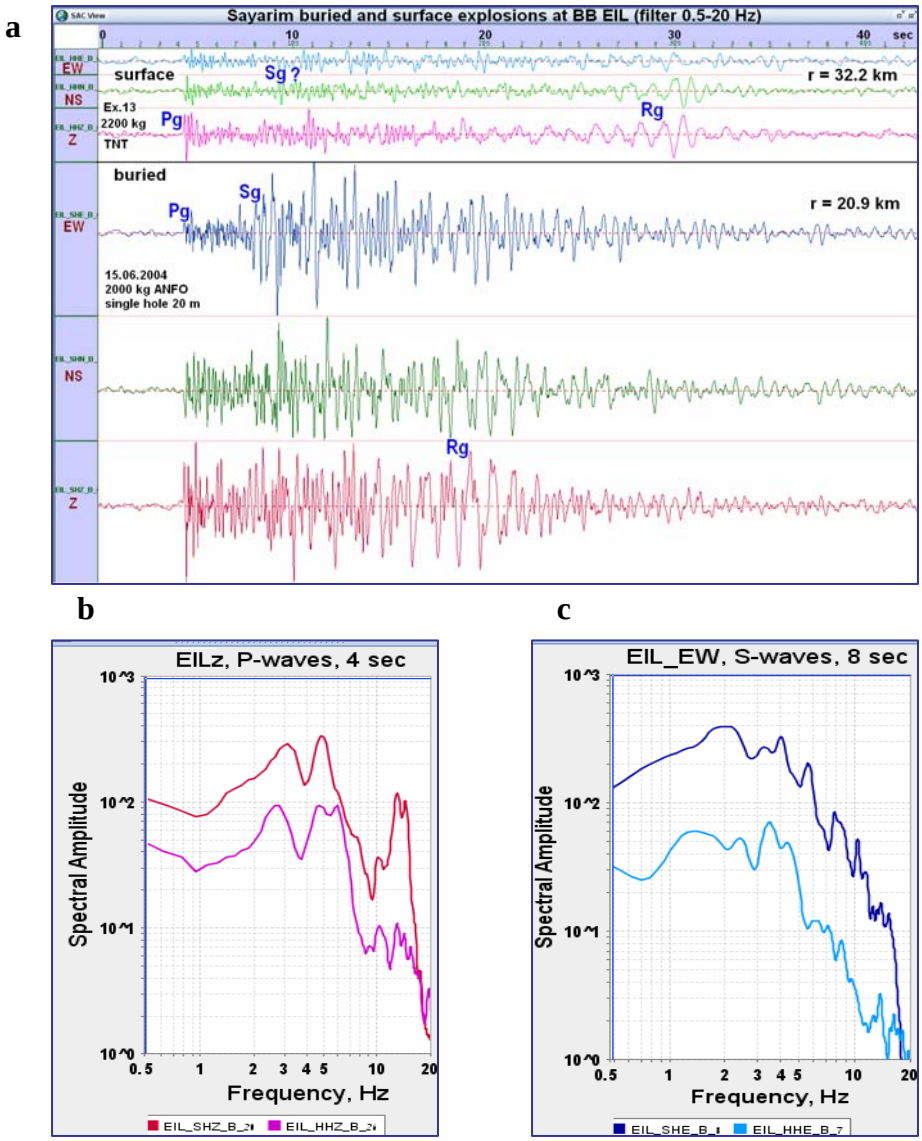

Figure 28. Seismograms in absolute scale (a) and spectra of Pg (b) and Sg (c) for surface and buried shots at EIL. Spectra colors correspond to the appropriate seismograms.

The first break of Rg, carrying most of the signal energy, cannot be distinguished due to the close distance; the Rg group velocity is rather low, 1.0-1.3 km/sec, for these close distances (21-32 km). No significant difference or shift to low-frequency is found in the spectral shapes of Pg and Sg waves for the surface shot compared to the buried one (Figure 28b,c) (see Stevens et al., 2003).

4.3. Beit-Alpha Charge Weight and Type of Explosive Series

We conducted a series of experimental explosions at Beit-Alpha basalt quarry, Northern Israel (Figure 1, Table 4), in boreholes of large diameter (0.5-0.55 m) with a depth of ~15 m, drilled in the Pliocene cover basalt flow, weathered and cracked in the subsurface layer (Figure 29). The largest shot Bα4 of 20 tons, designed as a large-scale in-land calibration explosion complementary to the Southern Sayarim shot S3 of 32.5 tons of similar design (but placed in soft alluvial sediments), was conducted in a MERC project (Gitterman et al., 2005b). Three smaller shots of 0.5 ton ANFO, 0.5 ton TNT and 2 tons ANFO in boreholes of the same design, jointly with the large explosion, provided a series for explosive and yield-dependent analysis of regional waveforms, similar to the Sayarim experiment, but in a different geological environment in terms of shot medium, upper crust structure, and tectonic setting. We also tested seismic energy generation at local distances for two similar single charges of 500 kg of different explosives: ANFO and TNT.

Table 4. Ground Truth parameters of Beit-Alpha experimental shots on June 6, 2005.

Ex. No.	Lat. Lon.	Origin Time, GMT	M_L	Charge, kg	Hole depth, m	Scaled depth, m/kg$^{1/3}$	No. of holes	Comments
Bα1	32.54499 35.46868	10:05:01.422	1.5	500	14.7	1.5	1	fully contained
Bα2	32.54506 35.46850	10:30:01.604	1.5	500 (TNT)	16	1.7	1	
Bα3	32.54522 35.46883	11:00:01.330	1.4	2000 (1000)	14.7- 15.5	1.0-1.1	2	poorly contained
Bα4	32.54549 35.46914	12:00:01.532	2.6	20000 (1000)	14-16	1.0-1.2	20	

a **b**

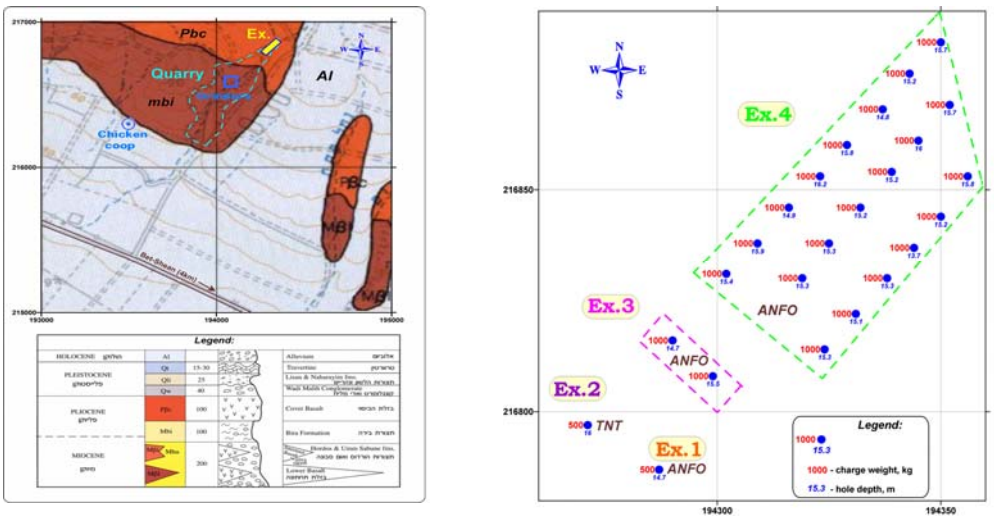

Figure 29. Geological setting (a) and parameters of the explosion holes (b).

The two 0.5 ton shots were fully contained, whereas for the two larger shots rock spall and energy loss into the air occurred, resulting in reduced magnitudes (Figure 30).

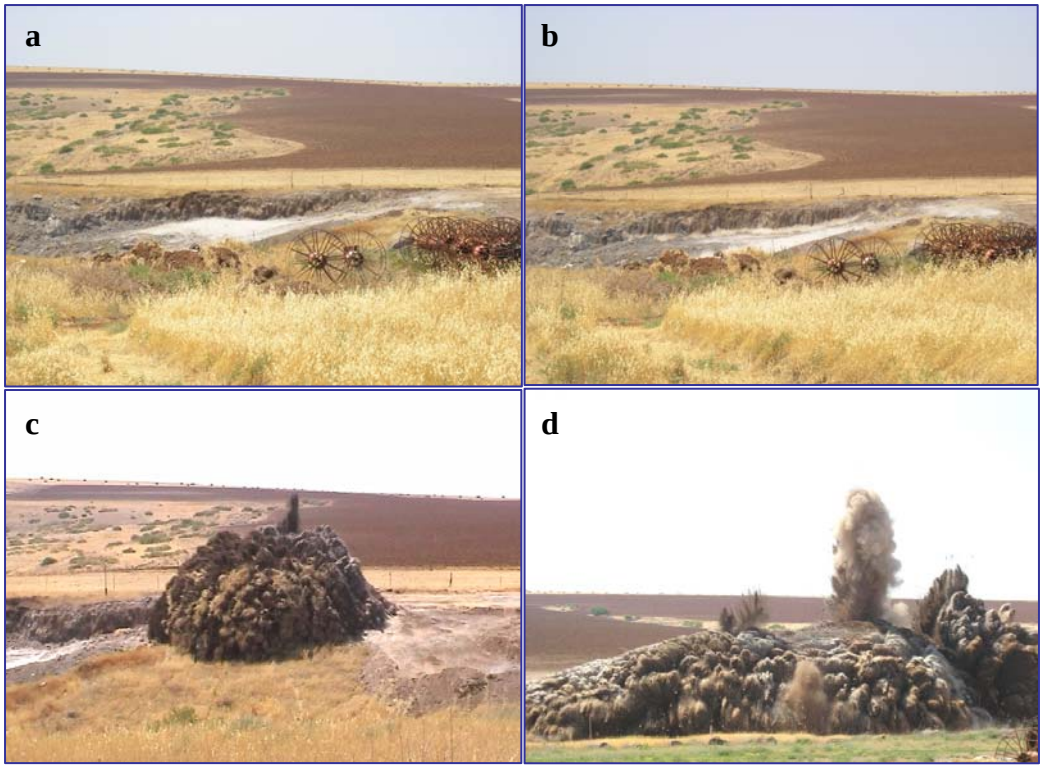

Figure 30. Explosions of 0.5 ton ANFO (a) and TNT (b) were fully contained, only dust denotes shot locations. Two larger explosions of 2 tons (c) and 20 tons (d) showed rock spall and energy loss into the air.

PGA Attenuation. A number of portable instruments were installed during the explosion experiment (Figure 31): nine accelerometers (ETNA and K2), three sensors (BlastMateIII) near sensitive structures for monitoring ground vibrations after each explosion; and five 3C seismic stations (L4C) at distances of 0.6-17 km. The map in Figure 31 shows the configuration of the blast site and observation instruments located at distances less than 1 km (two remote seismic stations are not shown).

Peak accelerations of ~2g were observed for the largest shot (Figure 24); source complexity was seen, with multiple phases corresponding to separate borehole charges. We estimated vector PGA attenuation with distance, the data were fit with the power relation $PGA_{(cm/s\^2)} = a*r_{(m)}^{-b}$. (Figure 33). Different power coefficients *b* were obtained for the four explosions, in the range 2.4-3.2, much higher than *b*~1.74 for Sayarim experiment. This feature can be related to the weathered and cracked basalt rocks of Beit-Alpha quarry.

Strong motion data obtained confirm the effects noted before, that in the near-source area observed amplitudes and signal energy for the 2-ton shot (Bα3) are similar or lower than for the two 0.5-ton shots, due to a lower scaled depth and energy loss into the air; energy generated for the 0.5-ton TNT shot (Bα2) is a little higher than for the 0.5-ton ANFO (Bα1).

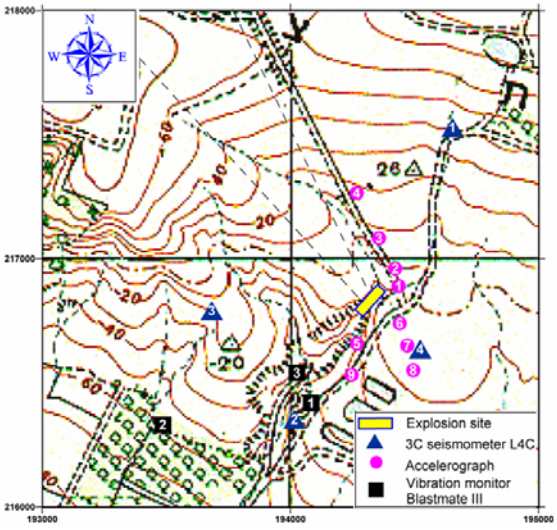

Figure 31. Location of close portable stations.

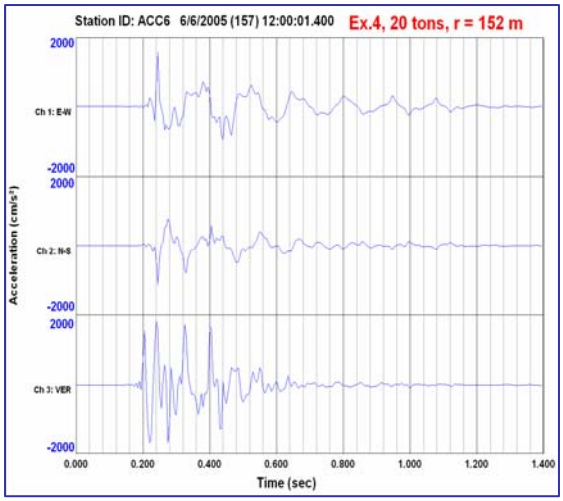

Figure 32. Accelerogram of the multiple-hole shot 20 tons at the closest sensor.

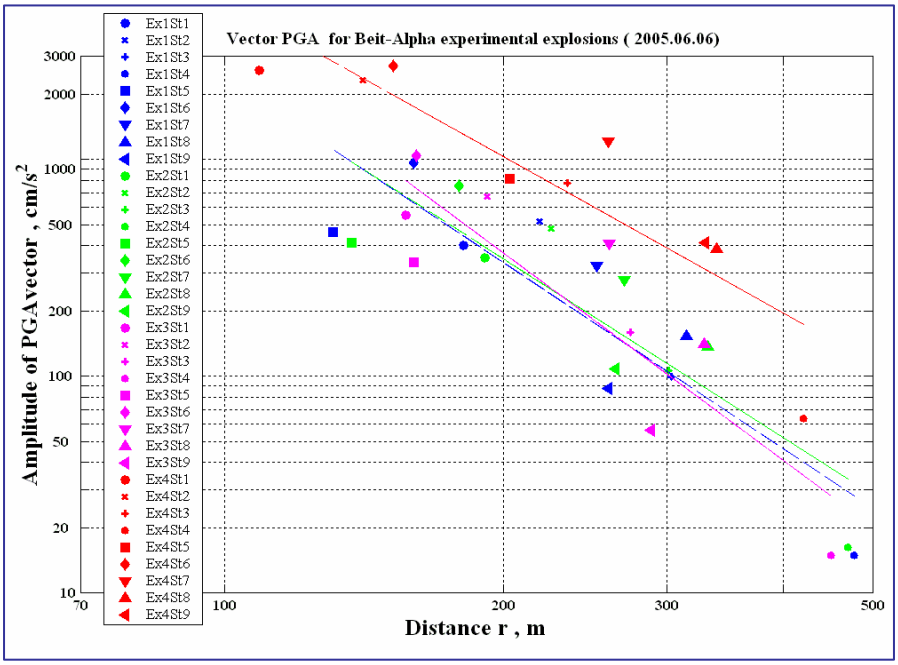

Figure 33. Estimation of distance attenuation parameters for the vector PGA.

Energy Estimations at Close Distances. We estimated relative seismic energy generated by the explosions and recorded at CNF BB station MMLI at r=13 km (see Figure 1). Maximum vector amplitude and seismic energy for the whole signal (time window 20 sec) were calculated from measured peak amplitudes for the 3 components (Table 5, Figure 34). Energy values (ratio) relative to the first explosion of 0.5-ton ANFO were also estimated.

Table 5. Maximum amplitudes, local magnitudes and energy from Beit-Alpha explosions at BB station MMLI.

Ex. No.	Mag. M_L	PGA Vector, counts	Amplit. Ratio	Energy, counts	Energy Ratio
Bα1	1.5	4147	1	654947	1
Bα2	1.5	4330	1.04	689228	1.05
Bα3	1.4	3277	0.79	429110	0.66
Bα4	2.6	25248	6.1	19822576	30.3

a **b**

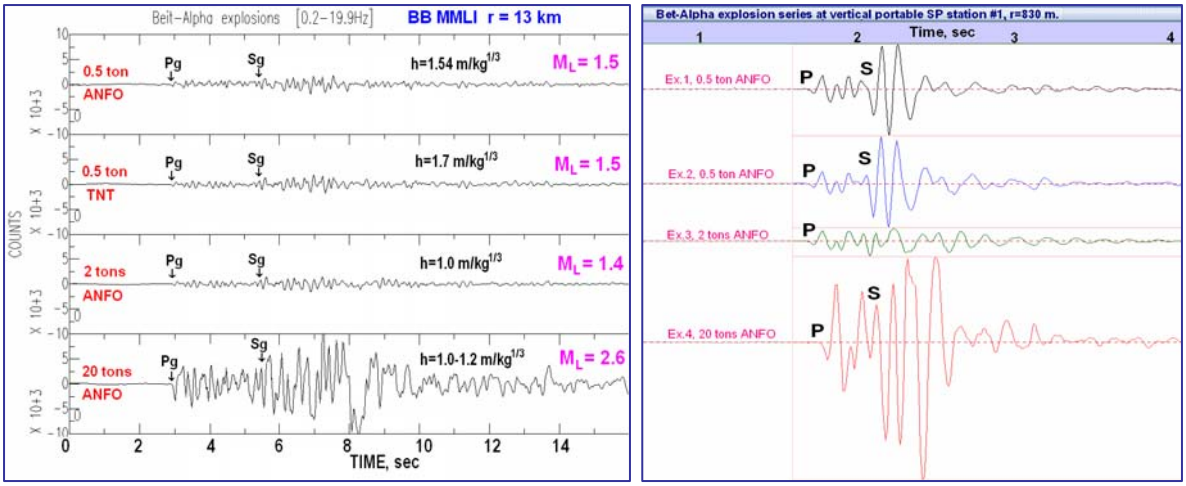

Figure 34. Seismograms (in absolute scale) of Beit-Alpha shots show reduced amplitudes and magnitudes at close BB MMLI (a) and portable SP station at ~1 km (b).

For this local seismic observation a relatively small increase of 4-5% in amplitude/ energy values is found for the 0.5-ton TNT shot compared to the 0.5-ton ANFO shot. Reduced amplitudes and an energy drop are found for the larger poorly-contained 2-ton shot (in two boreholes), resulting in a low local magnitude M_L=1.4 compared to the fully-contained 0.5 ton shot with M_L=1.5 (Figure 34a); a more significant energy decrease is observed at a near-source portable SP station (Figure 34b). For the largest 20-ton shot the estimated magnitude M_L=2.6 is also relatively small compared to an empirical relationship for simultaneous buried blasts (Gitterman, 1998); seismic energy is larger by more than 30 times relative to the 0.5-ton shots, compatible with about one unit larger magnitude (M_L).

Analysis of seismic source features and blast design parameters for the Beit-Alpha experiment shows that the main reason for reduced seismic signal strength is insufficient scaled charge depth $h=H/W^{1/3}$, where H is depth from the surface to the charge center, m, and W is charge weight, kg. The scaled depth for the 0.5 ton shot h=1.54 m/kg$^{1/3}$ is large enough to provide full containment of the explosion, whereas the two larger shots of 2 tons (h=1.0 m/kg$^{1/3}$) and 20 tons (h=1.0-1.2 m/kg$^{1/3}$) produced rock spall and energy loss into the air. These effects, clearly seen on explosion photos and video-records, provide an explanation of reduced magnitudes for the two explosions. These data show the importance of scaled depth of buried charges as a crucial factor of seismic coupling.

Regional Observations. The largest shot Bα4 of 20 tons was recorded at numerous seismic stations in Israel and Jordan; two stations in Lebanon - BHL (152 km) and HWQ (197 km), recorded the explosion (Figure 35), and the associated phase readings were used for location analysis. The explosion provided observations in the Southern direction including the IMS station EIL at 323 km, and can be considered as complementary (and close to reversed) to the Sayarim 32.5 tons explosion, located close to the EIL station; clear regional P and S wave groups were observed (Figure 36).

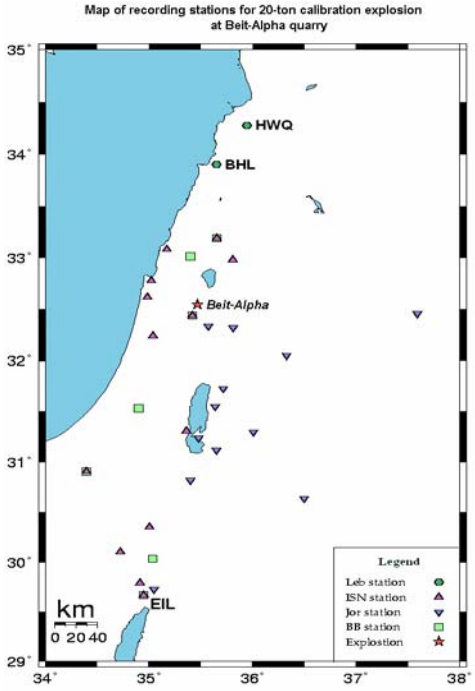

Figure 35. Location of SP and BB network stations in Israel, Jordan and Lebanon that recorded the largest explosion Bα4 of 20 ton.

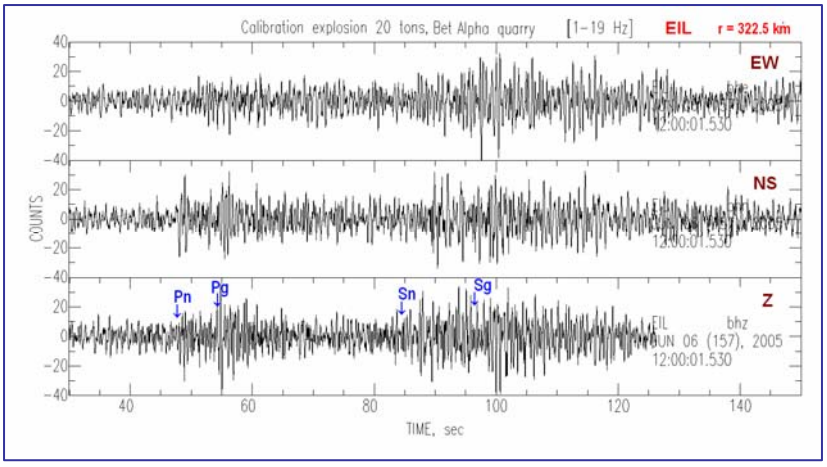

Figure 36. Seismogram of Beit-Alpha explosion of 20 tons recorded at the IMS station EIL. Regional phases Pn, Pg, Sn and Sg are marked according to the IASPEI91 model.

4.4. Source Phenomenology Explosion Experiments of Special Design

4.4.1. Background.

DOB Preparations. We conducted preparations of the DOB experiment, planned as the key project, for two years; there were three shots of the same near-spherical charges at different depths (about 20, 40 and 60 m). One of the main goals was to observe regional phases at remote stations, especially at the IMS array MMAI at Mt. Meron, located at ~230 km from the planned explosion site. The charge of ~5 tons was expected to provide explosion magnitudes of M_L~2.5, necessary for such observations, based on a local magnitude-charge relationship (Gitterman et al., 2005a).

Special technology was used: deployment of explosives in a cavity, created beforehand by a small charge, thus forming near-spherical sources (see Section 3.1.2). For the ANFO explosives (density ~0.8 gr/cm^3) planned the diameter of a cavity capable of accommodating this charge is ~2.5 m. The most important conditions for such an experiment are homogeneity of rock media for all the sources (i.e., for depths 15-65 m), and properties of the rocks allowing creation of large cavities; consolidated sediments of medium strength are suitable. An appropriate site was found at the Oron phosphate quarry, with thick upper layers of different types of marl rocks (Figures 38, 51).

This technology was first used in the Rotem 25-ton calibration explosion, conducted by GII (Gitterman et al., 2002); using boreholes of ~8", cavities of ~1 m size at depth ~14 m were created in kaolin rocks, near-spherical charges of ~1 ton were accommodated. However, there was no experience creating larger cavities at depths of more than 60 m in soft consolidated sediments using small diameter (6.5") boreholes, and preventing possible rock-falls in the cavity or borehole blockage. Therefore, a special trial shot series was conducted (April-June 2006) before the DOB experiment. The main goal of the trial shots was to test the technology in the new geological environment and estimate an optimal small charge or series of charges for creation of the appropriate cavities. A number of excellent cavities were created at depths of 25-63 m, with maximum size 3.5 m.

Ground Shaking Hazard Problems. The nearby location (~500 m) of quarry structures to the site of the planned 5-ton explosions required estimation of safety conditions using data from BlastMateIII vibration sensors obtained during the trial shots (see Figures 6c, and 37). Based on these data and well-grounded empirical relationships (Pergament et al., 1998) we found that the peak vibrations for 5-ton shots (Table 6) are lower than the threshold used in the USA Bureau of Mines Safety Code for modern residence buildings: PGV = 19 mm/sec (for frequencies f < 40 Hz).

In spite of these safety estimatess, the quarry administration decided that the DOB experiment with charges of 5 tons could not be conducted in the cavities prepared due to ground shaking hazard for nearby buildings, and the experiment was transferred to another location.

However, the cavities created presented an opportunity for conducting a “Decoupling Experiment”, not planned initially in the project, with smaller charges (~1.2 ton) filling only a part of the prepared cavities, producing a decreased (decoupled) seismic effect; this was acceptable and approved by the quarry administration. For completeness of the Decoupling Experiment a reference coupled explosion in an additional smaller cavity was

prepared; due to numerous rock-falls of the uppermost loose sediments into shot holes during small shots, this took almost two months.

Site	Distance, m	Estimated PGV, mm/sec
Laboratory	507	15
Dining room	672	10
Office	964	6

Table 6. Evaluation of Peak Ground Velocity near sensitive quarry structures for the planned 5 ton explosions.

Figure 37. Nearby location of planned 5-ton explosion boreholes to the quarry structures.

4.4.2. Oron Decoupling Experiment.

Geological Setting, Design and Parameters of Explosions. The site geology was near-surface alluvium and underlying consolidated marls and phosphates with similar mechanical and elastic properties (Figure 38a), providing homogeneous rock media for all the sources. Subsurface velocities were estimated from a refraction survey on the nearby DOB experiment site (Section 4.4.3).

A series of decoupled and fully coupled (reference) explosions with charges of 1240 kg ANFO (1000 kg TNT equiv.) in the cavities was conducted on July 17, 2006 (Table 7, Figure 38b). The spacing between the shots was 30-120 m (Figure 39). Note that this "Decoupling" experiment was not quite ideal, because the shots were placed at different depths, and the cavity volume could only be estimated approximately.

Table 7. Parameters of Decoupling Experiment explosions.

Ex. No.	Design	Local magnitude M_L	Coordinates		Detonation time, GMT
			X, km	Y, km	
1	h=26.5 m, decoupled	2.0	150.863	36.240	13:30:02.38
2	h=63 m, decoupled	1.5	150.922	36.286	13:56:40.99
3	h=30 m, coupled	2.4	150.890	36.360	14:15:02.14

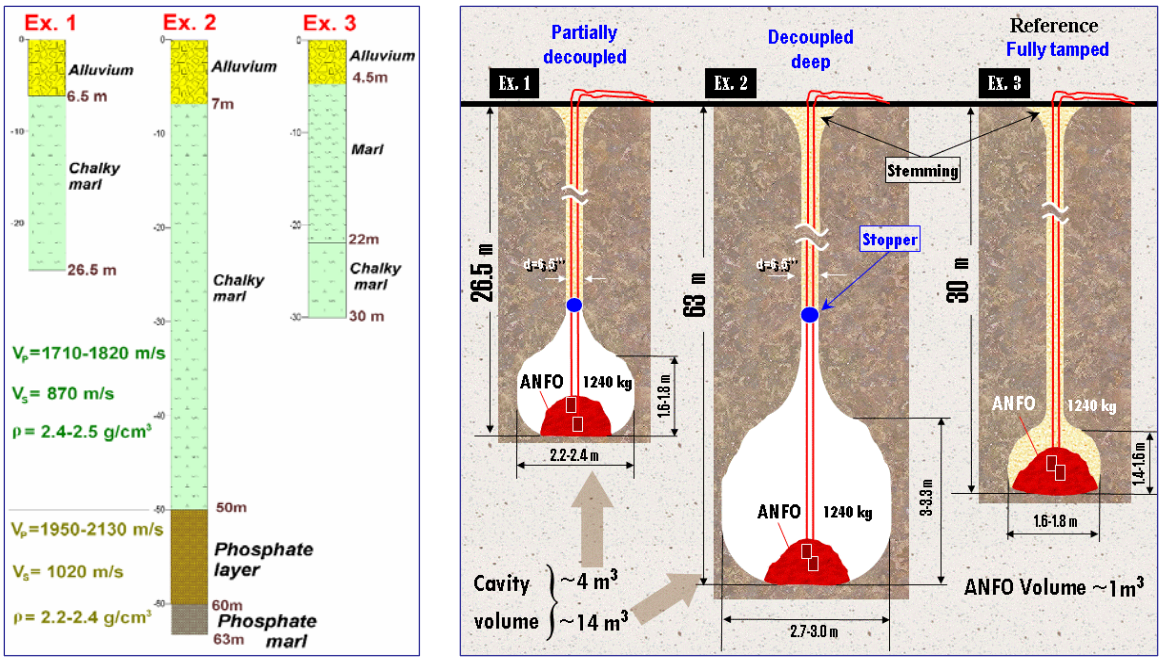

Figure 38. Geological settings of the Decoupling Experiment site from the shot borehole drilling logs (a) and the charge design (b).

The first two shots were decoupled (partially), charges of 1240 kg of ANFO were downloaded to the bottom of air-filled near-spherical large cavities of different size (Figure 38b). The cavity size was roughly estimated from observations of a borehole camera with an attached meter stick and a PC-based video-recorder (see Figure 4). Then the borehole was filled with loose stemming material using a stopper placed at the transition of the borehole to the cavity (Figure 38b). For the third shot the explosives filled most of a smaller cavity, then the rest of the cavity and the borehole were filled with stemming material. This shot was included in the experiment to provide a fully coupled reference source with the same charge, thus completing the decoupling experiment series. Note that the deepest Ex.2 is placed in phosphate rocks, and the other shots in chalky marls (Figure 38a). All explosions (with scaled charge depths $h=H/W^{1/3} > 2.3$ m/kg$^{1/3}$) were fully contained. No craters or cracks were observed on the surface around the explosion boreholes.

Near-Source Observations. Different 3C observation systems were deployed at near-source distances: 9 accelerometers ETNA, range 100-700 m; 3 sensors BlastMateIII, 500-1000 m; 5 SP seismic stations L4C, 4-23 km (Figure 39). Extensive good quality datasets were obtained for all shots in near-source zone and remote area showing signal characteristics and energy generation features related to these specific seismic sources.

Very high signal frequencies accompanied by the highest peak accelerations were observed at all near-source distances for the decoupled Ex.2 (Figures 40, 41). Possibly a smaller volume size of the seismic source, due to the larger depth (63 m) might contribute to this effect. However, it is problematic to explain a sharp raise of the radiated signal frequencies from 3-15 Hz to 30-40 Hz only by a twofold depth increase (as in the DOB experiment data, see Section 4.4.3).

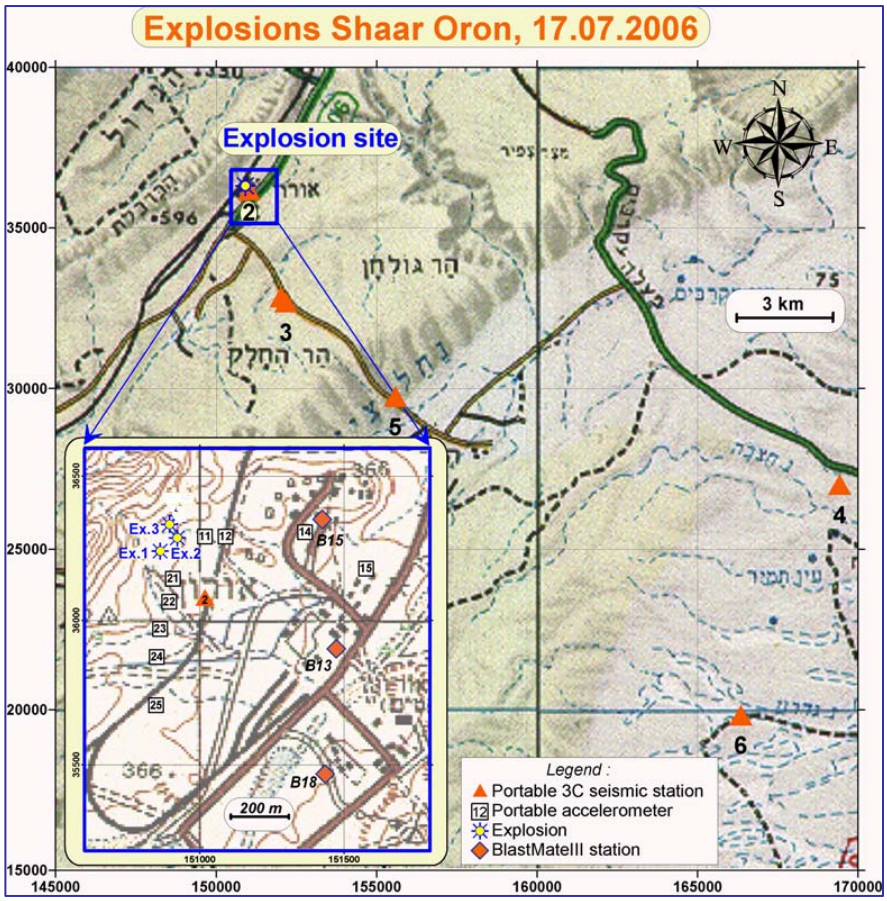

Figure 39. Location of the Decoupling explosion site and portable stations.

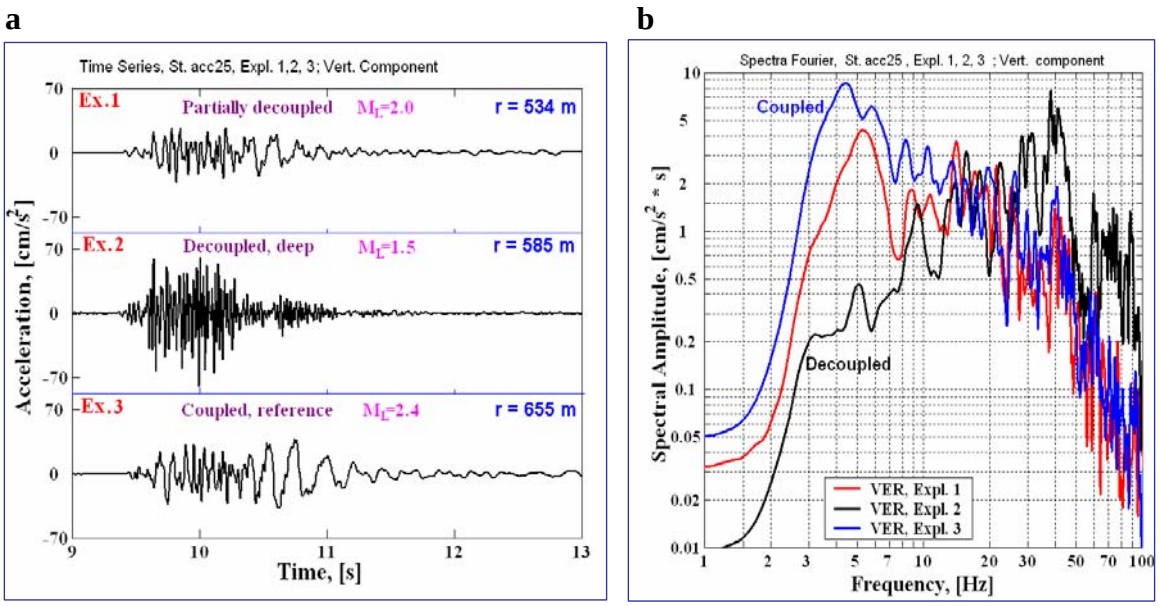

Figure 40. Vertical signal records (a) and spectra (b) at ~0.6 km (accelerometer ETNA). Local (duration) magnitudes M_L and epicentral distances are also shown.

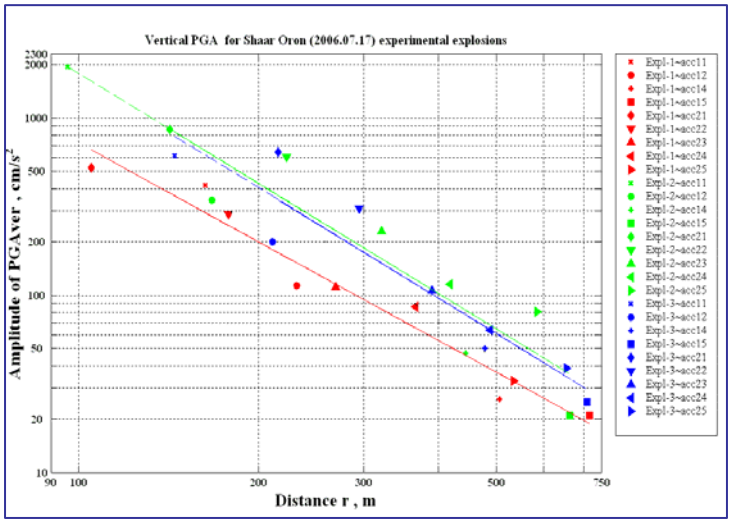

Figure 41. Vertical PGA for all accelerometers and regression curves for the 3 shots.

A more reasonable guess (A. Dainty, pers. communication) explains this effect by air-shock wave reverberations in the air-filled cavity. Taking the cavity maximum vertical dimension l_v~4 m, and the average shock wave velocity V~400 m/s, a rough estimate of the dominant reverberation frequency is $f_r = V/2l_r$ ~50 Hz, i.e., comparable to the observations. This phenomenon was modeled for cavity decoupled nuclear explosions in salt and tuff (Stevens et al., 1991), however much larger reverberation frequencies (>100 Hz) were obtained, possibly due to high temperatures and resulting high velocity of the air-shock wave.

The reverberation effect, if operative, should result in several modes, providing spectral modulation. A possible manifestation of this effect can be found in the closest accelerometer data (acc11, see Figure 39), shown in Figure 42. Coherent spectral maximums are visible in all components at ~40, 70 and 100 Hz.

a **b**

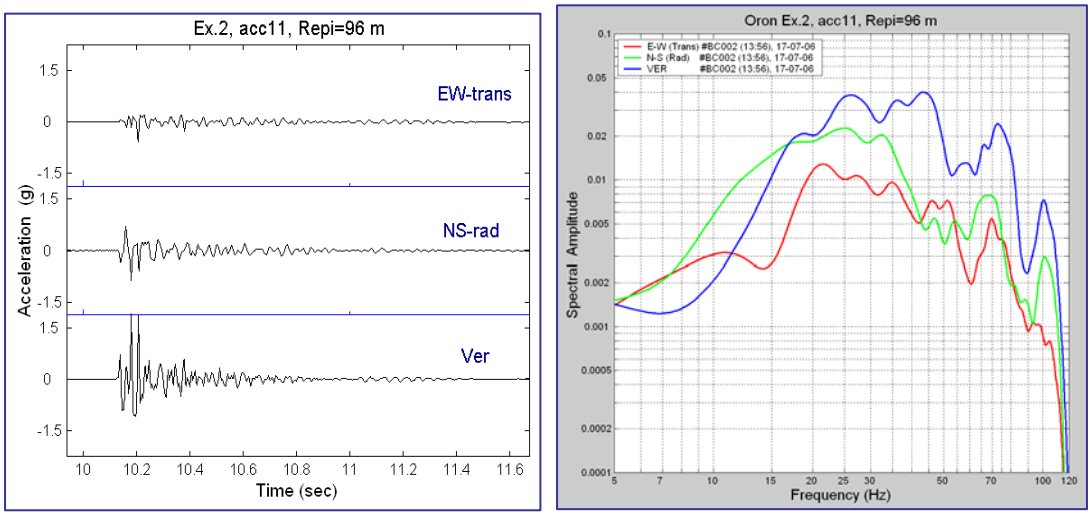

Figure 42. 3C records of decoupled Ex.2 at the closest epicentral distance 96 m (a) and smoothed FFT spectra (b) for 1.5 sec window.

Close Local and Regional Data. Rapid attenuation of high-frequency seismic energy for Ex.2 is already apparent at the closest portable station at 4 km, resulting in minimal signal amplitudes and spectra in the range 1-12 Hz, yet retaining energy at higher frequencies of ~12-20 Hz (Figure 43).

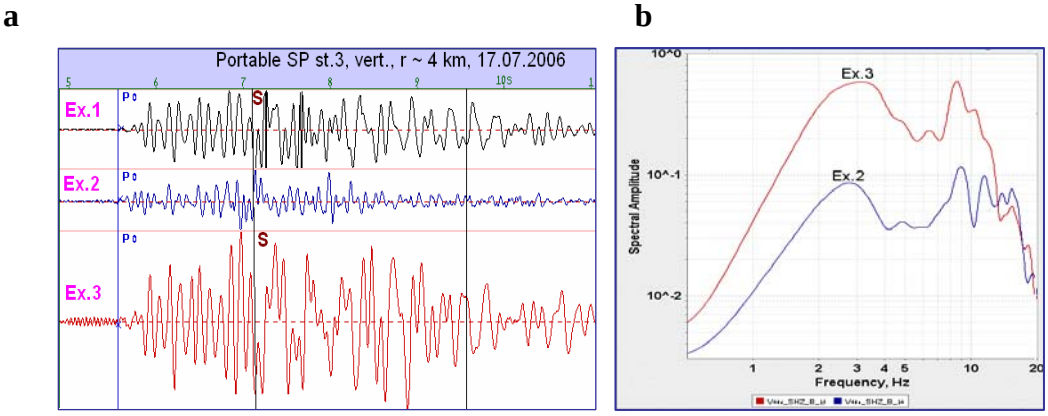

Figure 43. Vertical seismograms in absolute scale (a) and spectra for coupled (Ex.3) and decoupled (Ex.2) shots (b) at the closest portable seismic station.

A similar effect was observed at all regional stations (e.g. SP PRNI, Figure 44, and BB EIL, Figure 45), therefore a lesser magnitude of M_L=1.5 was estimated by the Israel Seismic Network, compared to M_L=2.4 for the coupled Ex.3. Note very weak S-waves for Ex.2, compared to Ex.3, at both PRNI and EIL. A clear maximum at high frequencies in P-waves, possibly at ~20 Hz (sampling 40 sps) is found at the EIL station (Figure 45b).

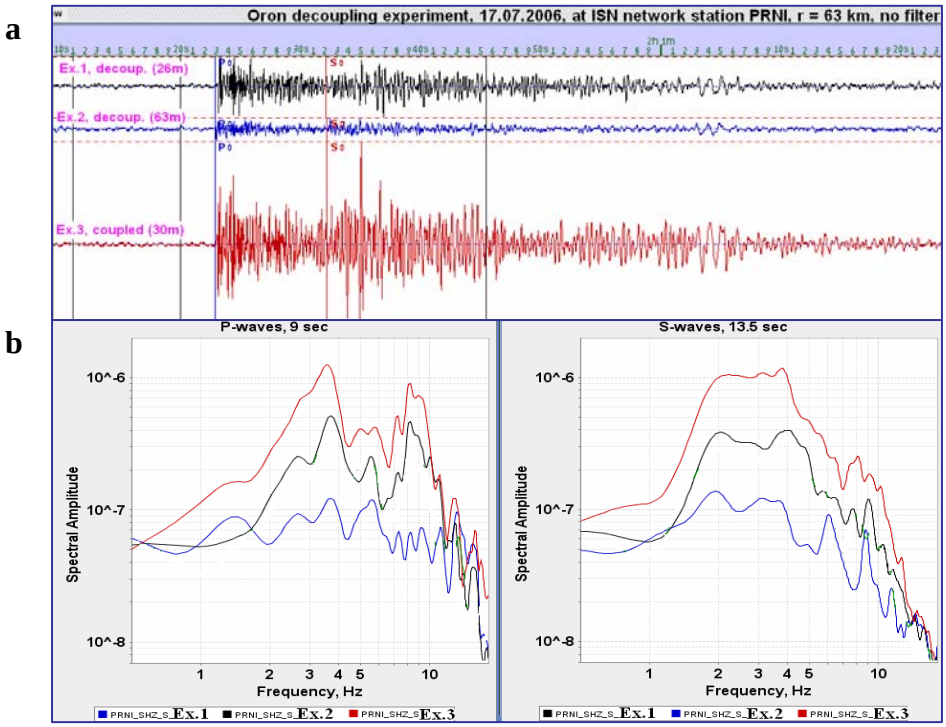

Figure 44. Vertical seismograms in absolute scale (a) and spectra (b) at SP st. PRNI.

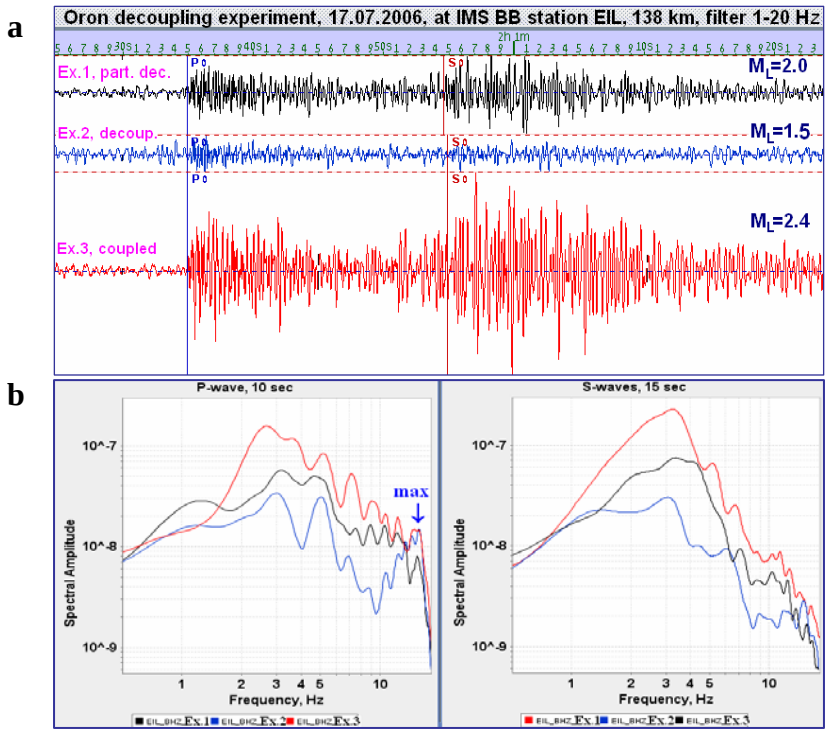

Figure 45. Vertical seismograms in absolute scale (a) and spectra (b) at BB station EIL.

All three explosions, even the decoupled Ex.2, were observed at IMS array MMAI, located at 236 km. The signal of the weakest, Ex.2 (M_L~1.5), was weak in raw data of the array elements, but after band-pass filtering from 1-10 Hz and array beamforming analysis a clear P-wave was found on the beam trace (Figure 46).

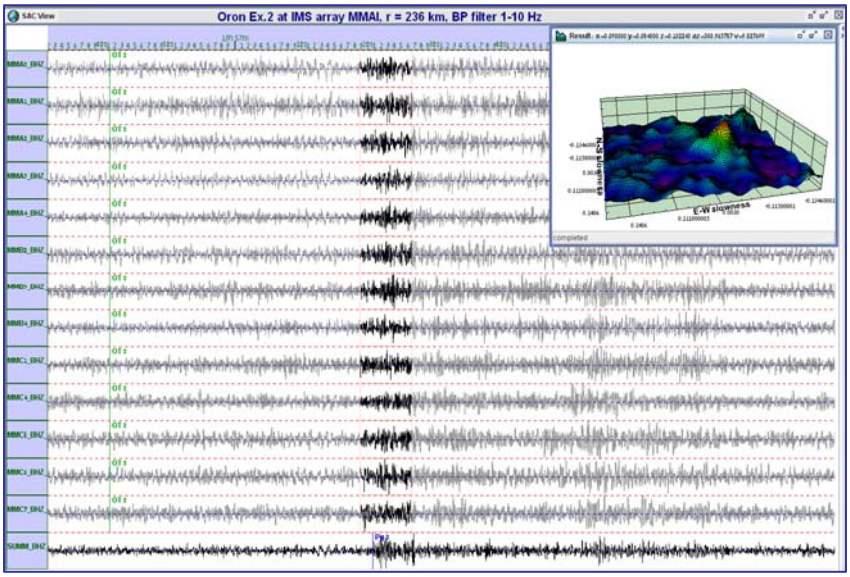

Figure 46. Observations of the weakest Ex.2 at IMS array MMAI (filter 1-10 Hz). Vertical lines on seismograms define time windows for the array beamforming analysis. An array location analysis is shown in the insert.

Energy Generation: Decoupling Factor. We measured signal peak (vertical) amplitudes for the three explosions and calculated the energy of the whole signal using vertical records of two SP (ZFRI, PRNI) and two BB (HRFI, EIL) stations in the distance range 40-140 km and the frequency range 1–20 Hz (Figure 47). We found that both parameters depend on distance in the same way. We estimated a Decoupling Factor (DF) as the ratio of peak (vertical) signal amplitude for the coupled (reference) shot (Ex.3) to the amplitude for a partially decoupled shot (Ex.1, Ex.2) (similar to the ratio of the Reduced Velocity Potential in Stevens et al., 1991) (Figure 48). We roughly estimated the cavity volume V as ~4 m^3 for Ex.1 and ~14 m^3 for Ex2 (see Figure 38b), and the TNT equivalent charge as W_{eq}~1000 kg (1240 kg ANFO); then the Charge/Volume ratio W_{eq}/V (kg/m^3) was calculated as ~250 for Ex.1 and ~70 for Ex.2. The average value DF_{av}= 6.4 obtained for Ex.2 (Figure 48) fits the predicted factor DF~6 for W_{eq}/V =70, calculated for a chemical shot in a 6.3 m spherical cavity in granite (Stevens et al., 2003).

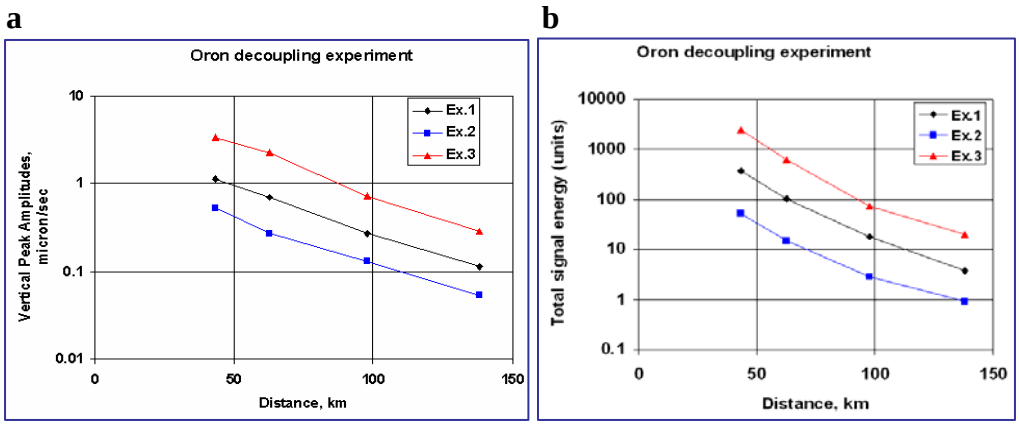

Figure 47. Vertical peak amplitude (a) and signal energy (b) at different distances.

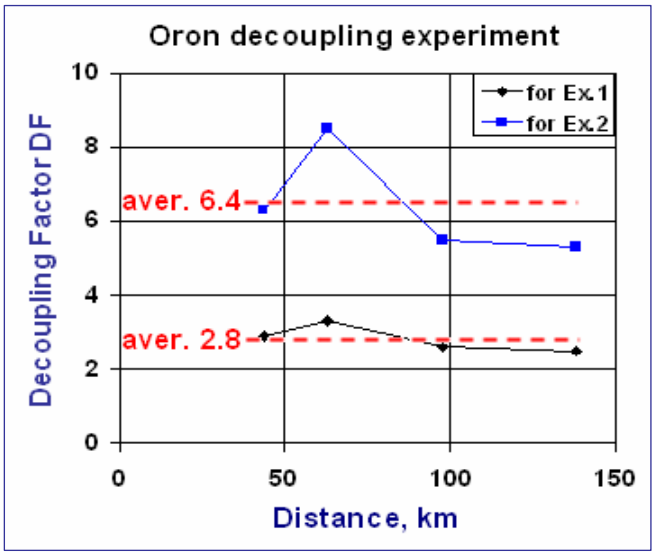

Figure 48. Decoupling Factor with range (frequency range 1-20 Hz) for partially decoupled shots in sediment (marls) media.

P, S Energy partition. We estimated seismic energy partition for the three explosions. For the four stations selected above and an additional portable SP station at ~4 km we calculated seismic energy for the phases P, S (vertical component) in time windows T with Ts/Tp~1.5 (Figure 49), and estimated S/P energy ratios (Figure 50). The results show that at all distances maximum S/P ratios are found for the coupled Ex.3, minimum S/P ratios for the deep decoupled Ex.2.

Note that the twofold larger shot depth for Ex.2 (compared to Ex.3) might result in smaller S-wave energy radiation (see below Section 4.4.3), and thus contribute together with the decoupling effect to the observed difference in S/P ratios.

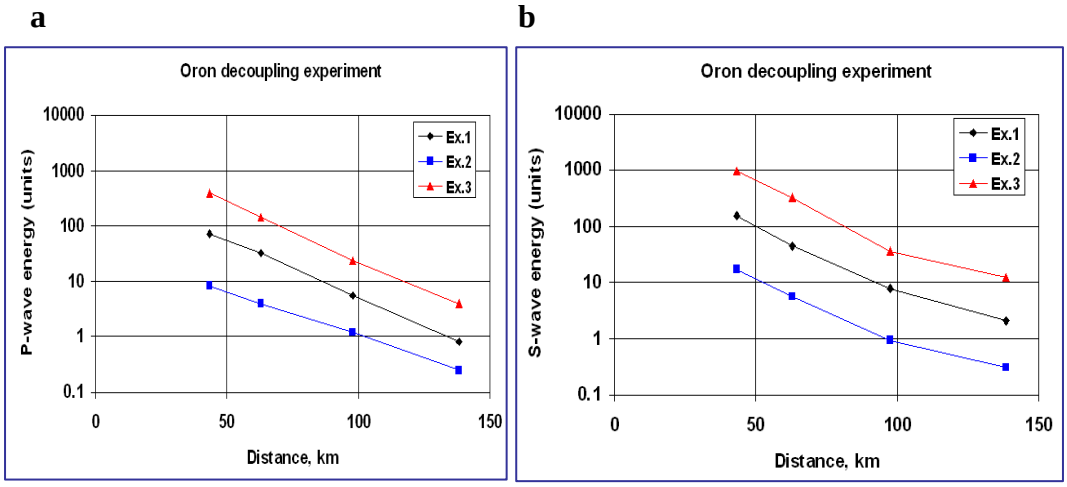

Figure 49. Seismic energy of P-waves (a) and S-waves (b) at different distances.

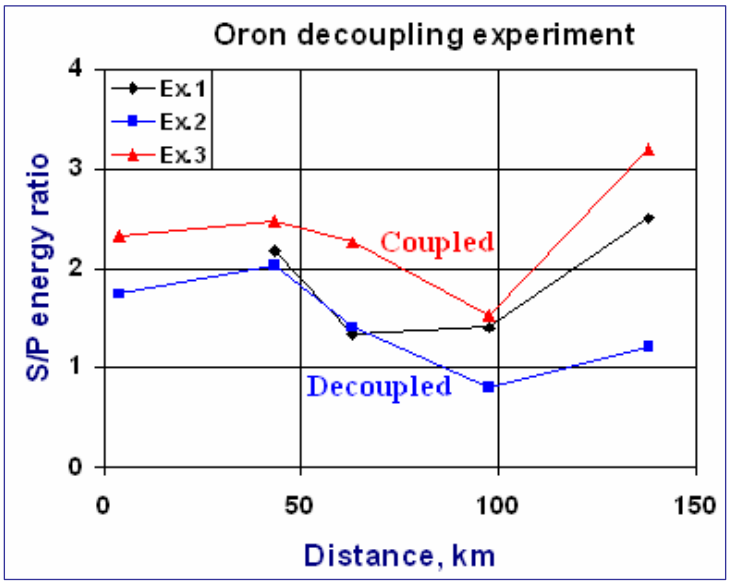

Figure 50. S/P energy ratios for the Decoupling series shots.

4.4.3. Oron Depth-of-Burial Experiment.

The key DOB experimental explosion series project was conducted on Jan 2, 2007. The main objective of the experiment was investigating relations between explosion depth and spectral/energetic/magnitude parameters of regional seismic phases, especially S/P ratio.

Geological Setting, Design and Parameters of the Explosions. The site geology was the same soft consolidated sediments as for the nearby (~2.5 km away) Decoupling Experiment site (Figures 51a, 52), thus the rock media was homogeneous for all the sources. The series included three equal near-spherical charges of 4200 kg ANFO at depths 26 m, 45 m and 59 m; spacing between the shots was 200-300 m (Table 8, Figures 51b, 52). The charge weight was the maximum which provided full containment for all 3 shots: we observed a small ground surface uplift on the video-record and thin cracks around the hole for the shallowest Ex.1, but no craters were seen (see Figures 56, 57).

Table 8. Parameters of DOB explosions.

Ex. #	Hole ID	Hole depth, m	O.T. GMT	M_L	Coord. (local)		Lat.	Long.
					X, km	Y, km		
1	OR4-21	26	09:31:12.317	2.7	149.294	34.058	30.89714	34.99353
2	OR4-19	45	10:01:13.442	2.6	149.428	33.858	30.89530	34.99498
3	OR4-22	59	10:30:31.276	2.5	149.082	33.994	30.89656	34.99133

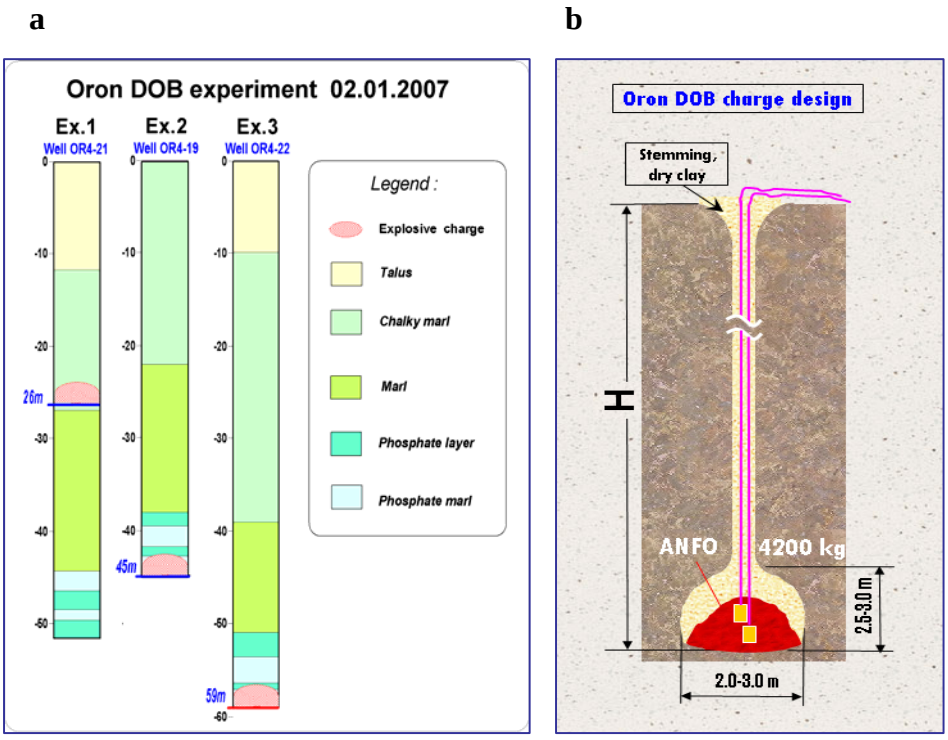

Figure 51. Geology of explosion boreholes from drilling logs (a); specific charge design providing large near-spherical seismic sources (b).

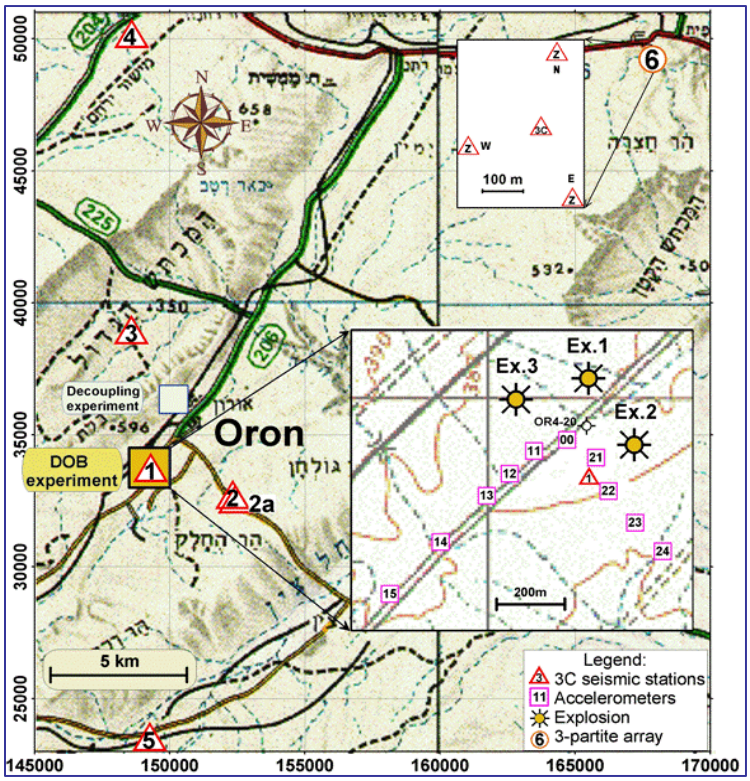

Figure 52. Location of the two experiment sites and portable stations, inserts show detailed location of the tripartite array elements (st.6) and configuration of the explosion boreholes and accelerometers.

Geophysical Site Survey. Seismic refraction and reflection surveys were conducted at the site along sections crossing the boreholes by the GII team before and after the experiment (Figures 53). Two goals were set: a) estimating subsurface velocity models in the near-source zone; b) search for changes after the shots in rock properties and characterizing the nonlinear source zone at different depths.

We planned 3 seismic profiles crossing all 3 explosion boreholes, using the same points before and after the explosions to determine any changes by comparing the results. One of the boreholes, OR4-20, was damaged by rain and replaced by an available spare hole, OR4-19, without a before profile (Figure 53b).

We present here some survey results, mainly for the refraction method. All survey details, measurements obtained and the main results are presented in a GII report (Ezersky et al., 2007). The refraction study was aimed at estimating Vp and Vs velocities of the subsurface before the explosion and estimating the velocity variation after the explosion. The data obtained show horizontal layering at the experiment site, enabling the use of a simple 1-D subsurface model (Figure 54, Table 9). The uppermost layer composed of the sedimentary Sahav (Talus) unit is largely plastic (Poisson Ratio ν=0.44). The second and third layers have similar velocities and dynamic Poisson ratio ν=0.33-0.34, typical for consolidated (rigid) rocks. The comparison of the seismic velocity before and after explosions showed velocity variations of 2-5%, on the order of the seismic refraction method accuracy.

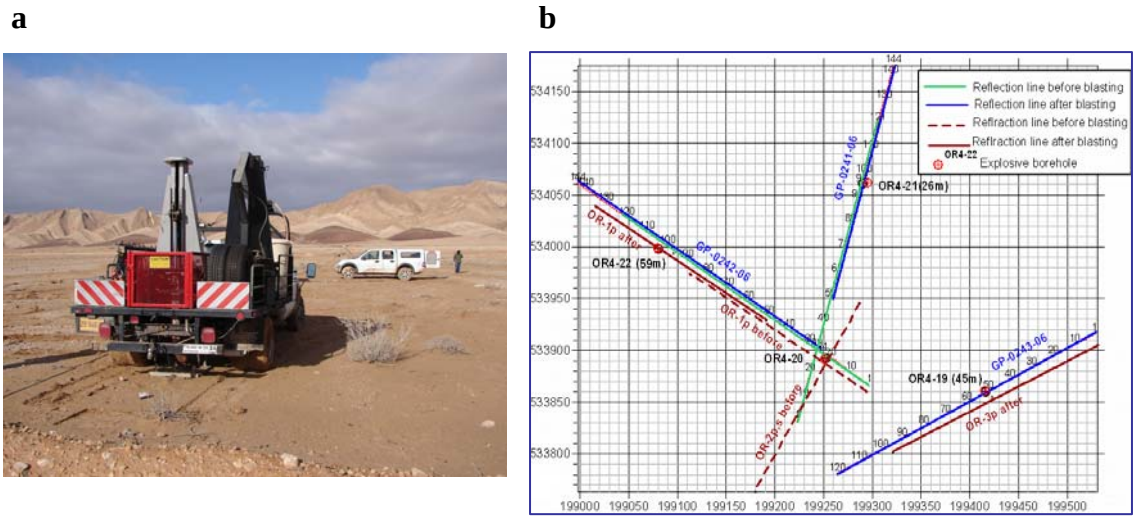

Figure 53. A vehicle-based hammer was used by as seismic source for reflection/ refraction profiling (a), map of seismic profiles planned at DOB site (b).

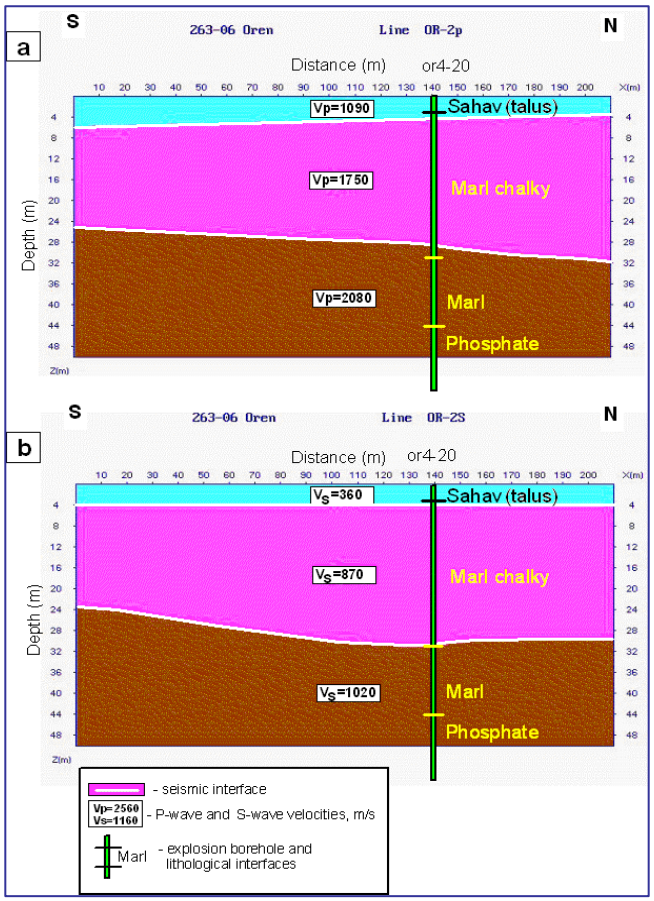

Figure 54. Refraction Vp (a) and Vs (b) depth sections along line "OR-2p,s before" (the DOB experiment).

Table 9. Subsurface velocity model (before the explosions).

Layer No.	Depth Interval (m)	Vp (m/sec)	Vs (m/sec)	Poisson Ratio, ν
1	0 to 5-7	1090-1140	360	0.44
2	5-7 to 24-32	1750-1800	870	0.34
3	Deeper than 24-32	1950 – 2080	1020	0.33

The reflection line records obtained are used for 2D imaging by means of diffraction waves. Diffraction waves can serve as an additional tool for detection of local heterogeneities (Landa and Keydar, 1998). The diffraction section, based on phase correlation of the diffraction signals on the observed seismic records, is used as an image for diffraction objects. The data are analyzed along different diffraction curves in order to find the curve closest to the travel time of diffracted waves; the result of this analysis is images of subsurface objects.

Figure 55 shows the diffraction section of line GP-0241 before and after the shallowest explosion No.1 (H=26 m) respectively. A clear anomaly located in the vicinity of station 93 and time 63 msec (Figure 55b) indicates a diffraction object (possibly a void, created after the large contained shot). This station position corresponds to the location of the explosion borehole OR4-21 (see Figure 53b). No anomaly is found in the data before the explosion (Figure 55a).

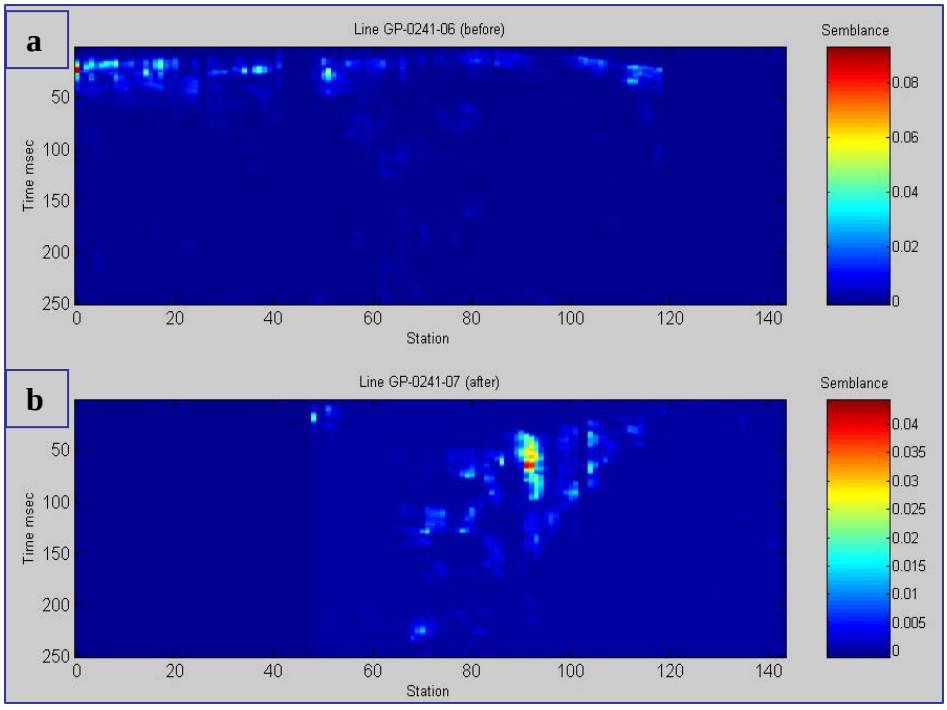

Figure 55. Diffraction section of line GP-0241, before (a) and after (b) Ex.1 (H=26 m).

Unfortunately, reflection data for the two deeper explosions did not provide any sign of changed media properties in the source vicinity, due to the limitations of the method for the method configuration and density of observations method.

Surface Explosion Effects. All three DOB explosions were fully contained, i.e., there was no rock spall and gas venting. The high fountain of dust for Ex.1 (H=26 m) was induced by the shock wave impact on the stemming column (Figure 56a); an additional role of the detonation cord is hypothesized in the lesser dust cloud for the deeper Ex.2 (Figure 56b); for the deepest Ex.3 a small cloud was barely observable (Figure 56c).

Figure 56. Surface effects during detonation for Ex.1 (a), Ex.2 (b) and Ex.3 (c).

No craters were observed on the surface around the boreholes after the experiment. For the shallow Ex.1 a clear ground surface uplift was observed on the slow-motion video-record, and a system of thin radial and tangential cracks was observed on the surface around the borehole to a radius of about 10-15 m (Figure 57).

Figure 57. Surface (radial) cracks around the Ex.1 borehole.

Recorded Data. Different 3C observation systems were deployed at near-source distances: 10 accelerometers ETNA, range 120-870 m; 4 SP seismic stations L4C, 3.5-16 km; a tripartite SP array (st.6) at 24 km deployed by the Israel NDC (Figure 52). Extensive good quality datasets were obtained for all explosions from portable and permanent regional seismic stations, including IMS BB stations EIL, MMAI array, and ASF, Jordan (Figure 1), in the distance range 0.15-238 km. The records showed signal characteristics and energy generation features related to these specific near-spherical seismic sources at different depths.

Near-Source Observations. On near-source accelerograms the highest amplitudes are observed for the deepest Ex.3, though it was the weakest event at regional distances with the smallest estimated magnitude (Table 8). A clear trend of peak amplitude and energy enhancement with charge depth is seen, with an increase of signal at higher frequencies. Sample vertical accelerograms for the closest (ACC00) and furthest (ACC15) accelerometer stations and the whole signal amplitude spectra (Figure 58) show that the largest PGA values for Ex.3 are accompanied by high frequencies: maximum energy at 10-20 Hz and significant spectral peaks at higher frequencies up to 40-50 Hz, unlike the shallow Ex.1 with maximum energy at 3-14 Hz and a sharp drop at higher frequencies.

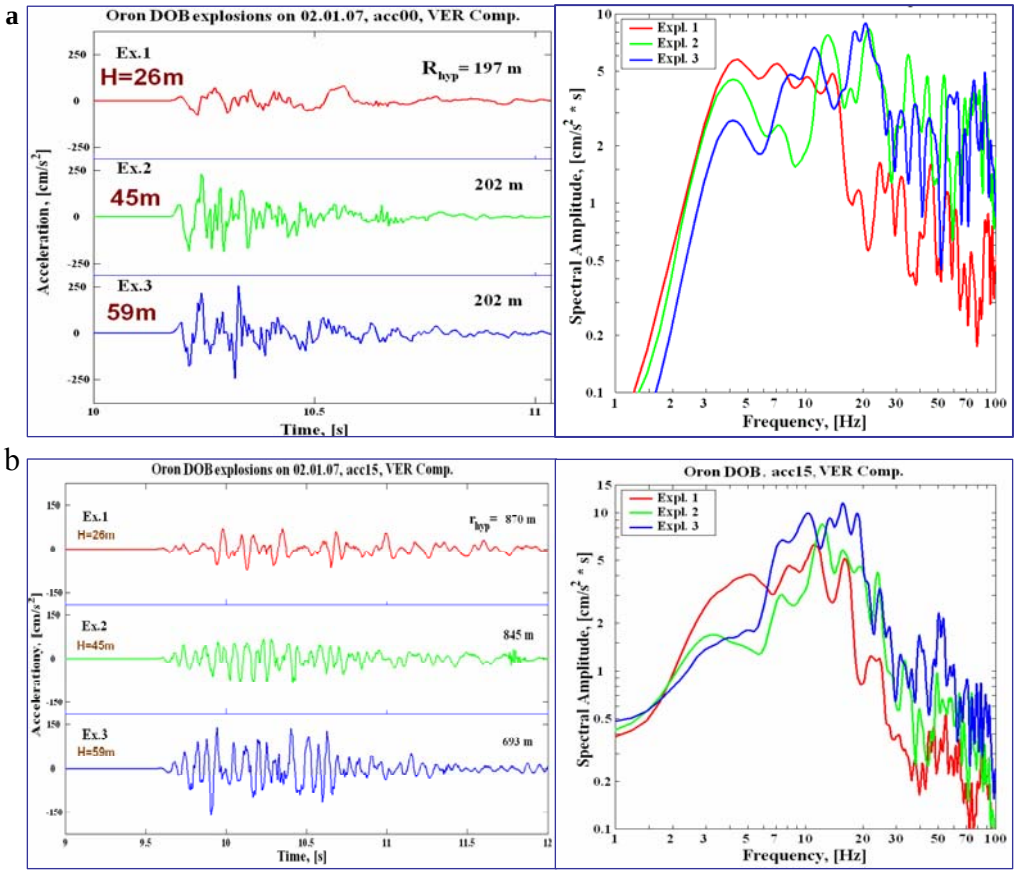

Figure 58. Vertical accelerograms and amplitude spectra at the closest station ACC00, equidistant from 3 DOB shots (a), and the remotest station ACC15 (b). Hypocentral distances to the shots are shown.

Horizontal Component Transformation. For better analysis of the signal horizontal components we transformed EW and NS records at the sensor AC00 (equidistant from all shots) to Radial and Transverse components for each explosion (Figure 59). At low frequencies (1-10 Hz) a trend of spectral amplitude decrease for deeper charges is observed, clearest and most systematic on the Transverse component. At high frequencies (10-100 Hz) this tendency is reversed, and the largest difference between the shallowest and deeper sources is seen on the Radial component.

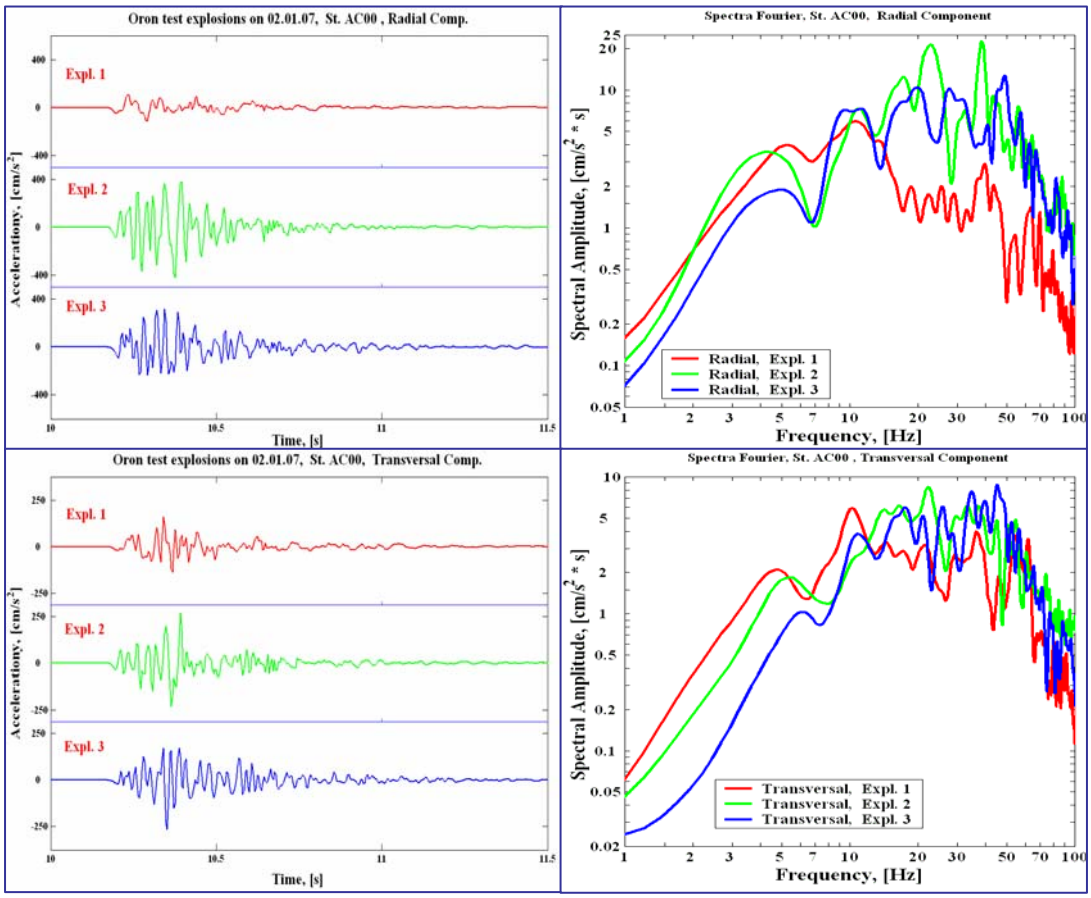

Figure 59. Transformed Radial and Transverse components and appropriate amplitude spectra at the sensor AC00 (equidistant from all shots, r~200 m).

Amplitude/Energy Attenuation Scaling in the Near-Source Zone. We calculated the Peak Ground Acceleration (PGA) vector (Eq. 4) and signal power (energy) vector (Eq. 8) at different distances.

$$POWER_{vector} = \sum(A_{EW}(t_i))^2 + \sum(A_{NS}(t_i))^2 + \sum(A_{vert}(t_i))^2 \qquad (8)$$

The results show (Figure 60) that in the near-source zone (200-870 m) signal peak amplitude and energy increase systematically with source depth. We found this effect at all accelerometers in all 3 components, confirming that it is not a site-effect, or a propagation feature.

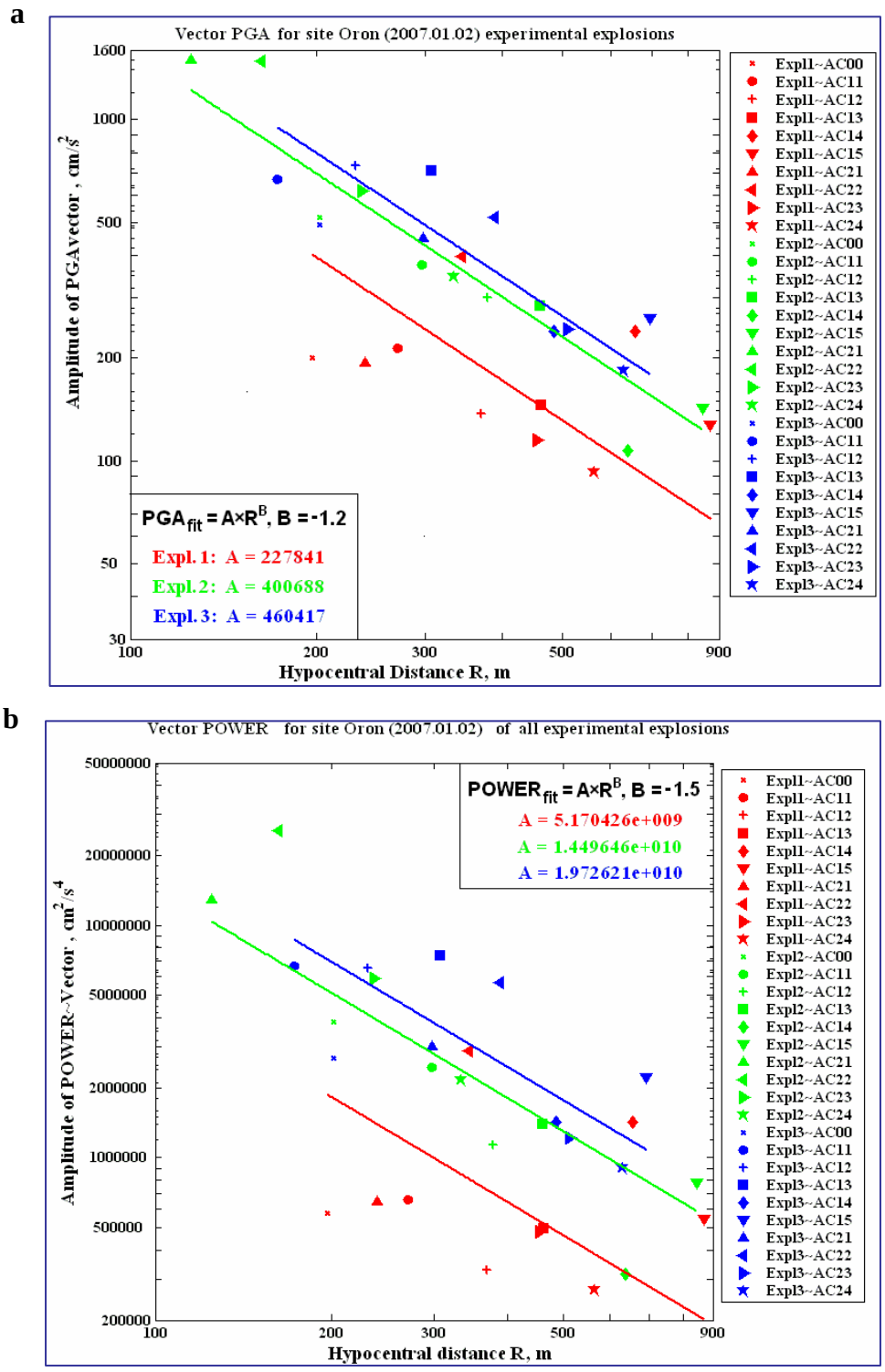

Figure 60. Attenuation of PGA (a) and POWER (b) vectors with distance.

Close Local and Near-Regional Distances. As close as r~3.5 km the attenuation of high-frequency seismic energy results in smaller peak amplitudes and spectra in the range 0.5-10 Hz for Ex.3 relative to the other explosions, even though it still has greater energy at higher frequencies (Figure 61). A drop in amplitude for the deepest Ex.3 compared to Ex.1 is clearly seen at on the record of the 3-component SP st.6 in the portable tripartite array at 24 km (Figure 62). Reduction of signal energy and event magnitude with source depth (e.g., Richards and Kim, 2005) is observed at all local and near-regional distances (Figure 63). Decrease of spectral amplitudes with increasing shot depth between about 1 and 10 Hz is reversed to the opposite trend at higher frequencies ~10-20 Hz (Figures 61-63b). Local (duration) magnitude M_L values for the 3 DOB shots, averaged over several stations of the Israel Seismic Network and plotted versus source depth, shows an approximately linear relationship (Figure 64a). A similar correlation for the analogous Balapan DOB experiment is plotted in terms of energy class K values estimated from regional stations (Mikhailova et al., 2001) (Figure 64b).

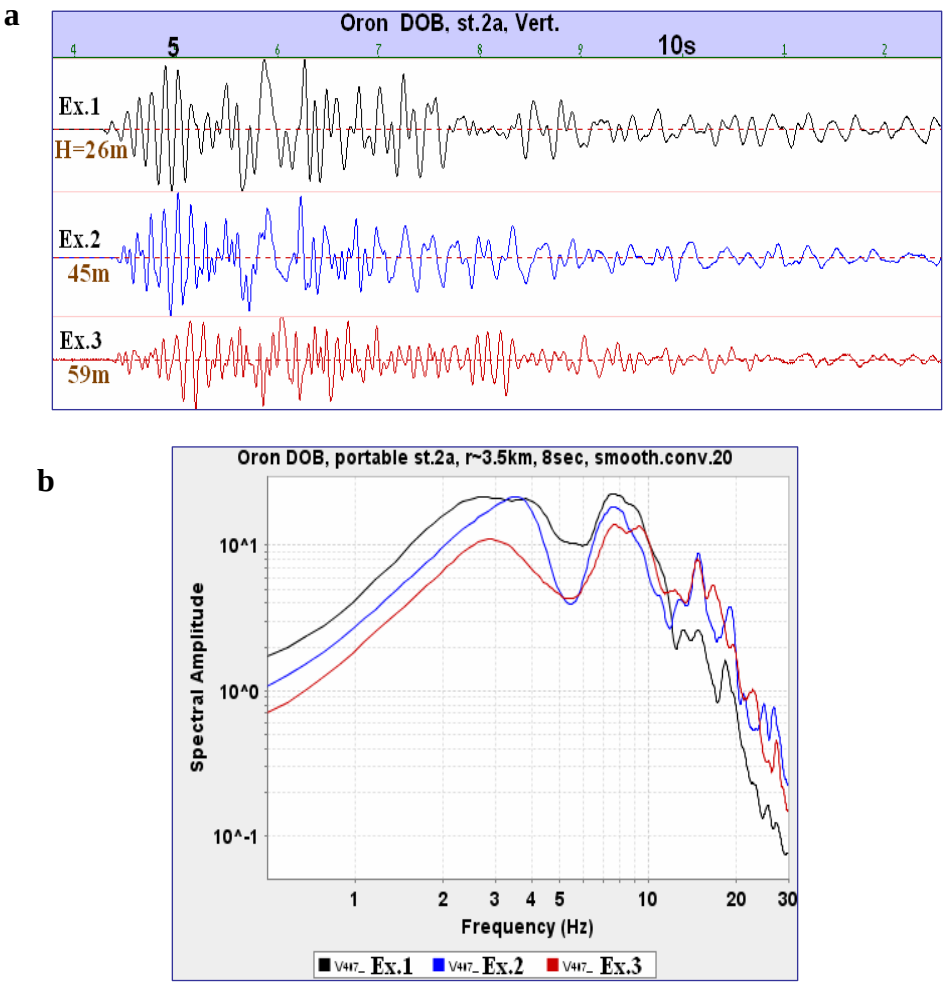

Figure 61. Vertical seismograms in absolute scale (a) and spectra of the whole signal (8 sec) (b) at the closest SP station at r~3.5 km. Note dominant energy for the deepest Ex.3 at high frequencies f >10Hz.

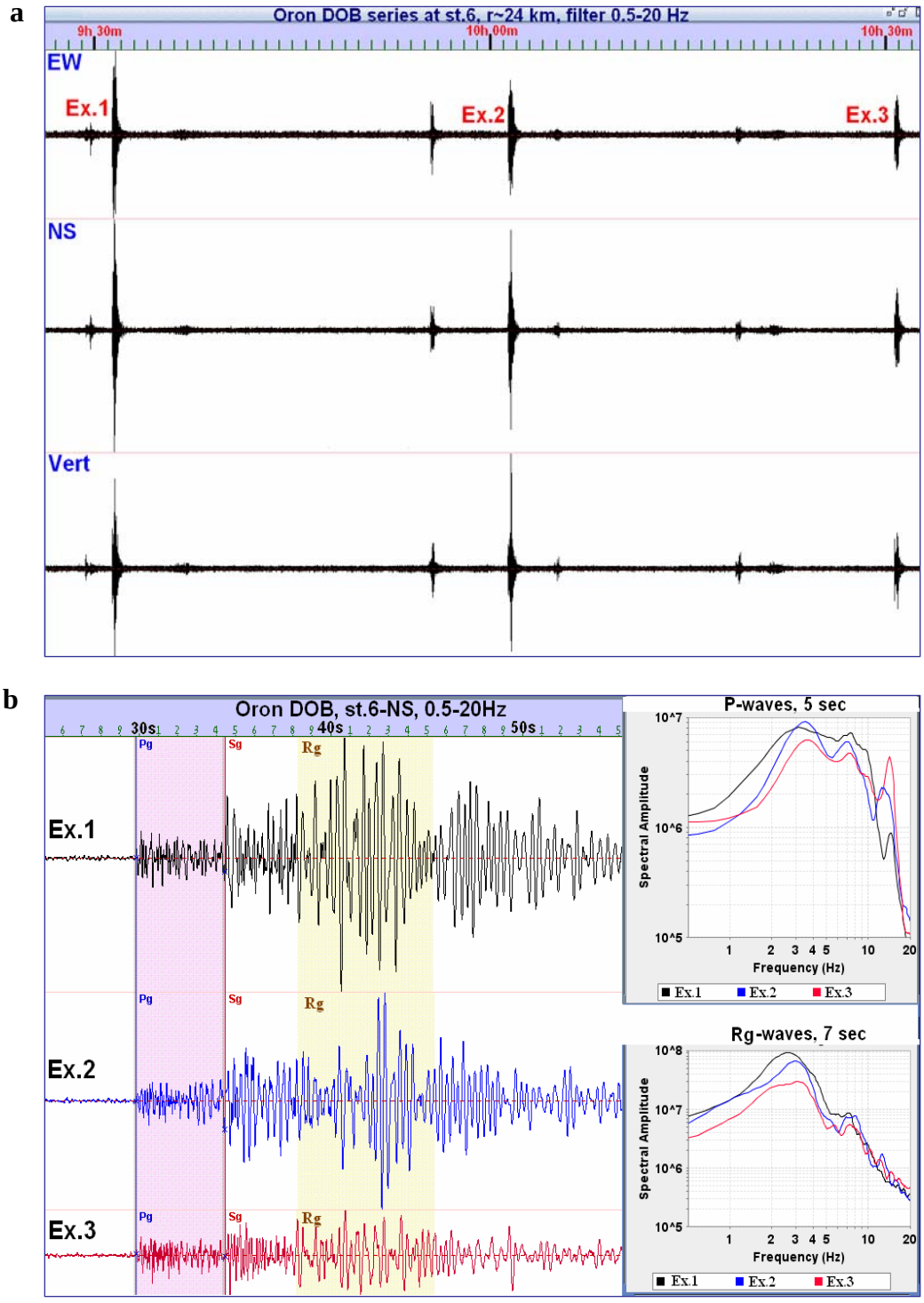

Figure 62. Close local recordings (in absolute scale) at the central 3C station of the SP tripartite array (St.6) at r~24 km: continuous 3C recording section of all 3 shots (a), NS records and spectra of P and Rg phases (b). A clear Rg onset is observed on vertical records (velocity ~2 km/s). Note a dominant spectral peak for Ex.3 at 13-15 Hz in P-phase which is not observed in Rg-phase.

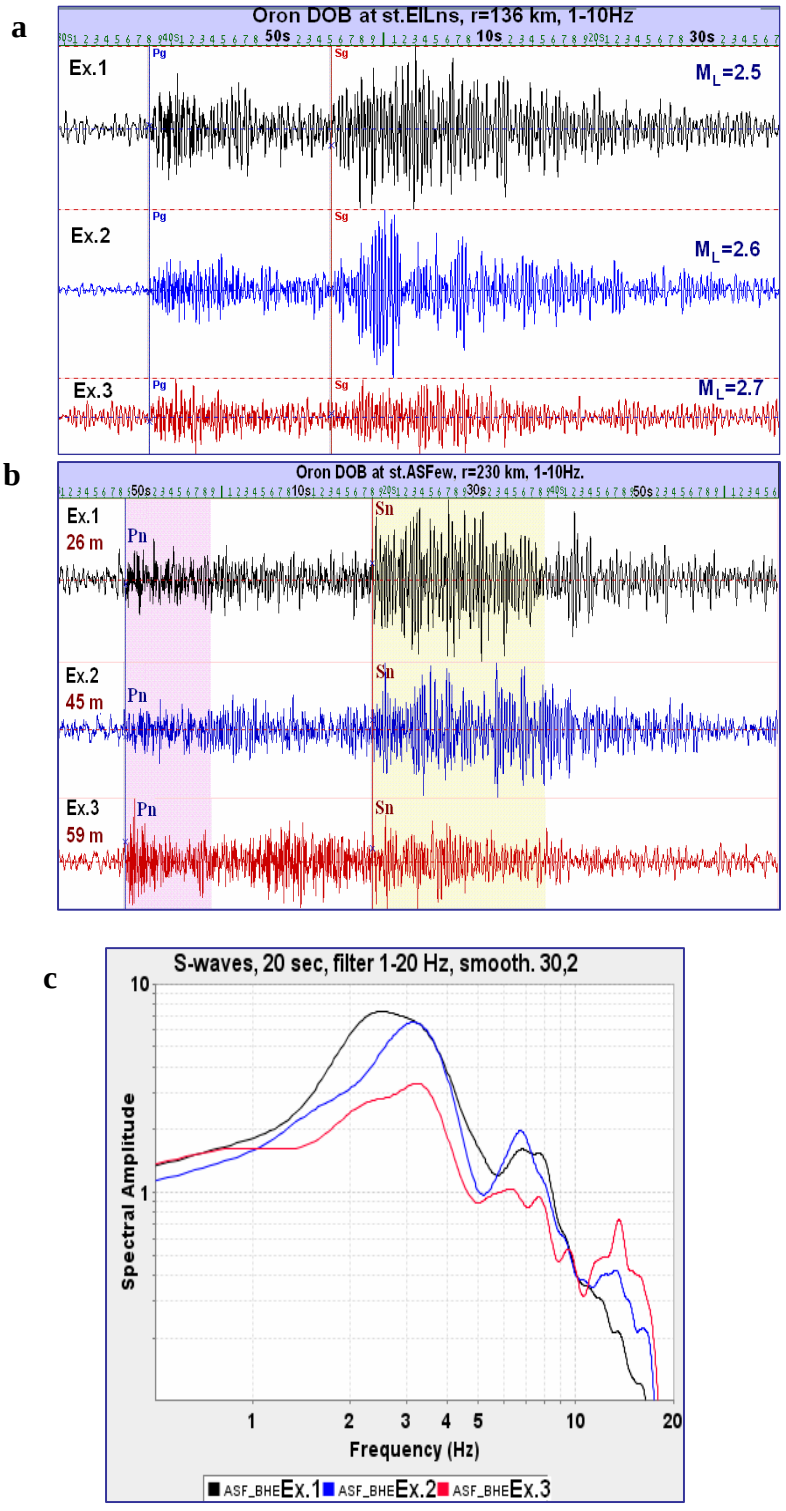

Figure 63. Horizontal seismograms (in absolute scale) at two IMS BB stations: EIL-NS (Radial) component (a), ASF-EW (~Transverse) component, windows for calculation spectra and spectral ratio are shown (b); crossover of spectral dominance for different shots at ~10Hz is clearly observed at ASF (c).

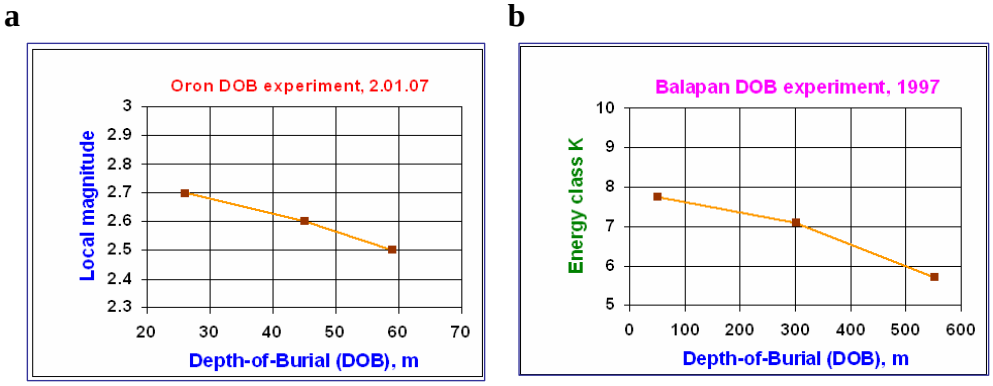

Figure 64. Magnitude versus source depth for two DOB experiments: local (duration) magnitude M_L at Oron (a) and Energy class K at Balapan (b).

Modeling of Seismic Sources at Different Depth. Based on the Mueller and Murphy (1971) model, spectra were predicted for explosions of the same (4.2 tons ANFO) small yield (nominal 0.01 Kt nuclear) at the source depths of 26, 45 and 59 m, used in the Oron experiment (J. Murphy, personal communication) (Figure 65a). It appears that the seismic observations (Figure 65b) are remarkably consistent with the model prediction of a crossover point of spectral dominance at ~10 Hz for different shot depths, This can be observed on accelerograms at near-source distances of 200-800 m, local seismograms at 3.5 and 24 km, and clearly at a regional distance of 230 km (st. ASF)

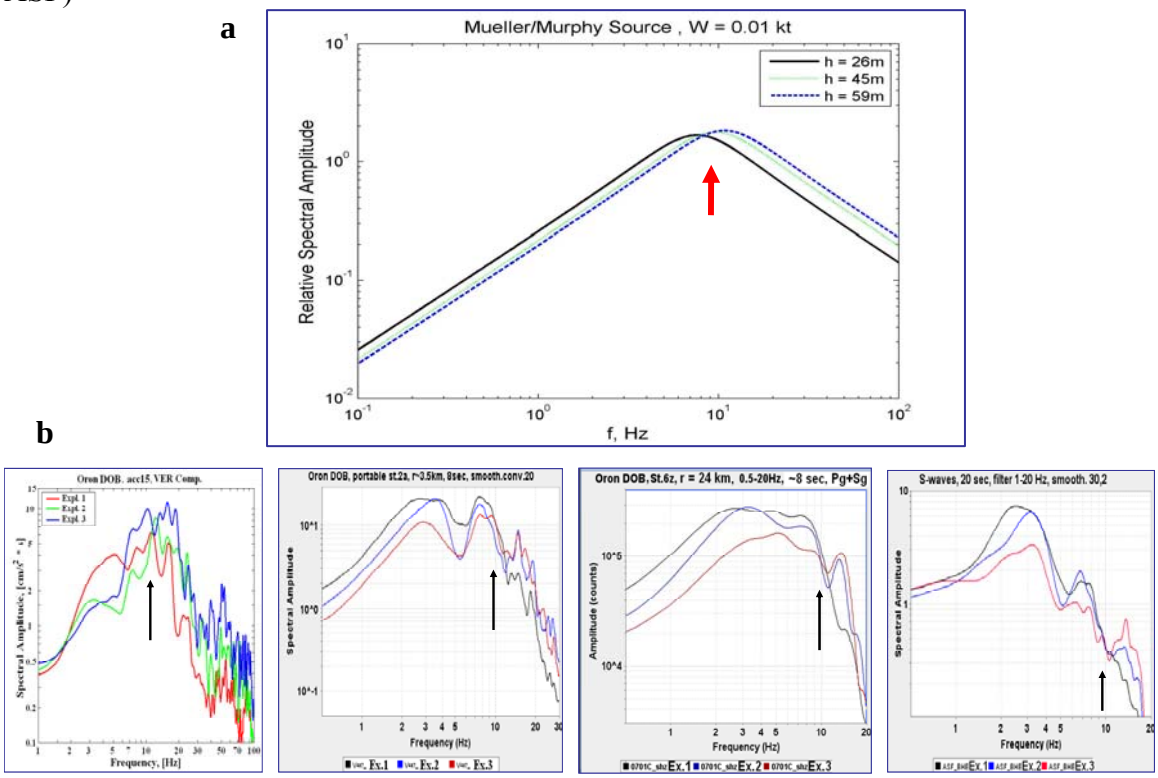

Figure 65. Comparison of Mueller-Murphy source model predictions (a) and observations (b) at different distances.

Energy Generation and Partition. To better characterize seismic energy generation for the Oron DOB explosions we calculated the whole signal energy in the time domain recorded at 3C stations in the distance range 24-238 km for different components – Vertical, Horizontal (the sum of energies for NS and EW components) and Vector (Figure 66). The Vertical energy shows a rather weak decrease with source depth, while the Horizontal and Vector values drop more sharply.

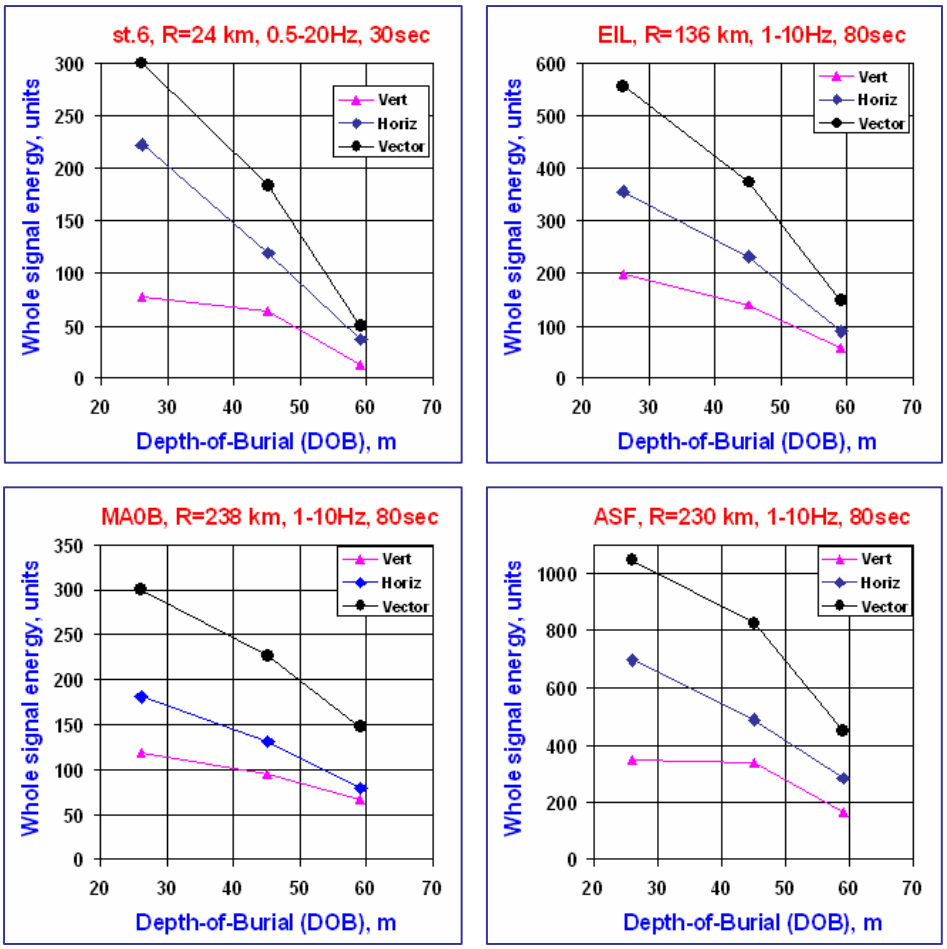

Figure 66. Seismic energy of the whole signal recorded at different components of several SP and BB stations versus source depth. Note different frequency range (filtering used) and signal duration.

As expected, at close local and near-regional distances observed amplitudes and energy of S-waves shows significant and systematic decrease with depth; P-waves remain approximately constant or even increase (Figures 62b, 63b). We evaluated the relative excitation of P and S energy using 3C stations, with identical propagation paths in the experiment, for differing source depths. We calculated P/S spectral ratios for smoothed amplitude spectra of P and S phases and S/P energy ratios for different regional phases (Figures 67, 68). Different time windows were used depending on distance and reliable

phase identification: equal short duration for clear phases Pg and Sg (4 sec), and Rg (7 sec) at the close SP st.6 (24 km) (see Figure 62b), and larger variable windows for the P-group (10 sec) and S-group (20 sec) at remote BB stations EIL, ASF and MMA0B (Figures 63, 67a), these include (Pn, Pg) and (Sn, Sg, Lg), because different P and S phases are not well separated at this distance range. Filtering was applied to the close (0.5-20 Hz) and remote (1-10 Hz) records.

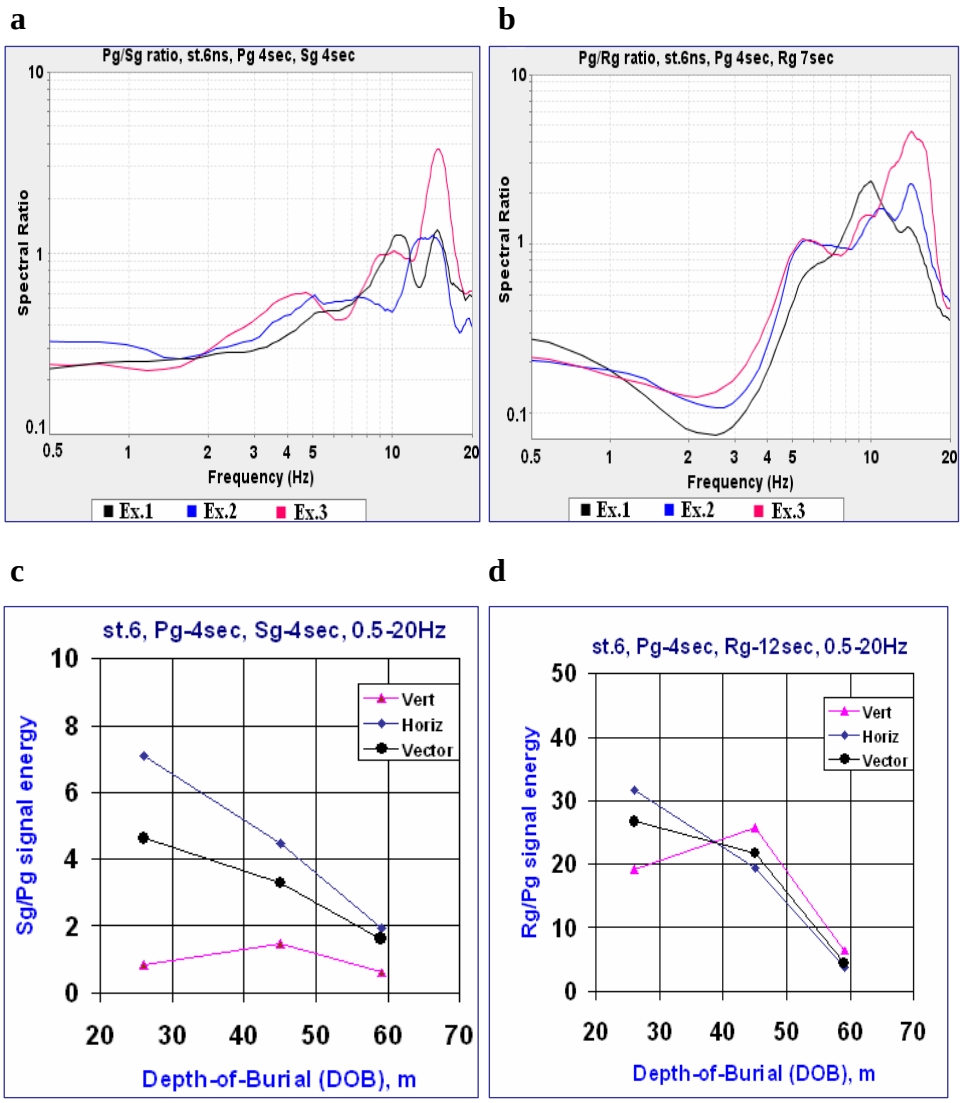

Figure 67. Energy partition at close local station st.6 (24 km): spectral ratios Pg/Sg (a) and Pg/Rg (b) show a weak dependence on source depth at 2-5 Hz; signal energy ratios Sg/Pg (c) and Rg/Pg (d) show an obvious decrease for deeper shots, especially for the Horizontal (EW+NS) component.

a

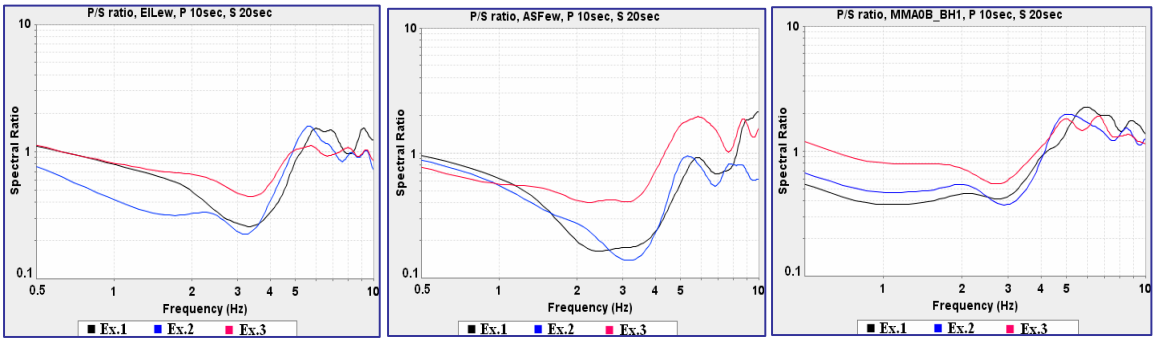

b

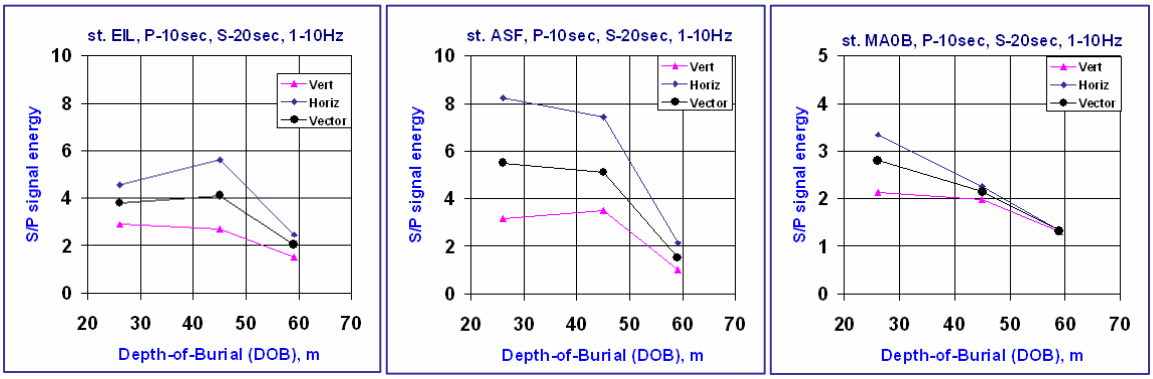

Figure 68. Energy partition at near-regional distances: spectral ratios P/S show decreased S-wave excitation for deeper shots in the range ~(0.5-8) Hz (a); signal energy ratios S/P decrease, in general, systematically with depth (b).

Spectral ratios of Pg/Sg and Pg/Rg at the close st.6 (24 km) (Figure 67a,b) show a weak dependence on DOB in a narrow band of 2-5 Hz, whereas at near-regional distances a clear strong rise in the ratios is observed with increasing explosion depth in a broader spectral range (0.5-8 Hz) (Figure 68a), similar to results obtained for the Balapan DOB experiment (Myers et al., 1999). Another characteristic of the radiated energy partition is that the signal energy ratio S/P shows a systematic (on average) decrease for deeper shots, especially for the Horizontal component.

P/S Energy Ratios vs Distance. P/S energy ratio was computed at 3C stations located at different distances from the three DOB explosions. A phase energy was estimated by Equation (8)by two methods. In the first method the time interval for the P and S phases was fixed and chosen equal to 2 sec, the start of the time interval was the visual phase arrival or the theoretical arrival, if the real arrival was not clear (Figure 69a). In the second method the time interval was chosen empirically to include most of the phase (P,S) energy and the energy computed was normalized to the time-interval length (Figure 69b). Both plots show increasing P/S ratios with distance and depth.

a **b**

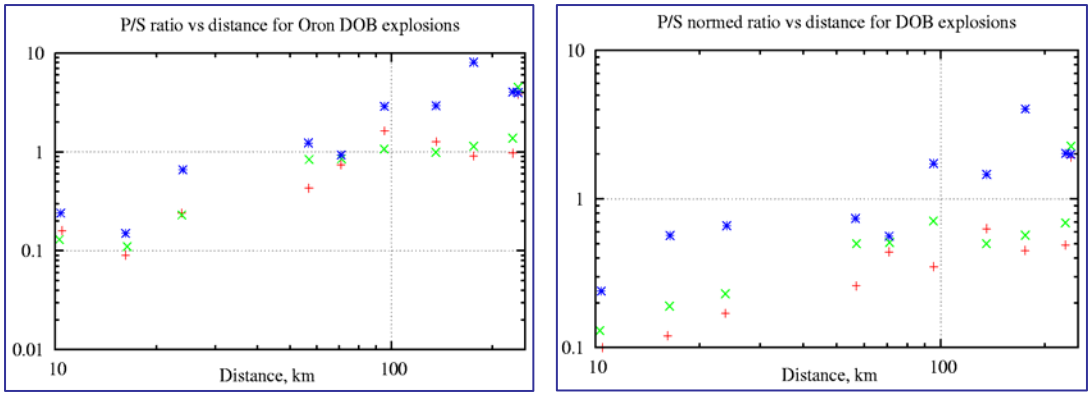

Figure 69. P/S energy ratios for fixed (a) and variable (b) time windows.

Location Analysis. A special feature of the Oron DOB experiment - the placement of the charges in holes, separated by only a few hundred meters, in order to eliminate variations in waveforms and travel times due to different propagation conditions - provided a good opportunity for a comparative location study. Using measured P onsets and a local 1D velocity model, the three explosions were located by two procedures: the standard grid-search least square procedure (LSQR), and a new model-free robust "Grid-Sign" algorithm (GS) (Pinsky, 2007) with the advantage of eliminating error of the unknown velocity model misfit (Figure 70, Table 10).

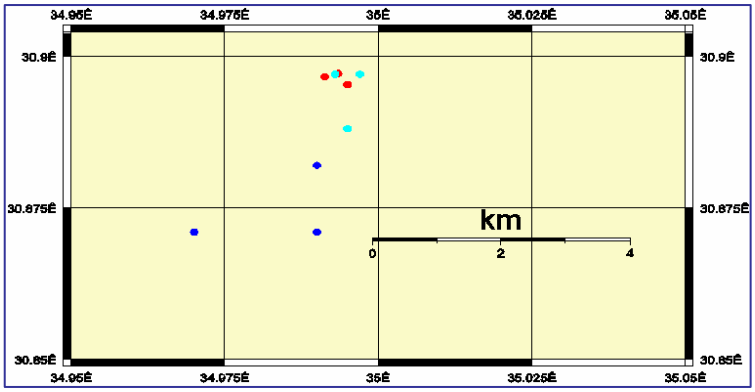

Figure 70. Location of the three DOB shots (● - Ground Truth) by the LSQR (●) and the GS (●) algorithms.

Table 10. Location error for three DOB explosions by different algorithms

#	Number of stations	GS Error, km	LSQR Error, km
Ex.1	17	0.5	2.2
Ex.2	22	1.2	3.1
Ex.3	14	0.6	3.1

4.4.4. Discussion

The Oron Decoupling experiment was not ideal, because the series shots were not placed at the same depth. However the main features of the decoupling effect were observed and estimated, roughly matching theoretical concepts. The high frequencies (40-50 Hz) which we observed for near-source accelerograms of the decoupled shot, are lower than modeled for shock-wave reverberation (100-600 Hz) from nuclear sources (Stevens et al., 1991). This can be explained by air shock-wave velocities for small chemical charges being much lower than for nuclear detonations with their extremely high temperatures and pressures. The results show that the unique design used of near-spherical sources can be used for preparation of a full-scale, ideal and cost-effective Decoupling Experiment.

The design and configuration of the Oron DOB series were preferable in some conditions compared to the previous Balapan DOB experiment (Table 11). Initially we planned much deeper and later somewhat smaller depths than realized, but after discussions (A. Dainty, personal communication) we decided the final charge depths in order to provide:

1) scaled depths in the range of NTS nuclear tests h=95-425 m/kT$^{1/3}$ (Springer et al., 2002);

2) full containment of all series shots.

Table 11. Comparison of design for two DOB experiments.

Parameter	1997 Balapan DOB, 25 ton TNT	2007 Oron DOB, 4.2 ton ANFO (~3.4 ton TNT)
Charge shape, aspect ratio AR	cylinder, L~34 m, AR~34	near-spherical, R~1-1.5m, AR~1
Scaled depth h=Hc/W$^{1/3}$, m/kT$^{1/3}$	113, 968, 1823	167, 294, 387
Rock homogeneity	50-m shot – in sediments (shales), others – in granites	Consolidated sediments: marls, chalky marls, phosphate marls
Explosion containment	50-m shot created a 40-m crater, for deeper shots the casing was ejected	all shots contained, 26-m shot created surface thin cracks
Spacing of the series shots	2.5-8.2 km	220-360 m (the same propagation path even for close stations)

Increase of overburden lithostatic pressure with depth opposes the opening and propagating of cracks, thus limiting the inelastic zone and decreasing source volume (Sharpe, 1942) and volume expansion δV (Richards and Kim, 2005). Higher dominant frequencies of the radiated signal that we observed in association with the largest near-source signal amplitudes for the deepest shot was followed by rapid attenuation of seismic energy with distance and the smallest local magnitude.

For a long vertical source the decrease in pressure at shallow depth causes much stronger non-linear deformation above the explosion than below it, and this asymmetry results in generation of shear waves, which would not be so strongly generated by spherical sources (Stevens, 2006). An important goal of our experiment was to ameliorate the asymmetry effect caused by the difference of lithostatic pressures above and below the vertical, lengthy, cylinder explosive source, typical for borehole chemical explosions. Nevertheless, we note that the observed small amplitude surface uplift for the shallowest Ex.1, H=26 m, may indicate an asymmetry effect caused by closeness to the surface, contributing to generation of larger S-wave energy.

4.5. Magnitude Scaling

We used data from Ground Truth simultaneous explosions conducted in the project for analysis of magnitude dependence on charge weight. Some other experimental in-land and underwater shots conducted before by GII in previous DSWA/DTRA projects (Gitterman et al., 2002, 2004) and in the MERC project (Gitterman et al., 2005b), were also included. The analysis results are shown in Figure 71, where the observation values and different curves fit for simultaneous shots are presented for comparison. Three of them were developed earlier for different type of explosive seismic sources:

[1] Under-Water Explosions (UWE) includes calibration and experimental shots in the Dead Sea conducted by GII (Gitterman, 1998, Gitterman and Shapira, 2001, Gitterman et al., 2005a): $M = 0.285 + \log10\ (W, kg)$. Two recent experimental shots (750 kg) in October 2004 agre well with previous data and the fit curve [1].

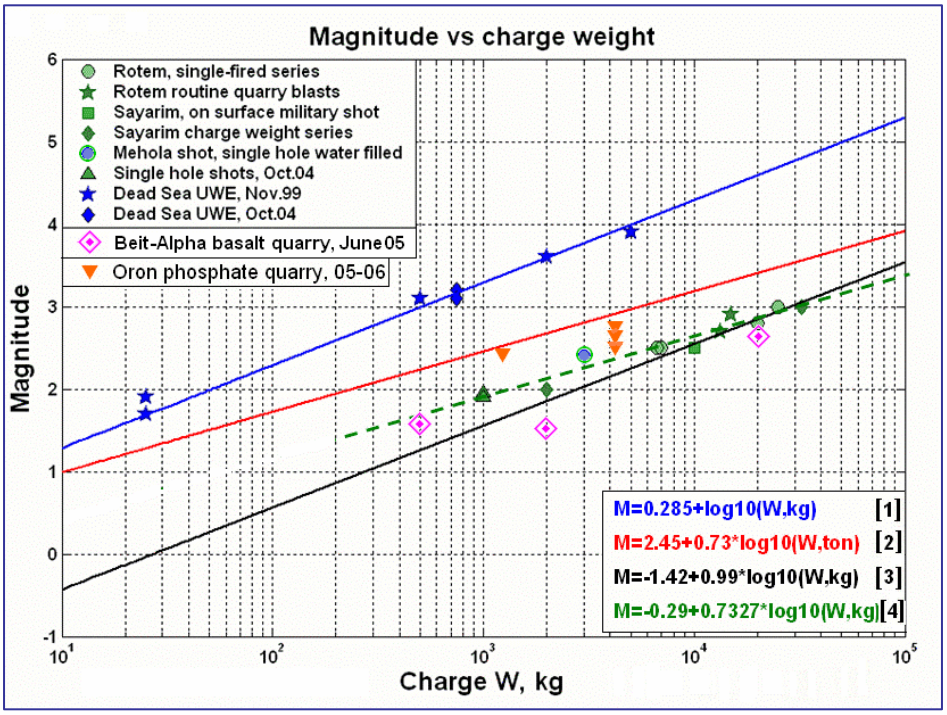

Figure 71. Magnitude versus charge for GT0 single-fired experimental explosions and quarry blasts conducted by GII in Israel.

[2] Upper limit of magnitude for known-yield sources in hard rocks (Khalturin et al., 1998): M=2.45+0.73*log10(W, ton). All values for the land explosions collected are below the curve [2].

[3] Single-fired controlled commercial blasts at Israel quarries, including a limited dataset (Gitterman, 1998): M = -1.42 + 0.99*log10(W, kg).

[4] The new data for experimental land explosions are not entirely consistent with curve [3], therefore we developed a new equation fitting the observed data: M = -0.2937 + 0.7327*log10 (W, kg). Note that the estimated scaling parameter (the curve slope) of 0.7327 is very similar to the upper limit curve [2].

Discussion. Analysis of the results leads to the following conclusions:

a) Comparison of local magnitude values for Sayarim buried explosions (June 2004) with the Rotem series data (Gitterman et al., 2002) conducted in consolidated rocks (kaolin) with concentrated near-spherical charges does not show any significant magnitude change. As obtained from regional observations, significant seismic coupling was achieved (M_L~2 for S2 and M_L~3 for S3) in spite of non-consolidated sediment media of dry alluvium, considered commonly as a low-coupling material (e.g. US Congress, 1988), and shallow burial depth that caused poorly contained explosions (scaled depth 1.1-1.4 m/kg$^{1/3}$). Possibly, the downward detonation direction and contact of the charge at the bottom with a consolidated rock layer contributed to the strong seismic effect.

b) Three large land quarry/military blasts conducted in 2004 showed unusual large seismic energy release, leading to high local magnitude M_L values estimated from Israel network observations. The Rotem quarry blast R2 of 15 ton ANFO in several dozen holes with delays produced a seismic event with magnitude 2.9 that is very close to the energy produced by the Sayarim experimental large simultaneous explosion of 32.5 ton ANFO in 11 holes (located ~120 km to the South) that yielded magnitude ~3.0.

c) Likewise, the surface military explosion of ~10 ton of TNT to destroy out-dated ammunition, in a trench and open to the air, produced a significant magnitude 2.5, and clear seismic signals are observed up to 160 km, along with very strong acoustic waves.

d) The Dead Sea underwater shots in October 2004 with charges of 750 kg of TNT at 50 m depth fit well to the previously developed curve [1] for UWE with less-energetic explosives (Henamon) but at a larger depth of 70 m.

e) Insufficient scaled charge depth *h* resulted in reduced seismic strength/magnitude for the Beit-Alpha explosions of 20 tons (h=1.0-1.2 m/kg$^{1/3}$), M_L=2.6 (instead of 2.8) and especially 2 tons (h=1.0 m/kg$^{1/3}$), M_L=1.4, producing rock spall and energy loss to the air. Unlike those two shots, the scaled depth h~1.5 m/kg$^{1/3}$ for the two 0.5 ton shots was large enough to provide full containment, and the magnitude M_L~1.5, fit the previously developed curve well.

f) Compared to single explosions in large-diameter holes in alluvium (Sayarim) and weathered basalt (Beit-Alpha), the coupled Oron shots in the Decoupling Experiment (Ex.3, 1240 kg) and DOB Experiment (4200 kg) demonstrated strong seismic strength, close to the upper limit of magnitude curve [2]. Several factors possibly contributed: favorable mechanical properties of the emplacement rocks (marls), full containment of the explosions, scaled depths closed to optimal, and near-spherical charge design.

5. CONCLUSIONS

The project event database was created to study empirical features of seismic energy generation for different seismic sources (especially for S waves from explosions), and how this energy is partitioned between P and S waves. The explosions selected have a broad variety of design features (buried and surface sources, tamped and decoupled shots, large diameter 0.5-0.8m borehole and near-spherical cavity charges), charge weight (100 - 32500 kg), depth (14 – 62 m), scaled burial depth (1.0-3.9 m/kg$^{1/3}$), emplacement rocks (alluvium, basalts, marls) and geological settings (graben filled by Quaternary alluvial conglomerates in Sayarim Valley, near Eilat; Pliocene cover basalt flow, weathered and cracked in the subsurface layer, Galilee).

A number of single-fired explosion experiments were conducted in the project by GII. Numerous vertical and 3C observations were acquired in a broad distance range: in the near-source zone (0.1-0.8 km) by accelerometers, by close local portable stations (3-20 km), at near-regional distances (390 km) by seismic stations of national networks in Israel and Jordan, and IMS stations, including a seismic array. GT1 parameters and local seismic station records were collected for number of large controlled quarry and surface military blasts. The extensive recording datasets collected provided a variety of waveform features, and spectral and energy estimates.

To fulfill the project goals existing software was modified and new programs and scripts were developed. The software package jSTAR developed at GII was modified to fit the objectives of the project and used for the processing and analysis of the waveforms collected. Numerous new features were added; the most significant procedures were transformation of the ground motion components, spectral and sonogram analysis of seismic and infrasound signals, and calculation of energy statistics for recorded waveforms in the time and frequency domain.

The newly-developed computer procedures were applied to the Sayarim experimental explosion series of variable charge weight (0.3-32.5tons). Results obtained show clear dependencies of S/P maximum amplitude and energy ratios on distance and yield. We analyzed the ratios for selected events in different time and frequency bands; the results confirmed the potential of the average ratio statistics for identification of explosion sources.

As seen from regional observations, significant seismic strength was achieved in spite of non-consolidated sediment media (dry alluvium), commonly considered low-coupling material, and shallow burial depth that resulted in poorly contained explosions (gas venting, rocks spall, and cratering). Source scaling estimates based on BB records at local distances of the same series show similar yield scaling parameters (0.87-0.93) for different regional phases. The power law parameter values (approximately a linear increase in peak amplitude with explosive weight) are in close agreement with the constants for nuclear explosions in Nevada and chemical explosions in Wyoming.

A series of single-fired explosions of different charge weight (0.5-20 tons) and type of explosives (ANFO and TNT) was conducted at the Beit-Alpha basalt quarry, in a different geological environment. The largest shot of 20 tons was reversed with repect to the Southern Sayarim shot of 32.5 tons of similar design. The important role of the scaled charge depth for seismic energy generation was demonstrated, and the explosion yield.

More seismic energy was seen at near-source and local distances for the TNT shot compared to the ANFO shot of the same design.

A new magnitude-charge equation for land shots was developed based on the GT0 data with a scaling factor similar to the estimate of magnitude upper limit for sources of known yield in hard rocks.

GT0 data and records collected for experimental military surface detonations in the Sayarim area provided observations of strong acoustic arrivals at remote seismic SP and BB IMS stations. Combined interpretation of the seismic and infrasound signals obtained will contribute to the analysis of energy generation and partitioning from explosion sources, source characterization, and related identification tasks.

Two source phenomenology experiments were conducted at the Oron phosphate quarry in Northern Negev. A special technology was used to create large cavities (up to 3.5 m) at different depths (up to 63 m), accommodating large near-spherical charges of ANFO explosive. A series of decoupled and fully coupled (reference) explosions with charges of 1240 kg in the cavities was conducted. Extensive observations in the near-source zone and further away showed signal characteristics and energy generation features related to these specific decoupled seismic sources. S/P energy ratios and decoupling factors were estimated at local distances, roughly matching theoretical concepts.

The Oron DOB experiment was conducted for empirical modeling of the relationship between shot depth and spectral/energy parameters of regional seismic signals; This experiment, which made constant all factors affecting signal properties except the DOB, seems more ideal than the previous Balapan DOB (1997), and has a unique charge design.

A clear, expected, magnitude/energy reduction with depth was observed at regional distances, complemented by near-source observations of higher frequencies (and larger amplitude/ energy) for deeper charges. S/P energy and spectral ratios and decoupling factors were estimated at close local and near-regional distances, matching roughly theoretical concepts and known observations.

Seismic spectra observations were found to be remarkably consistent with the Mueller/Murphy source model predictions: smaller spectral amplitudes for deeper sources, and the crossover point of spectral dominance at ~10 Hz, observed in a broad distance range 0.2-230 km.

in the project, unique explosion experiments were conducted, results and empirical relationships and estimates obtained, and an extensive database collected; these are an important contribution of the Geophysical Institute of Israel to improvement of nuclear test monitoring.

6. RECOMMENDATIONS

The two source-phenomenology Decoupling and Depth-of-Burial experiments demonstrated the feasibility of a method of seismic source design to create near-spherical charges of different size and at different depths. This blast technology can be used to conducting large-scale, low-cost experimental series of explosions of up to 10 tons at depths of up to 70-80 m, in consolidated sediments: decoupling, DOB, variable charge weight, etc.

REFERENCES

Blanford, R.R., 1995: Regional seismic event discrimination, in: E.S. Husebye and A.M. Dainty (eds.), *Comprehensive Test Ban Treaty, NATO ASI Series, Series E: Applied Sciences* - Vol. 303, 689-719.

Day, S. and K.McLaughlin, 1991: Seismic source representations for spall, *Bull. Seism. Soc. Am.,* **81**, 191-201.

Ezersky, M., S. Keydar and D. Pelman, 2007: Seismic refraction, reflection and diffraction survey at the experimental explosion site ORON quarry, GII Report No. 263/07, May 2007.

Glenn, L. A. and S.C. Myers, 1997: Depth of Burial experiments at Balapan. Report UCRL-JC-128313, Lawrence Livermore National Laboratory.

Gitterman Y., 1998: Magnitude yield correlation and amplitude attenuation of chemical explosions in the Middle East. In *Proceedings of the 20th Annual Seismic Research Symposium on Monitoring a CTBT*, Santa Fe, Sept.21-23, 1998, pp.302-311.

Gitterman, Y. and A. Shapira, 2001: Dead Sea Seismic Calibration Experiment Contributes to CTBT Monitoring, *Seism. Res. Lett.*, Vol.**72**, No.2, 159-170.

Gitterman, Y., V. Pinsky, and A. Shapira, 2001: Improvements in Monitoring the CTBT in the Middle East by the Israel Seismic Network, Contract DSWA01-97-C-0151, Final Report DTRA–TR-01-35, 196 pp.

Gitterman, Y., 2002: Implications of the Dead Sea experiment results for analysis of seismic recordings of the submarine "Kursk" explosions. *Seism.Res.Lett.,***73**, 14-24.

Gitterman, Y., V. Pinsky, A. Shapira, M. Ergin, D. Kalafat, G. Gurbuz, K. Solomi, 2002: Improvement in detection, location and identification of small events through joint data analyasis by seismic stations in the Middle East/Eastern Mediterranean region, In *Proceedings of the 24th Seismic Research Review, Ponte Vedra Beach*, September 17-19, 2002.

Gitterman, Y., V. Pinsky, K. Solomi, R. Hofstetter, C. Gurbuz, and M. Ergin, 2004: Using ground truth events for travel time calibration and studying seismic energy generation and partitioning into various regional phases. In *Proceedings of the 26th Annual NNSA Seismic Research Review: Trends in Nuclear Seismic Monitoring,* Orlando, Florida, September 21-23, 2004, LA-UR-04-5801, Vol. 1, pp. 61–72.

Gitterman, Y., V. Pinsky, R. Hofstetter, 2005a: Using ground truth explosions for studying seismic energy generation and partitioning into various regional phases. In *Proceedings of 27th Annual NNSA Seismic Research Review: Ground-Based Nuclear Explosion Monitoring Technologies,* Rancho Mirage, California, September 20-22, 2005. -UR-05-6407, Vol. 1, pp. 550–560.

Gitterman, Y., V. Pinsky, A.-Q. Amrat, D. Jaser, O. Mayyas, K. Nakanishi, and R. Hofstetter, 2005b: Source features, scaling and location of calibration explosions in Israel and Jordan for CTBT monitoring, *Isr. J. Earth Sci.;* Vol.54, No.4: 199-217.

Gitterman, Y., Pinsky, V., Kurpan, J., 2005c: Using ground truth explosions for studying seismic energy generation and partitioning into various regional phases. *Abstracts of the IASPEI General Assembly*, Santiago, Chile.

Gitterman, Y., R. Hofstetter and V. Pinsky, 2006a: Source features and scaling of buried and surface experimental explosions in Israel, In *Proceedings of the 28th Annual NNSA Seismic Research Review "Ground-Based Nuclear Explosion Monitoring Technologies",* Orlando, Florida, September 19-21, 2006.

Gitterman, Y., Hofstetter, R., Pinsky, V., Solomi, K., Amrat, A.-Q., 2006b: Calibration explosions in Israel, Cyprus and Jordan for CTBT monitoring, *Abstracts of the First European Conference on Earthquake Engineering and Seismology*, p. 284, Geneva, Switzerland.

Khalturin, V.I., T.G. Rautian and Richards P.G., 1998: The seismic signal strength of chemical explosions, *Bull. Seism. Soc. Am.*, **88**, 1511-1524.

Kurpan J., 2004: Discrimination of seismic events in Israel recorded by national seismic network, M. Sc. Thesis, *Tel-Aviv University*, supervisors Prof. Z. Ben-Avraham and Dr. Y.Gitterman.

Landa, E. and Keydar, S., 1998: Seismic monitoring of diffraction images for detection of local heterogeneities, *Geophysics*, 63, No.3, 1093-1100.

Leith, W. and L. J. Kluchko, 1998: Seismic experiments, nuclear dismantlement go hand in hand in Kazakhstan. *Eos, Transactions, American Geophysical Union*, v. **79**, no. 37, September 15, 1998. p. 437, 443-444.

Mikhailova, N., Germanova, T., Aristova, I., 2001: Estimation of energy and magnitude characteristics based on seismic records of chemical explosions in 1997-2000 on the former Semipalatinsk Test Site, in: *Geophysics and Non-Proliferation problems, 2001, Kazakhstan*, V.2, NNC RK, 93-98 (in Russian).

Mueller, R.A. and Murphy, J.R., 1971: Seismic characteristics of Underground Nuclear Detonations, *Bull. Seism. Soc. Am.,* **61**(6), 1675-1692.

Myers, S.C., W.R. Walter, K. Mayeda, and L. Glenn, 1999: Observations in support of Rg scattering as a source for explosion S waves: Regional and local recordings of the 1997 Kazakhstan Depth of Burial experiment, *Bull. Seism. Soc. Am.,* **89**, 544-549.

Negmatullaev S.Kh., M.I. Todorovska, M.D. Trifunac, 1999: Simulation of strong earthquake motion by explosions – experiments at the Lyaur testing range in Tajikistan, *Soil Dynamics and Earthquake Engineering,* **18**, 189-207.

Pinsky, V., Y. Gitterman, A. Hofstetter, A. Shapira, 2005: Robust location of surface explosions by a network of acoustic arrays, *Geophys. Res. Lett.* 33: L02317, doi:10.1029/2005GL024304.

Pinsky V., 2007: Accurate location of seismic sources with and without travel time model, in: *Earthquake monitoring and seismic hazard mitigation in Balkan countries, NATO ARW series*, edited by E. Husebye and C. Christova, Springer.

Richards, P.G. and W.-Y. Kim, 2005: Equivalent volume sources for explosions at depth: theory and observations, *Bull. Seism. Soc. Am.*, Vol.95, No.2, 401-407.

Sharpe, J.A., 1942: The production of elastic waves by explosion pressure: part I, theory and empirical field observations, *Geophysics*, 7, 144-154.

Springer, D.L., G. A. Pawloski, J. L. Ricca, R. F. Rohrer and D. K. Smith, 2002: Seismic Source Summary for All U.S. Below-Surface Nuclear Explosions, *Bull. Seism. Soc. Am.,* 2002; v.92; no.5; p.1806-1840.

Stevens, J., J. Murphy and N. Rimer, 1991: Seismic source characteristics of cavity decoupled explosions in salt and tuff. *Bull. Seism. Soc. Am.*, Vol.81, No.4, 1272-1291

Stevens, J., N. Rimer, H. Xu, J. Murphy, B. Barker, S. Gibbons, C. Lindholm, F. Ringdal, T. Kvaerna, and I. Kitov, 2003: Analysis and Simulation of Cavity-Decoupled Chemical Explosions. In *Proceedings of the 25th Seismic Research Review "Nuclear Explosion Monitoring: Building the Knowledge Base"*, Tuscon, Arizona, 23-25 September 2003, LA-UR-03-6029, Vol. 1, pp. 466–475.

Stevens, J., 2006: Development and Future of Explosion Source Theory, *Abstracts of the 2006 Annual SSA meeting*, San Francisco, California, 18-22 April.

Stump, B. W., S. M. McKenna, C. Hayward, and T.-S. Kim, 2002: Seismic and infrasound data and models at near-regional distances, in *Proceedings of the 24 th Seismic Research Review-Nuclear Explosion Monitoring: Innovation and Integration*, LA-UR-02-5048, Vol. 2, pp. 572–581.

Stump, B., D.C. Pearson and V. Hsu, 2003: Source scaling of contained chemical explosions as constrained by regional seismograms, *Bull. Seism. Soc. Am*. 93, 1212-1225.

U.S. Congress, 1988: Office of Technology Assessment, Seismic Verification of Nuclear Testing Treaties, OTA-ISC-361 (Washington, DC: U.S. Government Printing Office, Chapter 6, May 1988).

Vergino, E.S., and R.W. Mensing, 1983: Yield estimation using regional m_bP_n, *Bull. Seism. Soc. Am*. 80, 1200-1206.

Vogfjord, K., 1997: Effect of explosion depth and earth structure on the excitation of the Lg waves: S* revisited, *Bull Seism. Soc. Am.,* **87**, 1100-1114.

Wallace, T., D. Helmberger, and G. Engen, 1985: Evidence for tectonic release from underground nuclear explosions in long period S waves, *Bull. Seism. Soc. Am.,* **75**, 157-174.

LIST OF SYMBOLS, ABBREVIATIONS, AND ACRONYMS

AFRL	Air Force Research Laboratory
AFSPC	Air Force Space Command
DOB	Depth-of-Burial
ANFO	Ammonium Nitrate Filled Oil
IDF	Israel Defense Forces
IMS	International Monitoring System
BB	Broad Band
SP	Short-Period
GTI	Ground Truth Information
CTBT	Comprehensive Test Ban Treaty